MONITORING AND FAULT DIAGNOSIS OF MULTICONVERTER POWER ELECTRONIC SYSTEMS

by

RANJIT JAYABALAN

Presented to the Faculty of the Graduate School of

The University of Texas at Arlington in Partial Fulfillment

of the Requirements

for the Degree of

DOCTOR OF PHILOSOPHY

THE UNIVERSITY OF TEXAS AT ARLINGTON

December 2006

ACKNOWLEDGEMENTS

I am sincerely grateful to my advisor Dr. Babak Fahimi for his support. His guidance and encouragement has been vital to my learning. I thank him for mentoring me for completion of this dissertation.

I would like to thank Dr. Wei-Jen Lee, Dr. William E. Dillon, Dr. Raymond R. Shoults and Dr. Jean Gao for being on my supervising committee. Their views and suggestions have been valuable for completeness of the dissertation.

I wish to thank the Power Electronics and Controlled Motion (PECM) Lab. for the support in completion of this dissertation.

September 1, 2006

ABSTRACT

MONITORING AND FAULT DIAGNOSIS OF MULTICONVERTER POWER ELECTRONIC SYSTEMS

Publication No. _____

Ranjit Jayabalan, PhD.

The University of Texas at Arlington, 2006

Supervising Professor: Babak Fahimi

Over the recent years the electric loads in automobiles have increased considerably due to advancements in high-power semiconductor based converters. However, with increasing electrical and electrically driven loads, there have been increasing concerns on system reliability. Faults occurring in such application specific solid state converters can lead to fatal consequences as compared to their mechanical counter parts. Thus, it is vital to identify faults in such systems to develop necessary safety techniques and methodologies.

Detailed analysis of faults processes has indicated the need to act quickly following a device failure to prevent propagation of faults that may lead to catastrophic failure of the converter affecting the load, source and connected system. To minimize the effect of fault, it is essential to accurately identify the failed devices and their mode of failure.

The technique presented in the dissertation involves the use of statistical moments of higher orders to detect and identify a fault. This utilizes the existing current and voltage sensors (port parameters) of the multiconverter system without the need for any additional sensors. The technique not only detects system malfunction, but provides information on the device under fault and the nature of the fault. An accurate knowledge of the same will allow appropriate actions to be taken to avoid propagation of fault that may lead to catastrophic failure.

Analysis indicate third-order statistical moments are effective as they dynamically evaluate and monitor system deviations (voltages, currents) from normal operations and direction of the deviations that enable to detect and diagnose fault fast enough to prevent escalation. Thus idea behind the techniques is to detect, identify and act quickly on a single device failure to prevent escalation of the fault that would otherwise occur if the controller continued to operate without the knowledge of the fault situation. In addition, failure mode information derived from the system is essential for isolation of fault/reconfiguration of safety critical systems such as in Hybrid Electric Vehicle Power System to ensure sustainable operation and safety.

TABLE OF CONTENTS

LIST OF ILLUSTRATIONS

LIST OF TABLES

CHAPTER 1

INTRODUCTION

In multiconverter systems many power electronic converters such as AC-DC rectifiers, DC-DC choppers and DC-AC inverters are used as sources, loads, and distribution networks to provide power in different voltage magnitudes and forms. Recent advancements in semi-conductor technology, improvements in converter performance, and fault isolation such as that provided by DC-DC converters have enhanced the practicality, performance, flexibility, and reliability of networks based on multiconverter power electronic systems. These systems may constitute parts of DC or even hybrid DC and AC networks (see Fig 1). However, the interaction between tightly regulated converters can reduce power quality and in some cases affect system stability. They may also degrade static and dynamic behavior of both converter and system [1]. Figure 1 illustrates the existing application, technical challenges, and active fields of research in multi-converter systems.

Generally, design and analysis of converters have been done on a stand alone basis, due to the size and complexity of the multiconverter system. In addition, stability analysis has been mostly based on linearized small signal models which are

simple, fast and require less computational resources. This approach, however, neglects the inherent system level issues. Therefore, new approaches need to be developed that address the dynamics associated with multiconverters and account for the large signal perturbations that the system is highly prone to.

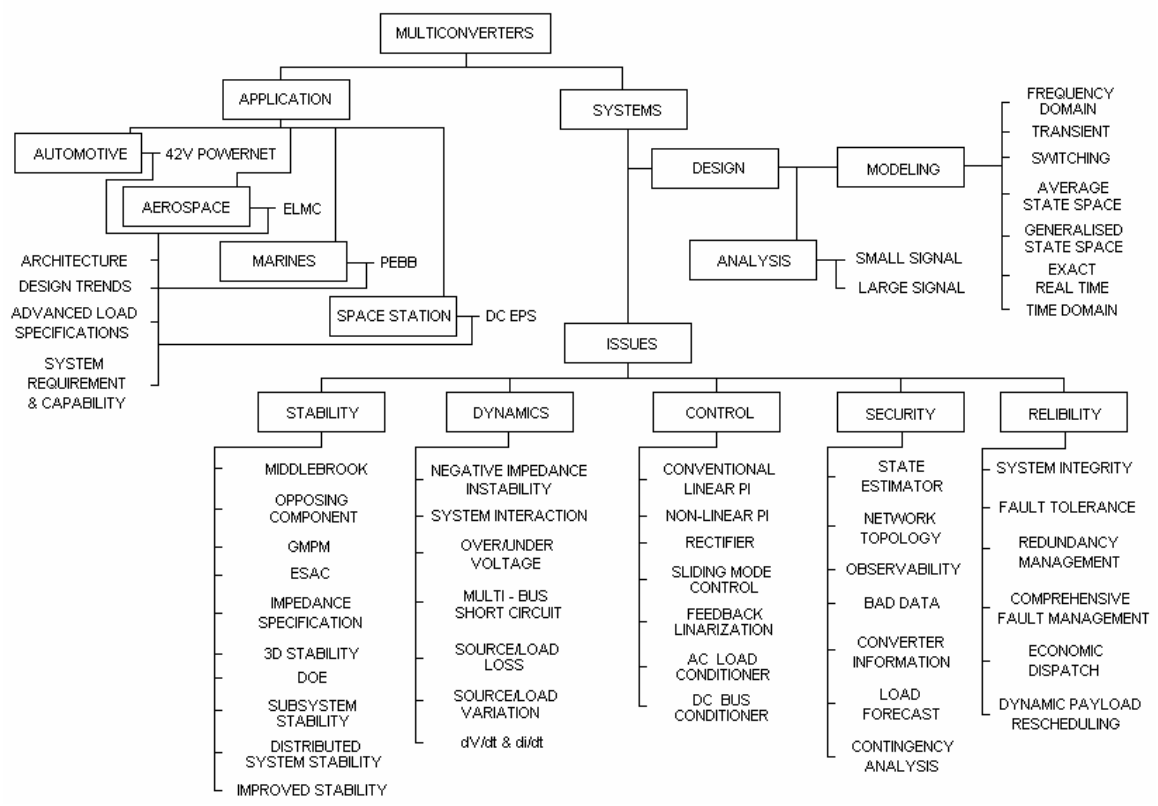

Fig 1. Graphical Representation of the R&D on Power Electronics-based Systems

1.1 Advanced Electrical Networks

Power electronics-based systems and components have been increasingly used in land, air, and sea vehicles over the past decade. This has turned the vehicular products into a primary market for power electronics applications. Moreover, the existing trend in more electrification of the vehicles represents an even bigger potential

for an increase in the existing demand. Although the primary incentive for introduction of multiconverter systems into vehicular technologies was to enhance fuel economy and environmental issues associated with vehicles; today, improvement of fault tolerance, cost, and compactness have boost the motivation for development of the more electric vehicles.

1.1.1 Automotive Power System

With increasing luxury and infotainment loads seeping into the automotive industry along with the need to replace the conventionally driven mechanical, hydraulic and pneumatic loads to be now driven electrically for improved performance and efficiency, has lead to significant rise in the electrical power demands which is anticipated to be as high as 5 kW average and peaks of about 12 kW in the very near future. The new vehicular power system architecture, the 42V PowerNet, will be the transition from the present 12V network of about 1.2 kW capacity to meet the increasing power demand Fig 2 [1]-[13].

Performance loads will constitute a significant part of the increased automotive loads, of which, many will be driven by tightly regulated converters and advanced electric drives. Performance loads such as Electromagnetic Valve Train (EVT) whose power demands vary as a function of engine rpm, 0.5 kW at low and 4 kW at high rpm, and while loads such as electric steering, whose demand vary from 1 – 2 kW, each represent a different kind of stress on the automotive power system.

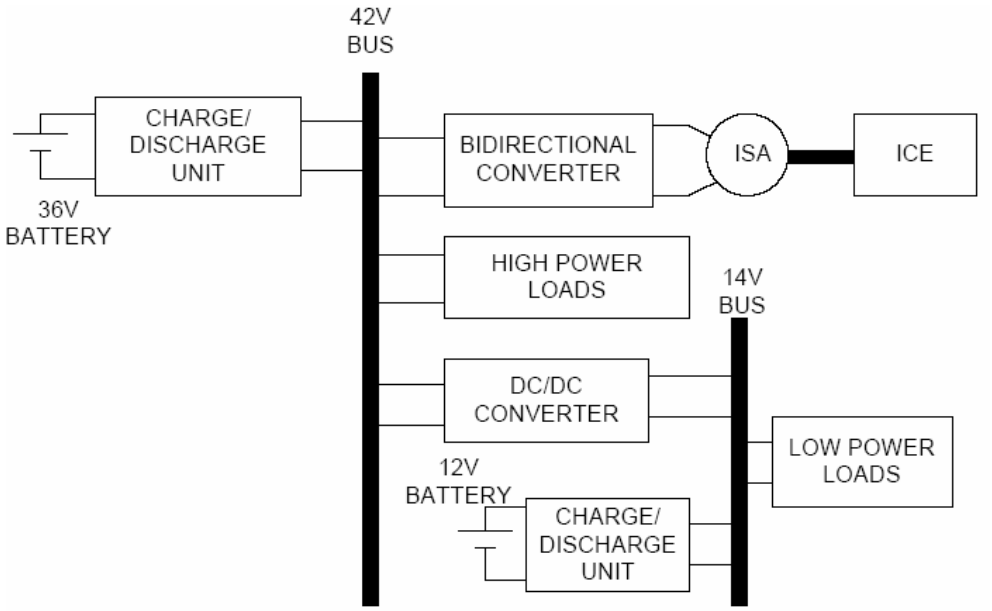

Fig 2. Advanced Automotive Power System Architecture

1.1.2 Aerospace Power System

The More Electric Aircraft (MEA) concept offers enhanced reliability, maintainability, supportability and survivability for the aircraft [14]-[20]. This is primarily possible to achieve due to recent advancements in solid state switching devices, high power converter technology, high power density motor/generator and drives, evolution of fault tolerant electrical power system (EPS) and breakthroughs in electrical actuators. The MEA will be a stepping stone for realizing more benefits from the All Electric Aircraft (AEA). Driving conventional loads electrically and addition of new loads have considerably increased power demands. Besides, increasing galley load of about 500W per passenger and in-flight entertainment (IFE) of about 100W per seat which are likely to total up to 350 kW for transport aircraft are also adding to the power demand.

To serve such demands, generation systems in MEA may be Constant Frequency Integrated Drive Generator (IDG), Variable Speed Constant Frequency (VSCF) or Variable Frequency (VF) system. These would deliver 3 Phase, 115 VAC, 400 Hz or 115 VAC wild frequency or even 270 VDC depending on electrical architecture. Using power electronic converters the voltage is transformed to 28 VDC and 24 VDC to supply the various kinds of loads. Thus a comprehensive Power Management System (PMS) will form an integral part of the MEA EPS that will manage loads to maintain the system at optimal condition Fig 3.

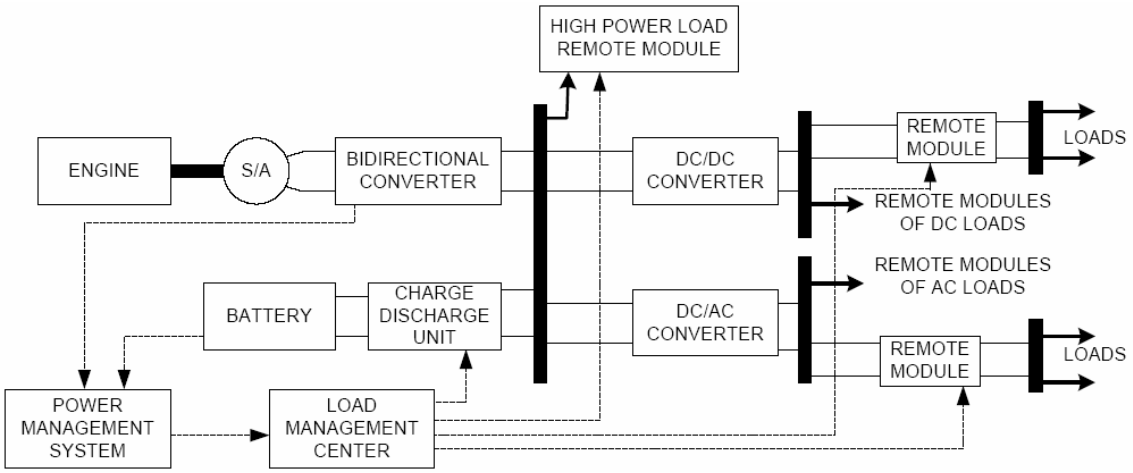

Fig 3. More Electric Aircrafts

1.1.3 Marine Vessel Power System

The power system architecture in ships and submarines can be of two types. In a segregate power system architecture different electrical loads are supplied by an independent generator set. However, in the more preferred Integrated Power System (IPS) architecture all the loads are supplied by a common electrical power bus. This

enables handling of the loads and generation sources more optimally and efficiently, and is able to direct power to vital loads on demand [21]-[24].

The distribution architecture is more of zonal design rather than a ring or radial type for the increased accessibility to sources and loads that it offers. In addition, it is more customized and readily lends itself to support DC and 60/400 Hz AC. With the zonal architecture, where DC loads are connected at the DC link, it leads to a need for an increased care in design and analysis of power system due to increased dynamics and probable instability. Figure 4 gives a graphical representation of zonal IPS system.

Power Electronic Building Blocks (PEBB) which are general purpose converters that can perform different electrical conversion function by just a simple software reconfiguration, are increasing entering into the marine power systems [25]-[30]. With generalized control hierarchy involving topology and application controllers among others, PEBB have become a more comprehensive subsystem unit. PEBB opens up the opportunity for electrical reconfiguration – whereby platform respond to assure power to vital loads during damage or failure and change state to varying readiness condition, which will prove to be asserted in marine time warfare.

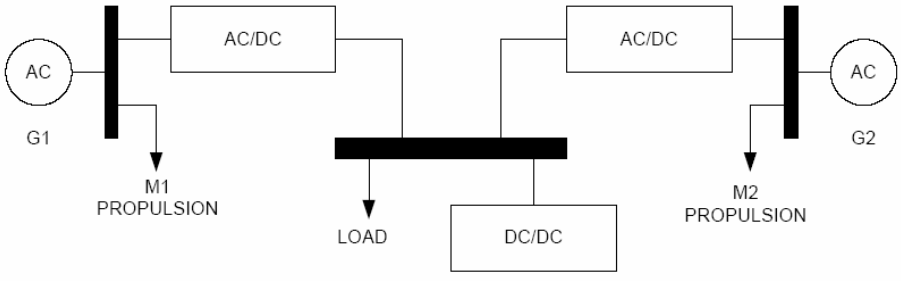

Fig 4. Diagrammatic Representation of a Zonal IPS

1.1.4 Space Power System

The Space Power System is an extensive network of DC electrical power system which comprises of many power electronic converters, variable loads, solar arrays and battery units [31]-[36]. Each power electronic converter either transforms the voltage for a set of loads or acts as power electronics drive system. The space power system would have multiple power sources both mechanical and electric that are transformed to 160 VDC as primary usable form. This is then segmented down to 120 VDC and further by DC-DC and DC-AC converters as per load requirements at lower level buses. Figure 5 shows a representative configuration of Space Station Power System.

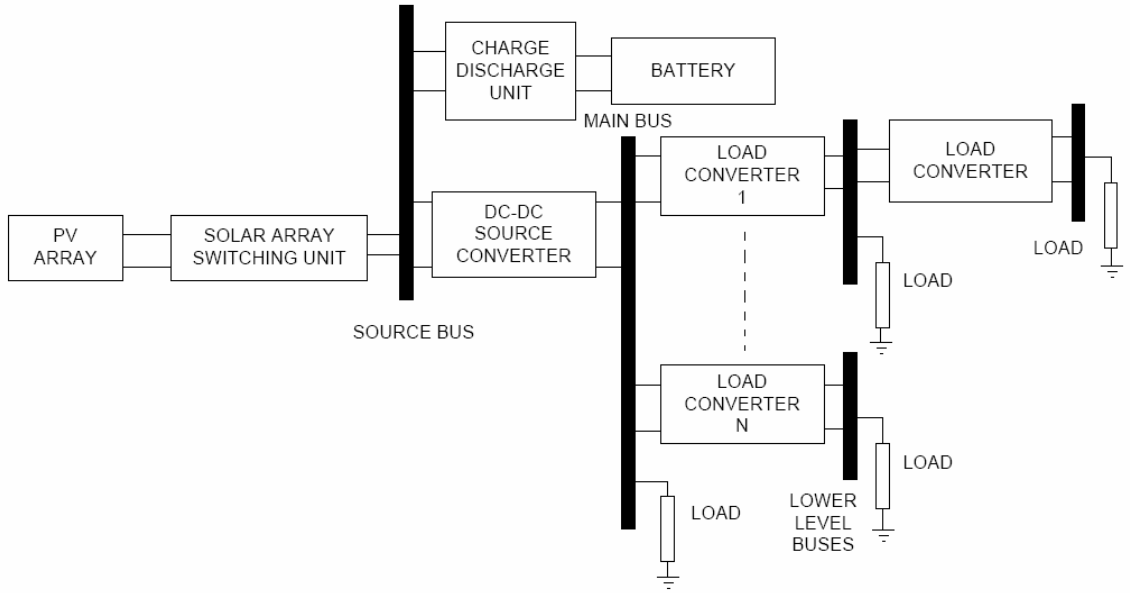

Fig 5. Space Station Power System

The use of such converters in space distributed power systems enable controlling the quality of power of different loads and subsystem, such as the DC-DC converter that allow close regulation of output voltage under wide variation of input

voltage and load. Besides, the system also benefits from high reliability by isolating system failures and thus providing high system redundancy. The solid state power converters in space power system give the added flexibility to address the complex sources, undefined loads and easier system expansion.

CHAPTER 2

MULTICONVERTER SYSTEMS

Multiconverter systems comprise of a number of power electronic converters such as AC-DC, DC-DC and DC-AC converters at source, loads and interconnections of large systems. The major attributes of multiconverter systems are their inherent capability to handle high power efficiently, and to provide high degree of reliability and fault tolerance. In addition they lend themselves to well structured distributed control. However, the system faces issues of instability, dynamics and security that need to be addressed [37].

2.1 Modeling and Simulation

Due to the switching operations, the power electronic converters are time dependant systems. Modeling and analysis of these converters in time domain would give static and dynamic system behavior and including the protection circuits, system control dynamics and limitation will improve the accuracy of the analysis [37]-[41]. However, it requires high computing resources and long simulation time. Therefore, averaging method can be used. However, they do not account for rapid and large signal variation and oscillatory behaviors. Thus the generalized/extended state space averaging method that overcomes these will be a more appropriate approach. The Extended state

space averaging method would enhance the accuracy of the system modeling and analysis.

The switching operations that make these power electronic converters time dependent systems can be viewed as dynamically changing electric circuit topologies. The rule of transition from one topology to another is realized by the virtue of the switching action which is periodic with frequencies decided by the controller. With energy storage elements forming an inherent part of these circuits, the analysis of the circuit dynamic can be performed by state space averaging of the time varying systems (see Fig 6). In such representations A_i, B_i and C_i describe the state, input and the output matrices of the system under consideration for the i^{th} time interval if the complete period of topological changes can be divided into m intervals.

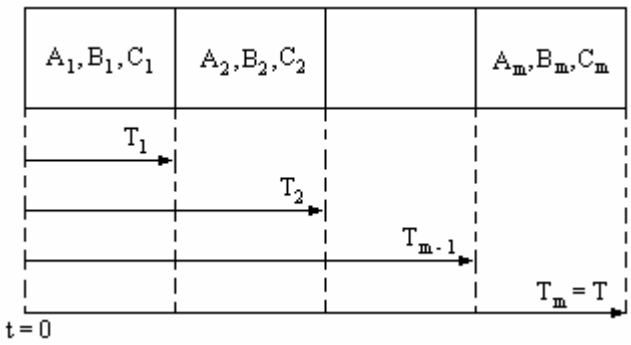

Fig 6. State Space Representation of Power Electronic Converters

The time varying representation of the entire system over one complete period can be expressed as in (1).

$$\begin{aligned} \dot{x} &= A_{eq}(t)x(t) + B_{eq}(t)U(t) \\ y(t) &= C_{eq}(t)x(t) \end{aligned} \tag{1}$$

Where $x(t)$ is the state and, A(t) and B(t) are the system matrix and the input matrix respectively that are functions of time that makes the system non-linear. The equivalent state space representation of (1) can be expanded using a step function as in (2)

$$\begin{aligned} A_{eq} &= \sum_{i=1}^{m} A_i \{u(t-T_{i-1}) - u(t-T_i)\} \\ B_{eq} &= \sum_{i=1}^{m} B_i \{u(t-T_{i-1}) - u(t-T_i)\} \\ C_{eq} &= \sum_{i=1}^{m} C_i \{u(t-T_{i-1}) - u(t-T_i)\} \end{aligned} \tag{2}$$

Applying Laplace Transformation to (1) and taking into account the time varying nature of the state matrices, convolution in frequency domain gives (3)

$$\begin{aligned} sX(s) &= \frac{1}{2\pi j}\left\{L(A_{eq}) * X(s) + L(B_{eq}) * U(s)\right\} \\ Y(s) &= \frac{1}{2\pi j}\left\{L(C_{eq}) * X(s)\right\} \end{aligned} \tag{3}$$

Using (2) and Taylor series expansion of the exponential functions, expression (4) for Laplace transform of state variables can be obtained.

$$\begin{aligned} L(A_{eq}) &= \sum_{i=1}^{m} A_i \left\{\frac{e^{-T_{i-1}s} - e^{T_i s}}{s}\right\} = \sum_{i=1}^{m} A_i \left\{\left[T_i - T_{i-1}\right] + \left[\frac{T_{i-1}^2 - T_i^2}{2!}\right] s + ...\right\} = \sum_{i=1}^{m}\left[\hat{A}_{i0} + \hat{A}_{i1} s + ...\right] \\ L(B_{eq}) &= \sum_{i=1}^{m} B_i \left\{\frac{e^{-T_{i-1}s} - e^{T_i s}}{s}\right\} = \sum_{i=1}^{m} B_i \left\{\left[T_i - T_{i-1}\right] + \left[\frac{T_{i-1}^2 - T_i^2}{2!}\right] s + ...\right\} = \sum_{i=1}^{m}\left[\hat{B}_{i0} + \hat{B}_{i1} s + ...\right] \\ L(C_{eq}) &= \sum_{i=1}^{m} C_i \left\{\frac{e^{-T_{i-1}s} - e^{T_i s}}{s}\right\} = \sum_{i=1}^{m} C_i \left\{\left[T_i - T_{i-1}\right] + \left[\frac{T_{i-1}^2 - T_i^2}{2!}\right] s + ...\right\} = \sum_{i=1}^{m}\left[\hat{C}_{i0} + \hat{C}_{i1} s + ...\right] \end{aligned}$$

(4)

Selecting only DC Component in (4) gives the classical state averaging method as in (5)

$$\begin{aligned} A_{eq} &\approx \sum_{i=1}^{m} A_i \left[T_i - T_{i-1}\right] = \sum_{i=1}^{m} \hat{A}_{i0} \\ B_{eq} &\approx \sum_{i=1}^{m} B_i \left[T_i - T_{i-1}\right] = \sum_{i=1}^{m} \hat{B}_{i0} \\ C_{eq} &\approx \sum_{i=1}^{m} C_i \left[T_i - T_{i-1}\right] = \sum_{i=1}^{m} \hat{C}_{i0} \end{aligned} \tag{5}$$

However, a better precision is obtained if higher order terms in (4) are also included. This will result in what is referred to as extended state space averaging method (6). Dropping the number of intervals for simplifying the derivation

$$\begin{aligned} L(A_{eq}) * X(s) &= \int_0^s \sum_{k=0}^{n} \hat{A}_k \tau^k X(s-\tau) d\tau = \sum_{k=0}^{n} \hat{A}_k \int_0^s \tau^k X(s-\tau) d\tau \\ L(B_{eq}) * U(s) &= \int_0^s \sum_{k=0}^{n} \hat{B}_k \tau^k U(s-\tau) d\tau = \sum_{k=0}^{n} \hat{B}_k \int_0^s \tau^k U(s-\tau) d\tau \\ L(C_{eq}) * X(s) &= \int_0^s \sum_{k=0}^{n} \hat{C}_k \tau^k X(s-\tau) d\tau = \sum_{k=0}^{n} \hat{C}_k \int_0^s \tau^k X(s-\tau) d\tau \end{aligned} \tag{6}$$

Where, k denotes the order of approximation, i.e. k = 0 for DC, k = 1 for first harmonic, k = 2 for second harmonic approximation. Recursive equation for formulation of the state space representation is obtained by applying integration by parts to (6).

$$\Rightarrow \sum_{k=0}^{n} \hat{A}_k \begin{bmatrix} \left|\tau^k X_1(s-\tau)\right|_0^s - k\left|\tau^{k-1} X_2(s-\tau)\right|_0^s + k(k-1)\left|\tau^{k-2} X_3(s-\tau)\right|_0^s \\ .....+k(k-1).....(k-(n-2))\left|\tau^{k-(n-1)} X_k(s-\tau)\right|_0^s \\ +k(k-1).....(k-(n-1))\left|\tau^{k-n} X_{k+1}(s-\tau)\right|_0^s \end{bmatrix}$$

$$\Rightarrow \sum_{k=0}^{n} \hat{B}_k \begin{bmatrix} \left|\tau^k U_1(s-\tau)\right|_0^s - k\left|\tau^{k-1} U_2(s-\tau)\right|_0^s + k(k-1)\left|\tau^{k-2} U_3(s-\tau)\right|_0^s \\ .....+k(k-1).....(k-(n-2))\left|\tau^{k-(n-1)} U_k(s-\tau)\right|_0^s \\ +k(k-1).....(k-(n-1))\left|\tau^{k-n} U_{k+1}(s-\tau)\right|_0^s \end{bmatrix} \qquad (7)$$

$$\Rightarrow \sum_{k=0}^{n} \hat{C}_k \begin{bmatrix} \left|\tau^k X_1(s-\tau)\right|_0^s - k\left|\tau^{k-1} X_2(s-\tau)\right|_0^s + k(k-1)\left|\tau^{k-2} X_3(s-\tau)\right|_0^s \\ .....+k(k-1).....(k-(n-2))\left|\tau^{k-(n-1)} X_k(s-\tau)\right|_0^s \\ +k(k-1).....(k-(n-1))\left|\tau^{k-n} X_{k+1}(s-\tau)\right|_0^s \end{bmatrix}$$

Introducing back the number of intervals over a complete period of topological changes in (7) and substituting in (3)

$$sX(s) = \frac{1}{2\pi j}\left\{ \begin{array}{l} \displaystyle\sum_{i=1}^{m}\sum_{k=0}^{n} \hat{A}_{ik} \begin{bmatrix} \left|\tau^k X_1(s-\tau)\right|_0^s - k\left|\tau^{k-1} X_2(s-\tau)\right|_0^s + k(k-1)\left|\tau^{k-2} X_3(s-\tau)\right|_0^s \\ .....+k(k-1).....(k-(n-2))\left|\tau^{k-(n-1)} X_k(s-\tau)\right|_0^s \\ +k(k-1).....(k-(n-1))\left|\tau^{k-n} X_{k+1}(s-\tau)\right|_0^s \end{bmatrix} \\ +\displaystyle\sum_{i=1}^{m}\sum_{k=0}^{n} \hat{B}_{ik} \begin{bmatrix} \left|\tau^k U_1(s-\tau)\right|_0^s - k\left|\tau^{k-1} U_2(s-\tau)\right|_0^s + k(k-1)\left|\tau^{k-2} U_3(s-\tau)\right|_0^s \\ .....+k(k-1).....(k-(n-2))\left|\tau^{k-(n-1)} U_k(s-\tau)\right|_0^s \\ +k(k-1).....(k-(n-1))\left|\tau^{k-n} U_{k+1}(s-\tau)\right|_0^s \end{bmatrix} \end{array} \right\}$$

$$sY(s) = \frac{1}{2\pi j}\left\{ \sum_{i=1}^{m}\sum_{k=0}^{n} \hat{C}_{ik} \begin{bmatrix} \left|\tau^k X_1(s-\tau)\right|_0^s - k\left|\tau^{k-1} X_2(s-\tau)\right|_0^s + k(k-1)\left|\tau^{k-2} X_3(s-\tau)\right|_0^s \\ .....+k(k-1).....(k-(n-2))\left|\tau^{k-(n-1)} X_k(s-\tau)\right|_0^s \\ +k(k-1).....(k-(n-1))\left|\tau^{k-n} X_{k+1}(s-\tau)\right|_0^s \end{bmatrix} \right\} \qquad (8)$$

Extending the above formulation to a multiconverter environment with p converters.

$$sX(s)=\frac{1}{2\pi j}\left\{\begin{array}{l}\displaystyle\sum_{j=1}^{p}\sum_{i=1}^{m}\sum_{k=0}^{n}\hat{A}_{jik}\left[\begin{array}{l}\left|\tau^{k}X_1(s-\tau)\right|_0^s-k\left|\tau^{k-1}X_2(s-\tau)\right|_0^s+k(k-1)\left|\tau^{k-2}X_3(s-\tau)\right|_0^s\\ .....+k(k-1).....(k-(n-2))\left|\tau^{k-(n-1)}X_k(s-\tau)\right|_0^s\\ +k(k-1).....(k-(n-1))\left|\tau^{k-n}X_{k+1}(s-\tau)\right|_0^s\end{array}\right]\\ +\displaystyle\sum_{j=1}^{p}\sum_{i=1}^{m}\sum_{k=0}^{n}\hat{B}_{jik}\left[\begin{array}{l}\left|\tau^{k}U_1(s-\tau)\right|_0^s-k\left|\tau^{k-1}U_2(s-\tau)\right|_0^s+k(k-1)\left|\tau^{k-2}U_3(s-\tau)\right|_0^s\\ .....+k(k-1).....(k-(n-2))\left|\tau^{k-(n-1)}U_k(s-\tau)\right|_0^s\\ +k(k-1).....(k-(n-1))\left|\tau^{k-n}U_{k+1}(s-\tau)\right|_0^s\end{array}\right]\end{array}\right\}$$

$$sY(s)=\frac{1}{2\pi j}\left\{\sum_{j=1}^{p}\sum_{i=1}^{m}\sum_{k=0}^{n}\hat{C}_{jik}\left[\begin{array}{l}\left|\tau^{k}X_1(s-\tau)\right|_0^s-k\left|\tau^{k-1}X_2(s-\tau)\right|_0^s+k(k-1)\left|\tau^{k-2}X_3(s-\tau)\right|_0^s\\ .....+k(k-1).....(k-(n-2))\left|\tau^{k-(n-1)}X_k(s-\tau)\right|_0^s\\ +k(k-1).....(k-(n-1))\left|\tau^{k-n}X_{k+1}(s-\tau)\right|_0^s\end{array}\right]\right\} \quad (9)$$

This equation (9) represents the extended state space averaging of multiconverter system of n^{th} order, having p converters with m topological states.

2.2 Stability and Analysis

The AC-DC, DC-DC, and DC-AC converters are non-linear, time dependant systems. Considering networks like automotive, aerospace and space power systems using numerous power electronic converters, the inherent interaction between these converters can make the system to deviate from its operating point. In addition, when these converters are tightly regulated, they behave as Constant Power Loads (CPL). A tightly speed regulated motor drive driving a one-to-one torque-speed mechanical load in a DC system is shown as an example of CPL in Fig 7 [38]. These constant power loads have positive instantaneous impedance but negative incremental impedance

leading to instability [42]. Thus, a deviation from equilibrium operating point due to disturbance tends to increase the deviation further as the system behaves as a positive feedback, unlike a positive incremental load where the system returns back to equilibrium due to negative feedback in the system Fig 8.

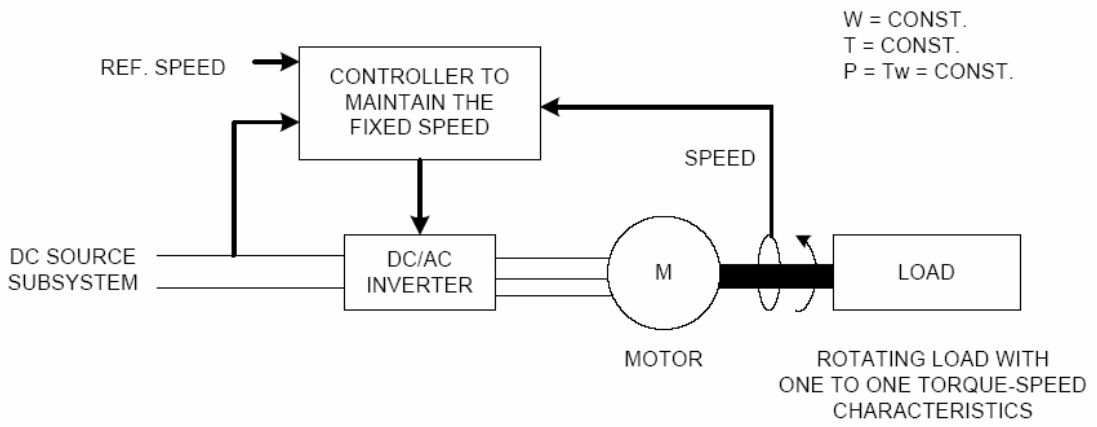

Fig 7. CPL with one-to-one Torque-Speed Characteristics

Stability analysis by Middlebrook Criterion is well established and is used extensively [43]. However, it introduces very large artificial conservativeness. In addition, the large forbidden region has little influence on the stability and leads to slow control loops and high bus capacitance. As a result, alternate stability method such as Opposing Component Criterion and Gain and Phase Margin (GMPM) that have smaller conservativeness were introduced. The major drawback is that the components are required to be moved across physical boundaries of subsystems. Thus, designing multiconverter systems becomes complex with the later two methods. The ESAC criterion is preferred because of the comparatively very small artificial conservativeness and most of all the fact that it does not require component rearrangement across

subsystem boundaries making it ideal for multiconverter system design. Figure 9 depicts these criterions.

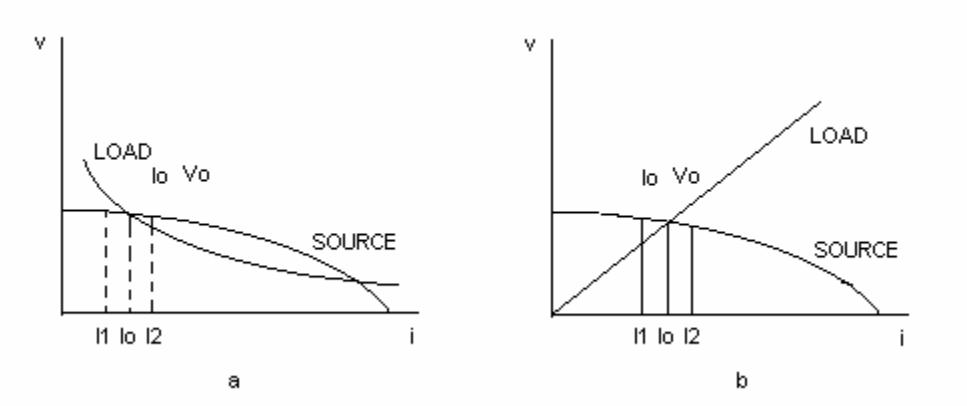

Fig 8. (a). Negative and (b). Positive Incremental Load Characteristics

In multiconverter systems with Constant Power Loads (CPL) and Constant Voltage loads (CVL), the necessary and sufficient condition for stability is

$$P_{CPL} < P_{CVL}$$

In the case of multiconverters in distribution systems where there are CPL and CVL, the necessary and sufficient condition for system stability takes the form

$$P_{CPL} < P_{CVL} + (V_{02} * R_{eq} * C_{eq})/L_{eq}$$

Where,
R_{eq}, C_{eq} and L_{eq} are the converter, input filter and the converter input side distribution system resistance, capacitance and inductance. V_{02} is the output nominal voltage of the converter.

$$P_{CPL} < (V_{02} * R_{eq} * C_{eq})/L_{eq}$$

represents a case of improved stability criterion where the system is stable even without resistive loads [36].

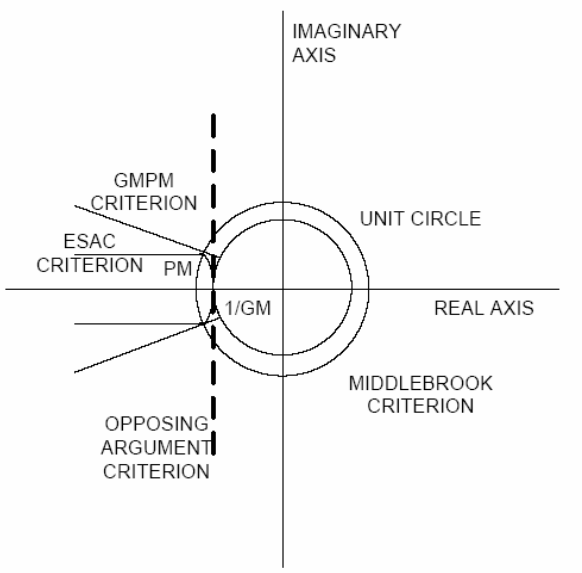

Fig 9. Representation of Stability Criterions

Constant power loads in the case of AC power system usually have a controlled or uncontrolled rectifier at the front end to supply DC power to the tightly regulated load as shown in Fig. 10. It is observed that if a controlled rectifier-based CPL approaches instability, decreasing the firing would increase the stability margin of the system. Hence, an uncontrolled rectifier-based CPL is more stable. The necessary and sufficient condition for stability of AC distribution system is similar to that of the DC but with rms voltage

$$P_{CPL} < P_{CVL} + (V^2_{rms} * R_{eq} * C_{eq})/L_{eq}$$

Figure 11 depicts the CPL and CVL in a hybrid (AC & DC) power system. The CPL is similar to that in AC power system however; the system stability is determined by the condition for which the eigenvalue of the system matrix have negative real part. The necessary and sufficient condition for stability is held only in the stable region (see

Fig 12). If in the analysis, the DC values on the AC side and the ripples on the DC side are neglected for simplicity, the approximation yields a larger stable region. Thus the reduced model obtained will not guarantee system stability for operating points close to the margin of stability region.

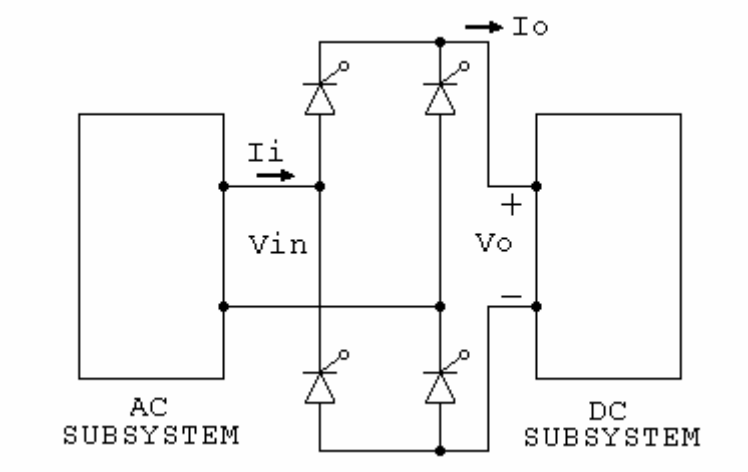

Fig 10. AC/DC Rectifier Connecting DC Subsystem with CPL to an AC Subsystem

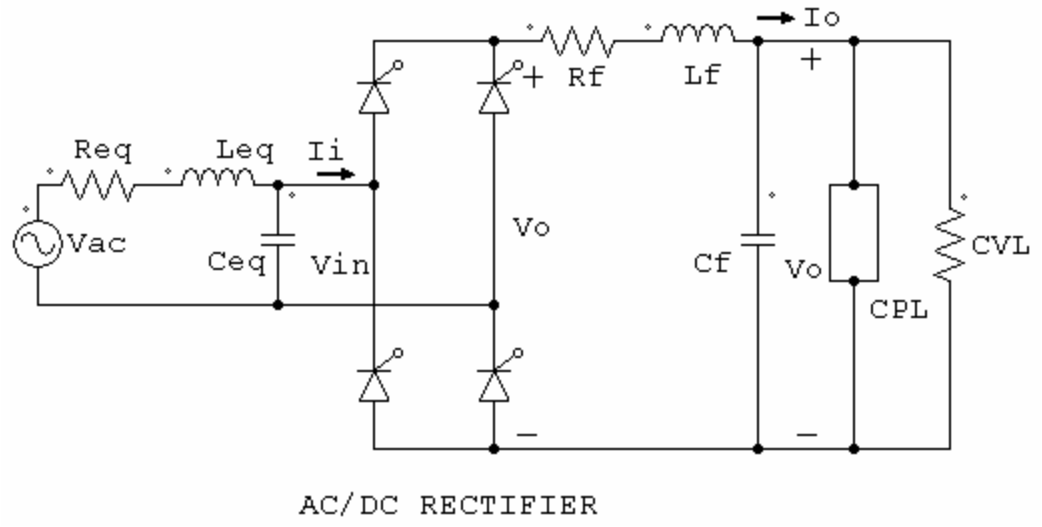

Fig 11. CPL and CVL in Hybrid (AC & DC) Power System

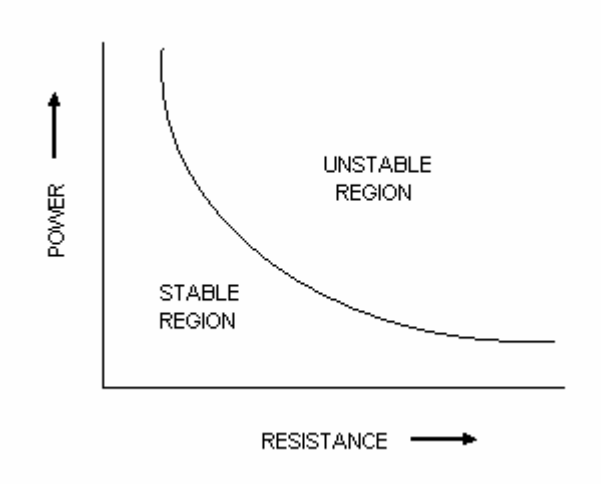

Fig 12. Stable and Unstable Region

However, power electronics converters with open loop as well as poor closed loop controller do not guarantee tight system regulation. Thus practical systems such as Uninterruptible Power Supplies (UPS) do not have negative impedance instability.

A more appropriate approach when considering large power systems such as space power system would be to use input impedance specification (Z_L) of the load subsystems and output impedance specification (Z_S) of the source subsystems. By ensuring $Z_S < Z_L$ at all frequencies, a stable source and load can ensure network stability, but would call for extremely conservative and expensive design.

However, the above cases are for small signal stability. The question that now stands is, how small is this small perturbation. What is the accuracy and validity of applying small signal, frequency domain, linearized, averaged reduced modeling, analysis and simulation to system which are primarily non-linear, time domain system and have large signal perturbations.

Thus, for stable and optimal performance of multiconverter systems, it is essential that large signal analysis in time domain be performed. In addition, incorporation of computer models to predict transients and non-linear characteristics and directed hardware analysis to identify scenarios degrading power quality or creating instability and performing transient stability test will ensure complete system stability even under unforeseen operating condition.

2.3 Dynamics and Control

New performance loads that will be added to advanced electrical networks are in the form of constant power loads that could lead to destabilization [50]. The interaction between various components of the converter and between source, load and interconnecting converters in cascade and parallel configuration in multiconverter networks could lead to significant system dynamics. Thus, designing controllers for the power electronic converters will be a major challenge [51], [52].

Conventional linear control methods can not be used due to stability limitations around the operating point, while the use of non-linear PI stabilizers would bring about variable switching frequency that are not desirable (Fig 13). Rectifiers are known to perform better with constant power loads than current control, however they cannot under such circumstances deliver constant voltage [38]. Similarly, sliding mode control provides a constant power output over a certain voltage range ($V_{0min} < V_0 < V_{0max}$), thus if implemented on converters such as DC-DC converters that are required to supply both constant power loads (CPL) and constant voltage loads (CVL), then an additional DC-DC converter will be required to regulate the voltage for CVL Fig 14 [38], [53].

However, feedback linearization control enables the converter to supply both constant voltage and constant power loads simultaneously [51], [52], [54]-[55].

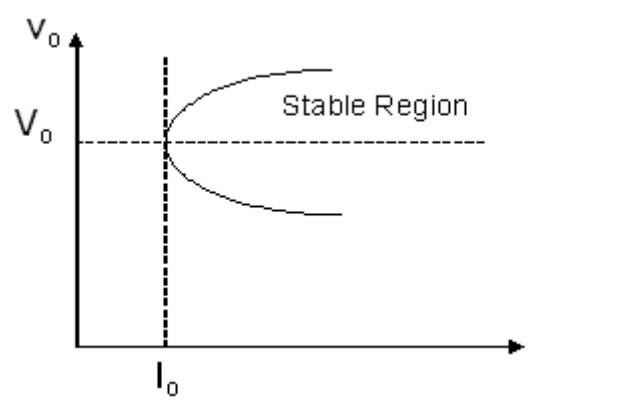

Fig 13. Stability Region

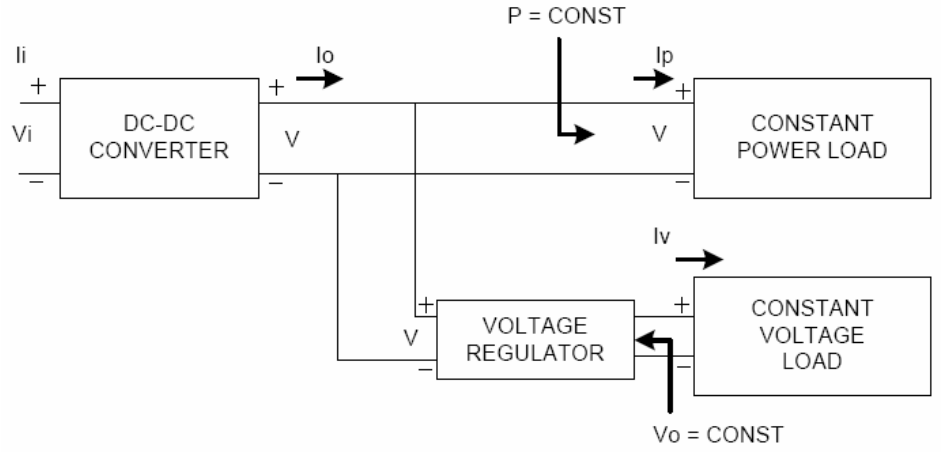

Fig 14. Representation of Constant Power and Constant Voltage Load.

2.4 Security and Reliability

It is essential to have system security to ensure continuity of system operation in its normal condition (no overload, over-voltage, under-voltage and loads being met) in real time [56], [57]. However if faults occur in system, they are identified, isolated, cleared and restored. To achieve system security, it is required to know the complete

system information from incomplete noisy set of real time measurements if state estimators are to be used (Fig 15). Alternatively, the knowledge of the contingencies and the frequency of their occurrence can also help in achieving system security. In such events, contingencies are based on probability mode such as Expected Contingency Mode (ECM) that gives a measure of system security level [57].

In the designing of multiconverter systems, particularly large EPS systems, system integrity will be of major concern. It is essential in the design process to ensure that minimum system interaction exists for stability and security in order to have high system reliability. The prognosis under fault conditions or even when the system begins to develop incipient failure should be well analyzed to receive complete system information. However, the issue that exists in fault diagnosis, is qualitative simulator sufficient or quantitative will be required and whether discrepancy identification involving computation of prognostic sets be determined statistically or dynamically. It is also required to define basis of hypothesis generation (Fig 16). In addition, it is crucial to identify and differentiate single/multiple faults in order to maximize system availability and capacity under faults [58]-[61].

Although economic dispatch addresses reliability through security, it is vital to have dynamic payload rescheduling particularly when autonomous multiconverter EPS of significant size and complexity are to be operated in closed loop. Redundancy management have proven to enhance reliability by using redundant subsystem, but such an approach cannot be always taken and it calls for a trade off between operating the system with higher reserves or at stability margins. The characteristic features of power

electronic based systems supports Comprehensive Fault Management that include identifying anomalies, diagnosing actual faults, isolating faults, recommending corrective actions for fault recovery and autonomous implementation of fault recovery action that make the system highly reliable and robust.

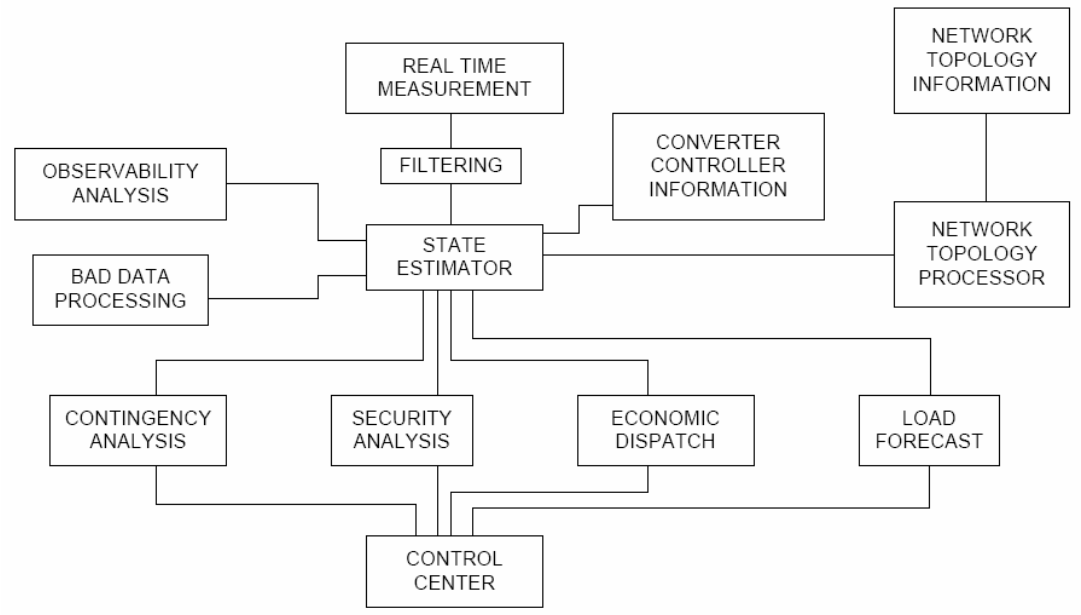

Fig 15. Control for System Security

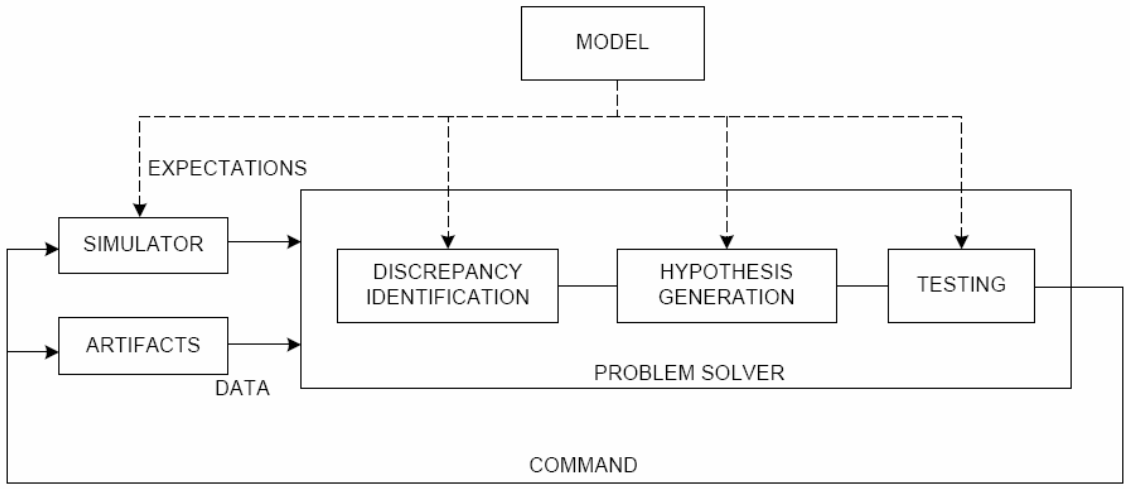

Fig 16. Representation of Fault Diagnosis Model

CHAPTER 3

FAULT ANALYSIS

Over the recent years the electric loads in automobiles have increased considerably. This has primarily been due to an increased need to change the traditionally driven mechanical, pneumatic and hydraulic loads to be now driven electrically for improved efficiency and performance. In addition, there have also been a surge in the number of infotainment and safety loads that have been added to the present vehicles. To address these requirements, new automotive power electronics-based power system architectures have been considered [2]-[4], [7], [12]. However, with increasing electrical and electrically driven loads, there have been increasing concerns on system reliability [37]. Faults occurring in such application specific solid state converters can lead to fatal consequences as compared to their mechanical counter-parts. Thus, it is vital to identify faults in such systems so as to develop necessary safety techniques and methodologies [62]-[65].

Detailed analysis of faults processes has indicated the need to act quickly following a device failure to prevent propagation of faults that may lead to catastrophic failure of the converter affecting the load, source, and connected system. To minimize effects of fault, it is essential to accurately identify failed device and its mode of failure.

A multistage DC-DC converter system consisting of two cascaded DC-DC buck converters is used as a representative system for the analysis and detection of various types of faults. The first DC-DC converter acts as a source converter that steps down 300 V input to 42 V. The second DC-DC buck converter behaves as a load converter stepping down 42 V to 14 V. Additional loads may also be connected to the source converter. These loads depending on the automotive power system requirements may be resistive or highly inductive loads. This is a close representation of the proposed hybrid electric vehicle automotive power system (Fig. 17).

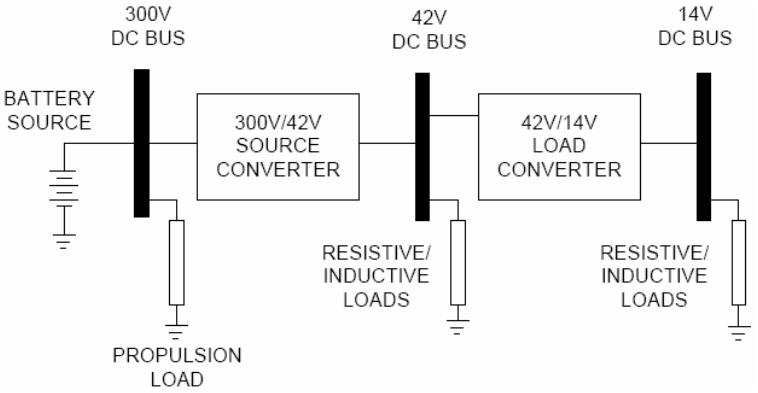

Fig 17. Simplified Representation of Hybrid Electric Vehicle Automotive Power System

3.1 Fault Analysis Techniques

Fault on a system may be defined as a physical defect or material damage of an element or system causing a failure. These faults may be classified by their duration – transient, intermitted or permanent, extent, or mode of propagation. Permanent faults will be discussed here. It is crucial to identify faults to effectively manage them to keep their impact minimal. Fault management may be achieved in four stages (1) Fault Detection – discovering the existence of a fault in the system, (2) Fault Identification –

identifying the nature and location of the fault, (3) Fault Localization – constraining the fault to a sufficiently small subsystem or functional module of the system, (4) Fault Correction – taking the appropriate corrective action to restore normal system operation. Traditionally, after detecting a fault, fault identification follows fault localization. That is, after a fault is detected in the system, a section of the system is immediately localized, disconnecting other loads too, and then the fault is identified by diagnosis and healthy loads are moved back into the system. However, in automotive systems, localizing a fault immediately following a fault without diagnosing the fault may lead to more catastrophic consequences as more safety or performance loads driven electrically are added into the hybrid electric automotive systems. In addition, with fault tolerant technologies, a system under fault may be able to continue sustained operation with reduced performance than having it disconnected that may impede safety. Thus, this would necessitate that after faults are detected they be identified before being localized. Hence, at this point it can be pointed that fault detection and identification is a collective subproblem and can be referred to as fault diagnosis.

Detecting a fault may involve different search strategies or a combination thereof. Topological search involves the use of normal system models to judge whether a field is good or bad and then examine the next field where fields in the same level are logically or physically adjacent. Although it has a dependence on the normal system operating models than models of malfunction, it is uneconomical from the point that, observations can only be used for good or bad judgment and may not lead to the diagnosis by itself. An alternative search strategy is the Symptomatic search, which

searches a library of symptom patterns to match observed symptoms and associate system states with the identified symptom patterns. In the event of ambiguity more observations are collected to resolve it. However, the drawback is, it is more complicated requiring dynamic and failure simulations, more memory and memory management. On the other hand, a combined search strategy of the two may be to an advantage, where in, observed symptoms can be associated to causes and from hypothesized causes possible symptoms can be related.

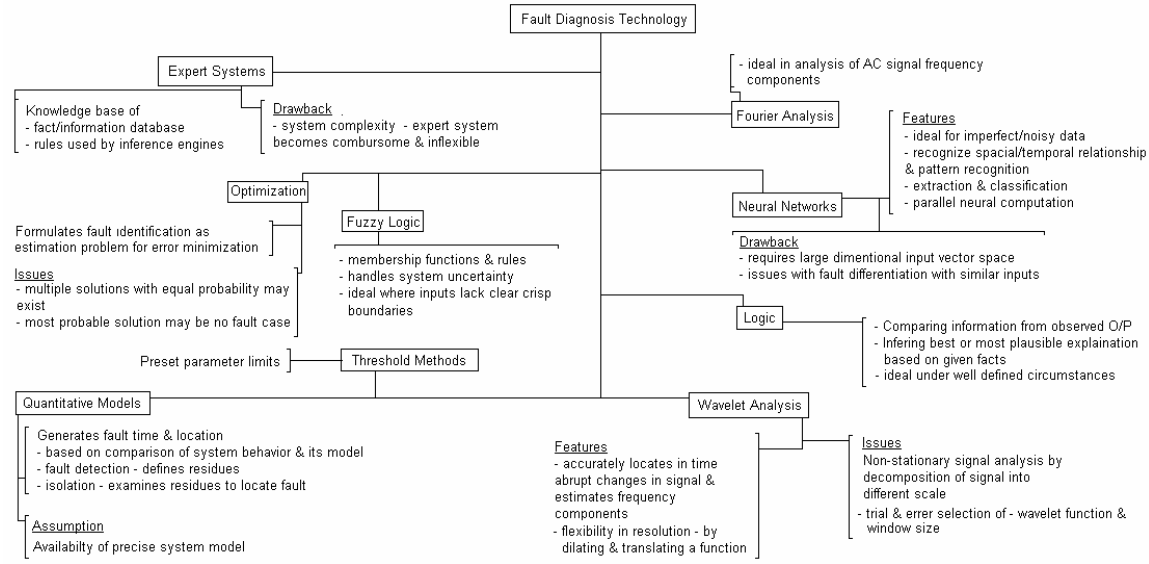

Fig 18. Fault Diagnosis Techniques

There have been many fault diagnosis techniques using expert systems, artificial neural networks (ANN), fuzzy logic and wavelets (Fig 18). Using expert systems in fault diagnosis involves the use of a knowledge-base consisting of a data base and rules [66] and [67]. The database involves facts and information about the system values, parameter characteristics and component interconnections details developed from reasoning methodologies of human experts, knowledge of normal working condition

obtained from steady state measurements and simulations, past experiences in fault diagnosis and statistical treatment of measurements. The rules in the knowledge-base are used by inference engines to diagnose the system condition from behavioral, functional and topological as well as even from circuit breaker status. However, depending on system complexity, expert system may become cumbersome and inflexible with little or no time to attend the fault without incurring catastrophic failure of the system under concern or cascading faults.

Neural Network based diagnosis involves modeling non-linear systems using training data offline or learn online with system knowledge [68] – [70]. With supervised training or leaning, error signal are fed back to alter the weights to reduce the errors in order to match the desired results. Alternatively, in unsupervised learning, prior fault classes are used to recognize new faults during system operation and, classifies the data and network so that it learns new faults and adapts them to similar faults that have already occurred, i.e. learned. However, it may prove to be extremely difficult and dangerous to acquire fault data from real system to train therefore in most cases model have to be used to generate training data and the efficiency of the training would depend on the quality of the training data set. Neural network may perform diagnosis either by generating residues and evaluating them or alternatively recognizing spatial, temporal relationship and performing pattern recognition including extraction and classification of faults. The main attributes of ANN are that it is ideal for fault diagnosis particularly when imperfect and/or noisy data is available and has the capability to learn, generalize and is capable of being fault tolerant. In addition, parallel neuron computation makes

ANN suitable for online environments. On the other hand, computationally intensive training time with unsupervised training, large dimensions of input vector space and issues with fault differentiation particularly when similar inputs belong to different faults are some of the shortcomings.

Fuzzy logic, a non-linear input/output mapping of a vector of features into scalar results involves creation of membership functions, application of rules, inferring from consequences of rules and resolving the output into a single number. It has the ability to handle imprecision of I/O variables by describing using linguistic variables making fuzzy logic ideal for handling system uncertainty and where inputs lack clear crisp boundaries. It has robustness to model uncertainty by ability to update empirical fits or maps with data previously not considered and robustness to data uncertainty due to nature of data acquisition [71].

Quantitative Model based fault diagnosis generates time and location of fault by comparing system behavior and its model. The fault diagnosis involves a two step process. First, fault detection phase where residues are defined and second, fault isolation phase wherein residues are examined to locate faults. However, the quantitative model is based on the assumption that precise system models are available, which unfortunately is not the case in most real systems.

Optimization based techniques look at fault identification as estimation problem that can be formulated as non-linear integer optimization problem treated as error minimization [72]. However, the main underlying issues are – in most cases the most probable solution may be a no fault case and multiple solutions with equal probability

may exist and need to be identified. Other method of fault diagnosis involves use of statistical method based on detecting faults on preset thresholds or using logic and abduction based on inferring best or most plausible explanation for given set of facts that involves comparing information from observed output and understanding the system that produces those outputs [73].

Wavelet analysis is yet another technique used in fault detection and diagnosis [74]. It primarily is a mathematical tool analyzing non-stationary signal by decomposing them into different scales that allows to accurately locate in time all abrupt changes in signal and estimate their frequency components if desired. In addition, it offers flexibility in the level of resolution by dilating and translating a function and the multi-resolution enable it to zoom into particular details of the signal of interest. The main issues are that it is computationally intensive with high computation time, the choice of optimal wavelet function and window size is by trial and error and it is most suitable for post fault analysis on captured waveform.

3.2 Fault Analysis in Cascaded Multiconverter Systems

Figure 19 shows the circuit diagram of the cascaded converter where C = Output Capacitor, L = Inductor with subscript 1 and 2 for load and source converter respectively. The voltage (V_{source} and V_{load}) and current sensors (I_{source} and I_{load}) placed at the output of each individual converter for their control, are also used for monitoring and detecting a fault. The cascaded topology of Fig. 19 has four legitimate modes of operation (under no fault) which are shown in Fig. 20a - d. Figure 20e and 20f present the intermediate topological states specific to diode open circuit faults and switch open

circuit fault scenarios while Fig. 20g and 20h show intermediate state in diode short circuit fault that are illegitimate modes of operation. The analysis performed here is limited to continuous conduction mode.

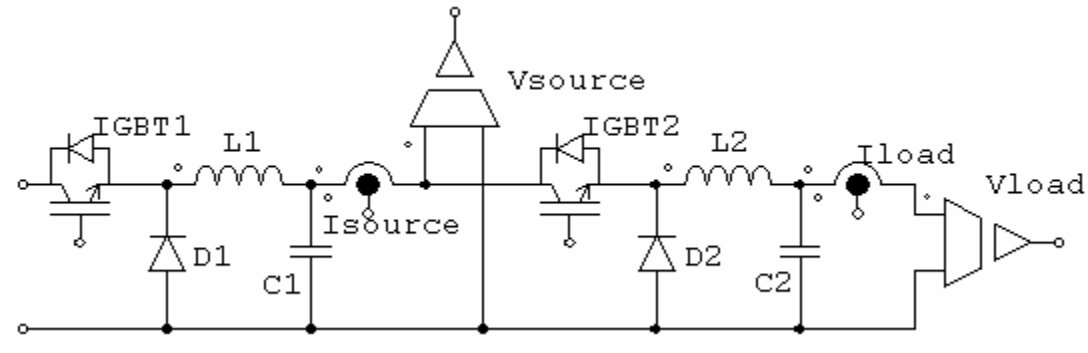

Fig 19. Circuit Layout of Cascaded Converter with Sensors

In Fig. 20a, the operation of two cascaded converters with the load converter switch off ($IGBT2$) with the diode ($D2$) completing the output circuit is shown. Figure 20c illustrates a topological state with both source and load converter switches ($IGBT1$ and $IGBT2$ respectively) in the on state. Fig. 20e and 20f although a legitimate operating mode with only source converter in operation is not a valid intermediate state under cascaded mode of operation.

Figure 21a – c present a short circuit fault on the 14V Bus. The bus fault may occur at any instant shown in Fig. 21a – c, however a fault when either $IGBT1$ or $IGBT2$ is off (Fig. 21c or Fig. 21a respectively) would finally lead to switching between states in Fig. 21b and 21c. 42V Bus short circuit fault is given in Fig. 21d – f. A fault under state shown in Fig. 21d would cycle through state in Fig. 21e discharging the load converter inductor $L2$ and the state in Fig. 21f, and leaves the load converter disconnected.

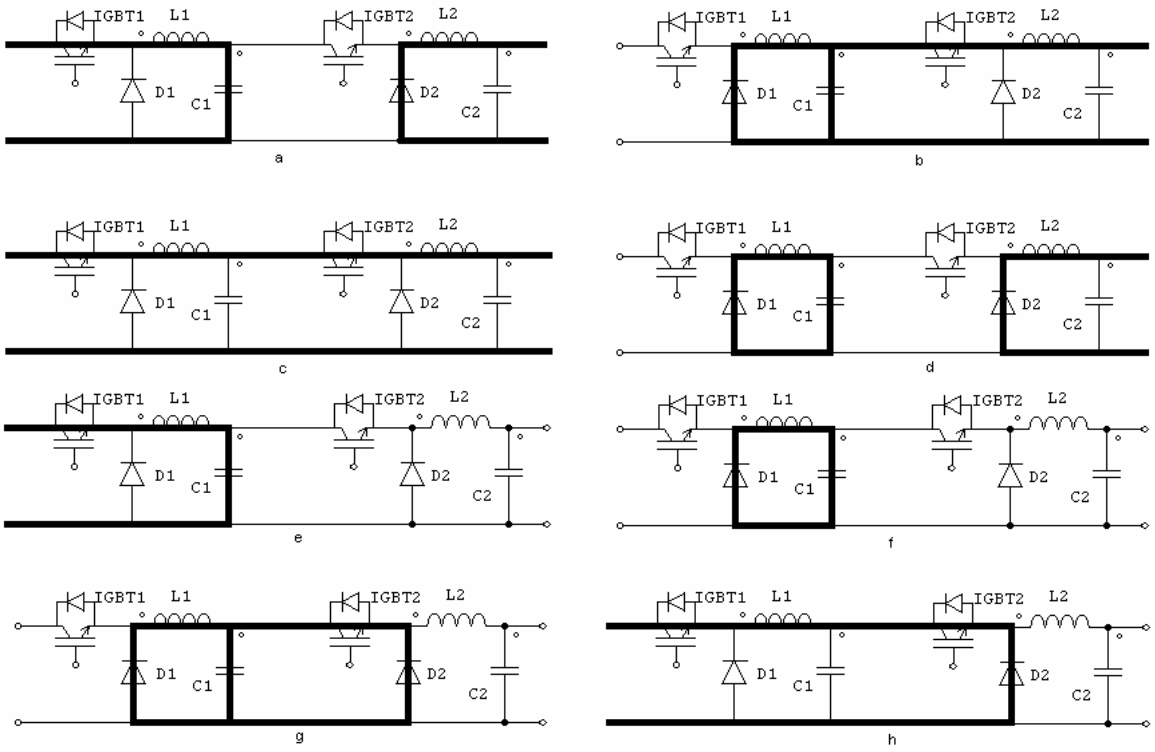

Fig 20. Operational States of Cascaded Multiconverter System

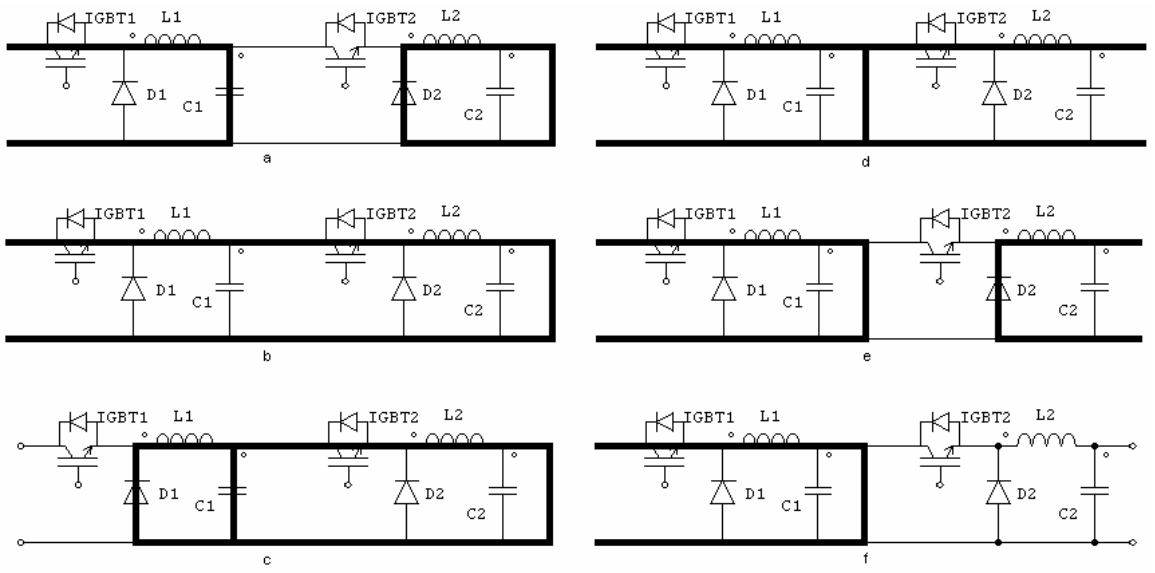

Fig 21. Topological States on 14V and 42V Bus Short Circuit Faults

It is observed from Fig. 22 that when the diode ($D2$) open circuit fault occurs, there is a sudden dip in the I_{load} and V_{load} as it is in state shown in Fig. 20e or Fig. 20f. Plot variables are identified as, V_{source} = Source Converter Output Voltage (V), I_{source} = Source Converter Output Current (A), V_{load} = Load Converter Output Voltage (V), I_{load} = Load Converter Output Current (A). Upon fault V_{load} momentarily drops to 5 V followed by a sustained 71% ripple in the load converter output voltage (V_{load}). Since a pure resistive load of 1Ohm has been considered at the load converter output, the voltage and the current have almost identical waveforms. In addition, the average input current at the input of the load converter or the output current of the source converter (V_{source}) has increased (from 5 Amp to approximately 10 Amp) and so has the current ripple. This is primarily due to freewheeling of the load converter current through the diode ($D1$) in the source converter Fig. 20b. The voltage waveform of the source converter (V_{source}) indicates some instability. Thus the load converter switches in and out of the healthy topological state Fig. 20b and 20c by cycling through state shown in Fig. 20b, 20c, 20e and 20f.

A 14V DC bus short circuit pulls down the 14V bus voltage (V_{load}) while the 42V bus undergoes a short circuit via 14V bus when the load converter switch is turned on each time Fig. 21b and 6. Thus, V_{source} is unstable and fluctuate between zero and 95V at a frequency of 540 Hz with an average output voltage of 46V, a 9.5% increase in nominal voltage. The large spike observed in the output current (I_{load}) of the load converter is because the load converter inductor was fully charged towards the end of its

charging cycle when the 14V Bus short circuit fault occurred. This spike occurs within 20 microsecond of bus fault and has a magnitude of 450A that can damage any connected load. This is not observed when the bus short circuit fault takes place when the inductor is in the discharge cycle. The load and the source converter output currents increase to extremely large values that will damage both converters. This is illustrated in Fig. 23.

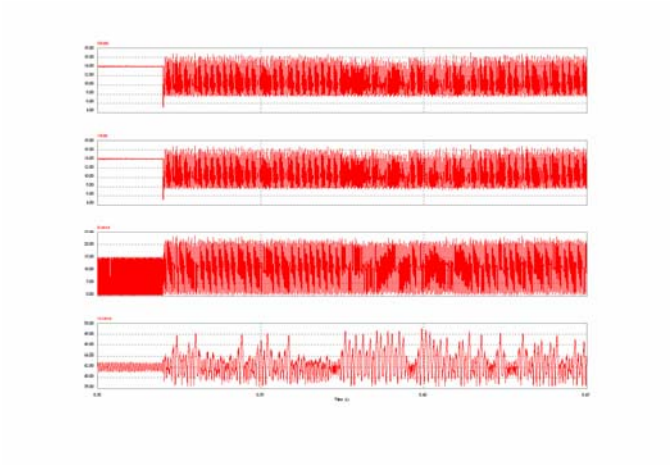

Fig 22. Diode Open Circuit Fault in Load Converter

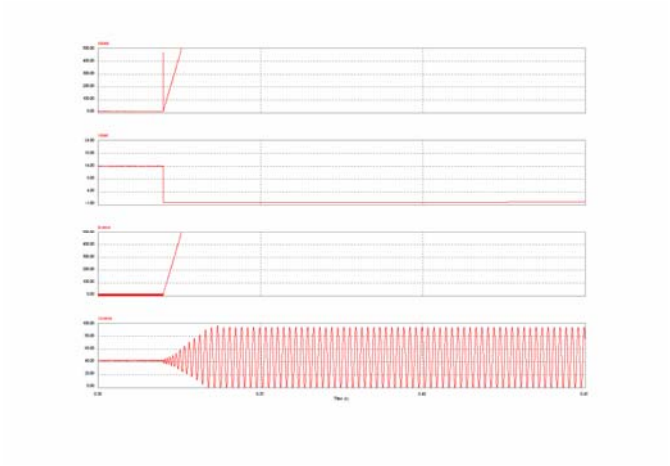

Fig 23. 14V DC Bus Short Circuit Fault

From observations in Fig. 23 it is anticipated that a cascaded fault would occur with the load converter switch short circuit ($IGBT2$) following the 14V DC bus short circuit. However, since the load converter is a current intensive system as compared to the source converter, the switch and diode current ratings of former would be higher. Upon Bus fault, $IGBT2$ remains on continuously however the source converter switch ($IGBT1$) and diode ($D1$) continue operating with a duty cycle in an attempt to maintain the required 42V output. When $IGBT1$ turns off, diode $D1$ conduct and freewheels the fault current in the load converter Fig. 21c. Since $D1$ has lower current rating, it would get short circuited. This would short the 300V DC bus when $IGBT1$ turns on the first time after the diode ($D1$) short circuit and the load converter would be disconnected from the cascaded system without any damage.

3.3 Analytical Representation of Faults in Converters

The transmission matrix as a frequency domain representation directly presents the effect of the input on the output or vice-versa. Thus the matrix gives the system characteristic information of how each port parameter influences other parameters. This matrix largely draws on the system configuration and its component values. Thus, any change in either is likely to reflect in the transmission matrix and hence how the port parameters would affect each other.

The transmission matrix of a DC-DC buck load converter under normal operating conditions is presented in parametric form in (10) defined by C = Output Capacitor, L = Inductor, d = duty cycle, $v_{out}(s)$ = converter output voltage, $i_{out}(s)$ = converter output current, $v_{in}(s)$ = converter input voltage and $i_{in}(s)$ = converter input

current. $v_{out}(s)$ and $i_{out}(s)$ are the system output port parameter and $v_{in}(s)$ and $i_{in}(s)$ are the system input parameters. The effect of the input voltage on the output voltage can be seen to be related by the duty cycle. In addition, the input current is also found to affect the output voltage depending on the value of the control parameter d (duty cycle) and component parameter L (inductor). Similar observation can be made for the dependence of output current on input voltage by output capacitor, C and duty cycle and the effect due to input current by L, C and d. The later is also observed to be a second order dependence.

$$\begin{bmatrix} v_{out}(s) \\ i_{out}(s) \end{bmatrix} = \begin{bmatrix} d & -\dfrac{sL}{d} \\ sCd & -\left(\dfrac{1+s^2LC}{d}\right) \end{bmatrix} \begin{bmatrix} v_{in}(s) \\ i_{in}(s) \end{bmatrix} \tag{10}$$

In the event of a diode open circuit fault the transmission matrix takes the form of (11). The large voltage spikes that occur when the switch is open and so is the diode (due to diode open circuit fault) and the inductor is energized appear in the transmission matrix as an additional term x. The x term (a function of inductor current) represents the effect of the large negative di/dt of the inductor when the switch and the diode are both open (which results in significant voltage spikes across the inductor). From the matrix it is also observed that the output voltage and current relationship to the input voltage are not affected and remains the same as in the normally operating converter. However, the input current distinctively impacts the output voltage and current.

In the case of diode short circuit and switch open circuit, the transmission matrices are the same but are different from the normal converter transmission matrix.

In the former transmission matrices the output voltage and current do not relate to the input voltage indicating that no output would be obtained from the load converter (12).

$$\begin{bmatrix} v_{out}(s) \\ i_{out}(s) \end{bmatrix} = \begin{bmatrix} d & -\left[\frac{sL+x}{d}\right] \\ sCd & -\left[\frac{1+sC(sL+x)}{d}\right] \end{bmatrix} \begin{bmatrix} v_{in}(s) \\ i_{in}(s) \end{bmatrix} \tag{11}$$

$$\begin{bmatrix} v_{out}(s) \\ i_{out}(s) \end{bmatrix} = \begin{bmatrix} 0 & -\frac{sL}{d} \\ 0 & -\left(\frac{1+s^2LC}{d}\right) \end{bmatrix} \begin{bmatrix} v_{in}(s) \\ i_{in}(s) \end{bmatrix} \tag{12}$$

Extending the analysis for the entire multistage system, it is found that the form of the transmission matrix may not always represent the complete information, in this case, the presence of fault. Here again the subscript 1 and 2 indicate the source converter (300/42 DC-DC Buck Converter) and load converter (42/14 V DC-DC Buck Converter) parameters respectively. The representation below relate the output voltage (V_3) and output current (I_3) of load converter to the input voltage (V_1) and input current (I_1) of source converter.

Analyzing the diode open circuit fault in an overall cascaded system, it is observed from (13) that output voltage (V_3) of the load converter is still related to the input voltage (V_1) of the source converter by the same relation as two normally operating cascaded converters but have an additional term of $d_1(sXC_1)/d_2$ that projects

the voltage spike of V_3 due to the large negative di/dt on diode open circuit. This also impacts the output current (I_3) of load converter.

The cascaded Transmission Matrix with diode short circuited/switch open circuited (14), indicates a reduced voltage at the output of the load converter (V_3) as the element $d_1 d_2$ is eliminated in the relation between V_3 and V_1. However, it does not project distinctively that V_3 is zero. In addition, such cascaded final representations do not indicate the effect on V_2 and I_2 parameters which could have given distinctive indication of a fault.

Analysis of the average model indicates that the system state matrix remains the same under all fault conditions except in the diode open circuit case where the term x appears (10). However, each fault influences the input matrix. An example for the diode short circuit/switch open circuit case is given in (15).

$$\begin{bmatrix} V_3 \\ I_3 \end{bmatrix} = \begin{bmatrix} d_1\left[d_2 + \frac{1}{d_2}\left[s^2 C_1 L_2 + sXC_1\right]\right] & -\frac{1}{d_1}\begin{bmatrix} s\left(L_1 d_2 + \frac{L_2}{d_2}\right) \\ +\frac{1}{d_2}\left[X + s^2 X L_1 C_1\right] \end{bmatrix} \\ d_1\begin{bmatrix} sC_2 d_2 \\ -\frac{1}{d_2}\left[s^3 C_1 C_2 L_2 + s^2 C_1 C_2 X + 1\right] \end{bmatrix} & \frac{1}{d_1}\begin{bmatrix} -s^2 L_1 C_2 d_2 \\ +\frac{1}{d_2}\begin{bmatrix} s^4 L_1 L_2 C_1 C_2 + s^3 L_1 C_1 C_2 \\ +s^2\left[L_1 C_1 + L_2 C_2\right] \\ +sX + 1 \end{bmatrix} \end{bmatrix} \end{bmatrix} \begin{bmatrix} V_1 \\ I_1 \end{bmatrix} \quad (13)$$

$$\begin{bmatrix} V_3 \\ I_3 \end{bmatrix} = \begin{bmatrix} \dfrac{s^2 C_1 L_2 d_1}{d_2} & -\dfrac{sL_2 + s^3 L_1 L_2 C_1}{d_1 d_2} \\ \left[\dfrac{sC_1 + s^3 C_1 C_2 L_2}{d_2}\right] d_1 & \dfrac{1}{d_1 d_2}\left[1 + s^2\left[L_1 C_1 + L_2 C_2\right] + s^4 L_1 L_2 C_1 C_2\right] \end{bmatrix} \begin{bmatrix} V_1 \\ I_1 \end{bmatrix} \tag{14}$$

$$\begin{bmatrix} \dot{i}_L \\ \dot{v}_{out} \end{bmatrix} = \begin{bmatrix} 0 & -\dfrac{1}{L} \\ \dfrac{1}{C} & -\dfrac{1}{RC} \end{bmatrix} \begin{bmatrix} i_L \\ v_{out} \end{bmatrix} + \begin{bmatrix} 0 \\ 0 \end{bmatrix} V_{in} \tag{15}$$

CHAPTER 4

FAULT DIAGNOSIS

The proposed technique for detection of faults involves the use of statistical moments of higher orders to detect and identify a failure. This utilizes the existing current and voltage sensors (port parameters) of the cascaded system without the need for any additional sensors. The technique not only detects system malfunction, but provides information on the device under fault and the nature of the fault.

Analysis indicate third-order statistical moments are effective as they dynamically evaluate and monitor system deviations (voltages, currents) from normal operations and direction of the deviations enable to detect and diagnose fault fast enough to prevent escalation. Thus idea behind the techniques is to detect, identify and act quickly on a single device failure to prevent escalation of the fault that would otherwise occur if the controller continued to operate without the knowledge of the fault situation. In addition, failure mode information derived from the system is essential for isolation of fault/reconfiguration of safety critical systems such as in Hybrid Electric Vehicle Power System to ensure sustainable operation and safety.

4.1 Circuit Description

The circuit diagram of the cascaded converter of Fig. 1 has the circuit parameters given in Table 1. The subscript 1 and 2 is used to identify the source and load converter components respectively. Each converter is rated for 200W with the output voltage regulated by PWM (Pulse Width Modulated) signal using conventional PI control. The switching frequency of each converter is 20 kHz. The voltage (V_{source} and V_{load}) and current sensors (I_{source} and I_{load}) placed at the output of each individual converter providing feedback for their control, are also used for monitoring and detecting a fault. An eZdsp TMS320F2812 series digital signal processor (DSP) is used for signal acquisition (at 50 kHz) and control. The high computational speed of 150 MIPS (Million Instructions per Second) of TMS320F2812 leverages the ability to perform on chip monitoring, detection and diagnosis computation.

TABLE 1. Converter Parameters

S. No.	Description	Source Converter Parameter	Load Converter Parameter	Units
1	Input/Output Rated Voltage	300 / 42	42 / 14	VDC
2	Rated/Peak Output Current	5.25 / 9.5	14 / 20	A
3	Switching Frequency	20	20	kHz
4	Inductance	1.0 (L1)	0.5 (L2)	mH
5	Output Capacitor	600.0 (C1)	100.0 (C2)	uF
6	Gain	0.1944	0.07502	const
7	Time Constant	0.002	0.00022	sec

4.2 Monitoring and Fault Diagnosis

The measured output voltage and current at the source and load converters are continuously monitored to detect an abnormality. Using statistical moments of sampled window of continuously measured voltage and current enables one to detect a fault within the failure withstand time of the power devices or the cascading fault events. Differentiation of the fault is achieved by the third moment of measured signal that provides information on the direction of the variation of the measured signal. The general expression for the n-th order moment (s^n) is given in (16), wherein, the mean of the moving sampled window measures (M) is compared with the current measure (y) of a defined sample window size of N. The third statistical moments of the measured signals that offers complete diagnosis information and is less computationally intensive that higher order is selected and are represented by flv, flc, fsv and fsc for load voltage, load current, source voltage and source current respectively.

$$s^n = \frac{\sum_{k=1}^{N} (y_k - M)^n}{N-1} \tag{16}$$

Table 2 maps the possible conditions of device firing signals and third moment of measured signals. When the cascaded load converter is unfaulted, the system maps to the No Fault. Deviation to any other block other than the ‘No Fault’, will cause a fault detect flag to be set and will identify the fault type.

The above faults may be represented as a cross-variance matrix of third order statistical moments of system parameters (17). To simplify the representation, a

common sample window size (N) is taken for all the system parameters (voltage and currents). It is observed that certain elements in the matrix distinctively project a presence of a fault along with the type of fault. Other elements in the matrix that do not project a distinct relation to a fault are ignored and are not shown in the matrix.

TABLE 2. Fault Detect Status Table

Gate Signal		flv	flc	fsv	fsc	Fault	Fig*
T_{IGBT1}	T_{IGBT2}						
x	x	~ 0	~ 0	~ 0	~ 0	No Fault	a/b/c/d
x	1	< 0	> 0	-	-	14V Bus sc	4a/4b/4c
x	0	> 0	-	-	-	IGBT2 sc	b/c
x	1	< 0	-	>= 0	-	IGBT2 oc	a/d
x	1	< 0	-	< 0	-	D2 sc / 42V Bus sc	g/h/4d/4e/4f
x	0	-	-	< 0	> 0	42V Bus sc	4d/4e/4f
x	x	> 0 / < 0	dc > 0			D2 oc	e/f

* Refers to Fig 3 unless noted.

x – Don't care
dc – second moment of load converter duty cycle
1 – Device On
0 – Device Off

$$V^3 = \frac{1}{N-1}\sum_{t=1}^{N}\begin{bmatrix} (x_{1t}-\overline{x_1})^3 & (x_{1t}-\overline{x_1})^1(x_{2t}-\overline{x_2})^2 & (x_{1t}-\overline{x_1})^1(x_{3t}-\overline{x_3})^2 & - \\ - & - & - & - \\ (x_{3t}-\overline{x_3})^1(x_{1t}-\overline{x_1})^2 & - & - & (x_{3t}-\overline{x_3})^1(x_{4t}-\overline{x_4})^2 \\ - & - & (x_{4t}-\overline{x_4})^1(x_{3t}-\overline{x_3})^2 & - \end{bmatrix} \quad (17)$$

X_1 - flv (Load Converter Output Voltage - Vload)
X_2 - flc (Load Converter Output Current - Iload)
X_3 – fsv (Source Converter Output Voltage - Vsource)
X_4 – fsc (Source Converter Output Current - Isource)
$X_t = (x_{1t}, x_{2t}, x_{3t}, x_{4t})^T$ - Vector denoting t = 1, 2, 3… N observation for time series of X_1, X_2, X_3, X_4 vectors

Element (1, 1) in (17) is the third moment of the load converter output voltage (V_{load}) or X_1 when positive indicates a presence of an $IGBT2$ short circuit fault in the load converter. This coincides with $IGBT2$ short circuit fault noted in Table 2. $(x_{1t} - \overline{x_1})^1 (x_{2t} - \overline{x_2})^2$, element (1, 2) is a cross-variance between load converter output voltage (V_{load}) or X_1 and load converter output current (I_{load}) or X_2, which project a 14V bus short circuit fault while, element (1, 3), $(x_{1t} - \overline{x_1})^1 (x_{3t} - \overline{x_3})^2$ a cross-variance between load converter output voltage (V_{load}) or X_1 and source converter output voltage (V_{source}) or X_3, indicates $IGBT2$ open circuit fault. Similarly, element (3, 1) indicates load converter diode short circuit fault while (4, 3) indicates 42V bus short circuit. The 3rd order cross-variance matrix in (17) can be generalized to an nth order. In addition, inclusion of input parameters (voltage and current) of the converters would shed more light into fault diagnosis from the cross-variance matrix.

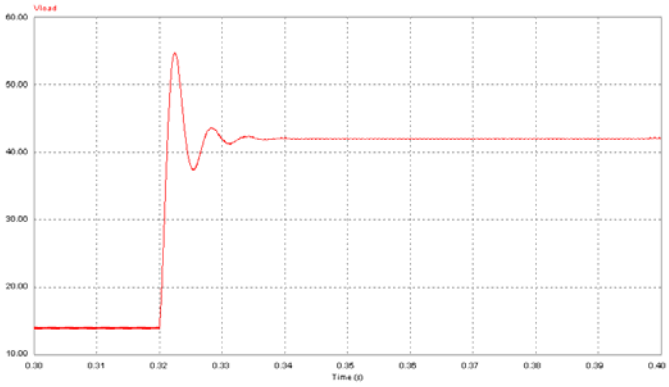

Fig 24. Simulated IGBT2 Short Circuit in Load Converter when Operating under Steady State

Consider the case of switch short circuit fault ($IGBT2$) of Load Converter which results in two possible states as shown in Fig. 20b and 20c depending on the

topology prior to the occurrence of fault. Fig. 20b and 20c are legitimate operating states under normal switch ($IGBT2$) operation when it can be turned on/off by gating signal and can change over to the next state Fig. 20a or Fig. 20d. From Table 1 it is observed that flv > 0 and T_{IGBT2} = 0 (gating signal off) triggers fault detect flag and identifies an $IGBT2$ device short circuit. To conduct the fault test an 8 Ohm output load resistance at the 14V bus was used to safely limit fault current to a value of approx 5.25 A as against 14 A under rated and 42A under fault conditions. In addition all semiconductor switches have been overrated for fault analysis. Figure 24 shows the switch ($IGBT2$) short circuit fault in load converter that occurs at a run of 0.32 seconds when the cascaded system is operating in steady state. Figure 25a shows the measured output voltage for $IGBT2$ short circuit fault and Fig. 25b is the zoomed view of the fault instant. From Fig. 25b it is observed that upon $IGBT2$ short circuit fault 42V appears at the 14V bus in 2 msec. The corresponding flv signal on fault is shown in Fig. 26 and 27 for the simulated and measured case respectively. It is observed that an $IGBT2$ fault is detected in 400 microseconds in both cases, the time within which bus voltage increased to only 20V, a 43% increase compared to 200% if 42V appeared that may damage most of 14V loads.

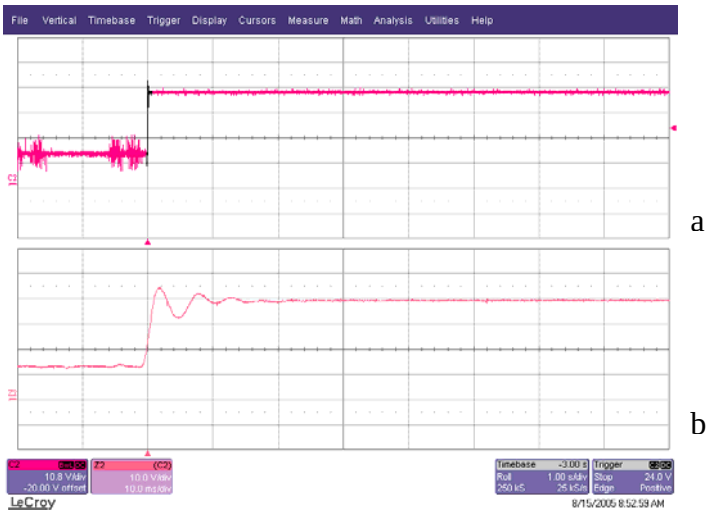

Fig 25. Measured IGBT2 Short Circuit in Load Converter when Operating under Steady State, (a). 14V Bus Voltage Waveform (b). Zoomed Projection of the Fault Point

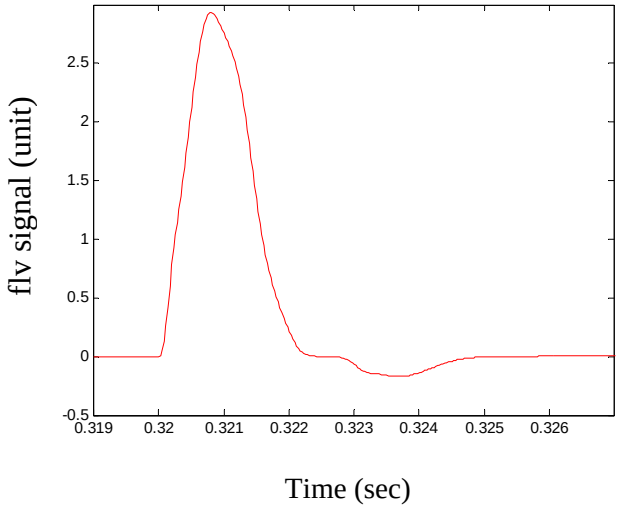

Fig 26. Third Moment of Simulated Load O/P Voltage (flv signal) Detects Switch (IGBT2) Short Circuit Fault in the Load Converter in 400 Microseconds

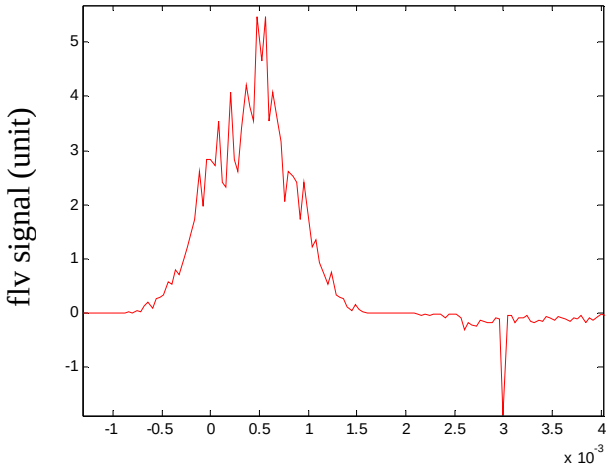

Fig 27. Third Moment of Measured Load O/P Voltage (flv signal) Detects Switch (IGBT2) Short Circuit Fault in the Load Converter in 400 Microseconds

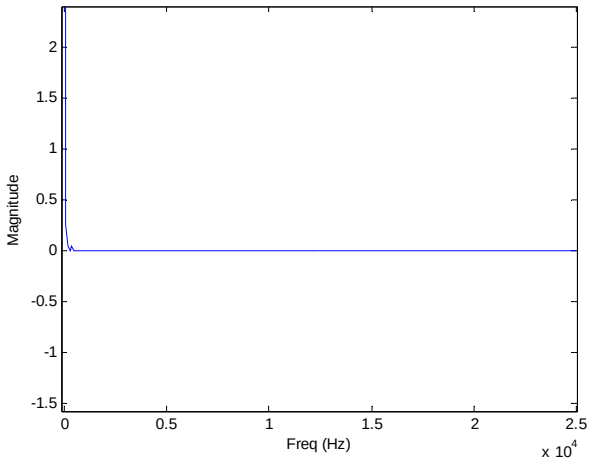

Fig 28. FFT Plot for IGBT2 Short Circuit Fault

A Fast Fourier Transform (FFT) of the IGBT2 short circuit fault does not project any frequency components other than the DC component that is present under steady state operating condition in the cascaded DC/DC system Fig 28. An alternative analysis tool such as the Wavelets that enables detecting trends, breakpoints,

discontinuities in non-stationary waveform is considered. The Daubechies Wavelet db4 detects sudden changes/discontinuity in waveforms and suggest the presence of high frequency information is used for fault diagnosis on IGBT2 short circuit fault Fig 29. Fig 29 shows that db4 was able to detect a malfunction or fault but does not project the direction of deviation or how the 14V bus voltage is changing that is required for diagnosing an IGBT2 short circuit fault.

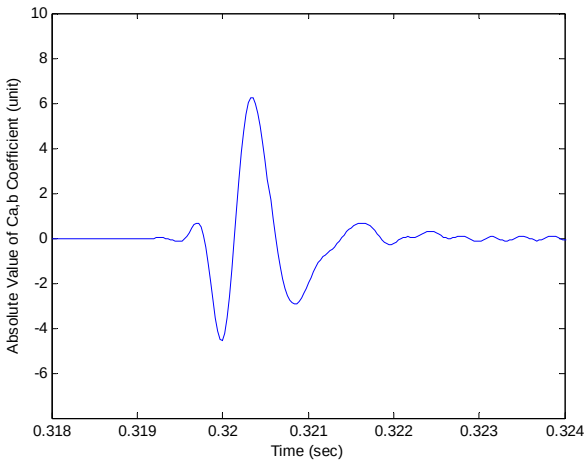

Fig 29. Wavelet db4 Detects Sudden Change/Discontinuity in Load Converter O/P Voltage on IGBT2 Short Circuit Fault

The 14V DC bus short circuit fault analyzed in Fig 23 is again considered here but with a load of 8 Ohms at the load converter output. Upon a short circuit fault the change in the 14V DC bus voltage and current are shown in Fig 30 and Fig 31. No current limit is set on the load converter however; the current at the input side is limited to 10A to safely conduct the test. This is done in order to present how fast the effect of the short-circuit fault is. It is observed that the fault current increases to 10 A in approximately 300 microseconds and then overshoots to a maximum of 64A before

being limited to 10A by the system at the input size of the converter. The current although exceed the device (IGBT2) rated current of 50A, it is still within the short circuit current failure limit of 100A. The device short-circuit withstand time is approximately 1msec for IGBT2. Further, upon bus short-circuit the 14V bus voltage falls much faster compared to rate of rise of current due to the presence of a large inductor at the output of the load converter Fig 30 and 31. The fault signals – third moment of load converter O/P (output) voltage (flv) and current (flc) are plotted in Fig 32 and 33 respectively. Both flv and flc together identify the presence of a 14V DC Bus short circuit fault in approximately 1.5 milliseconds. A comparison of Fig 27 and 32 indicate that the third moment of the load converter O/P (output) voltage (flv) provides an insight into how the output voltage is varying and the use of the flc in Fig 33 differentiates the 14V Bus short circuit fault from IGBT2 open circuit or D2 short circuit fault as in Table 2.

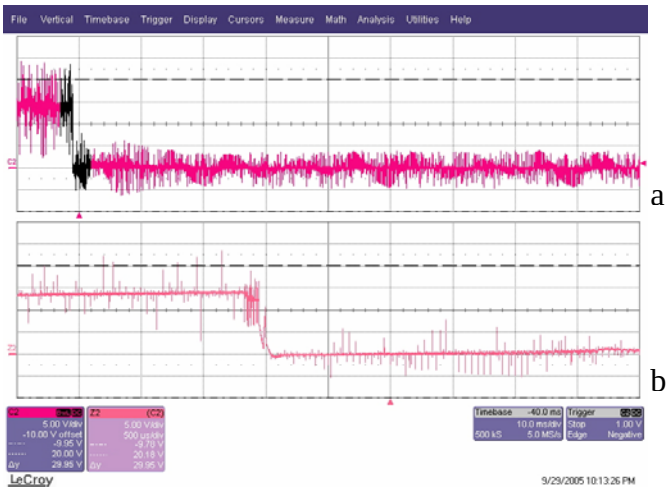

Fig 30. Measured 14V DC Bus Short Circuit Fault when Operating under Steady State, (a). 14V Bus Voltage Waveform (b). Zoomed Projection of the Fault Point

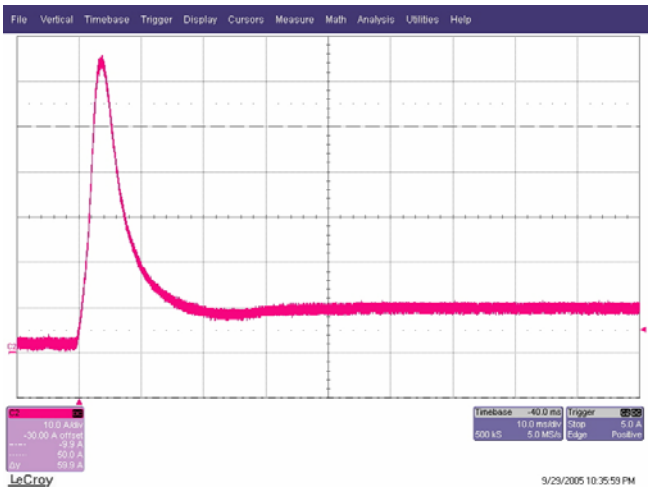

Fig 31. Measured 14V DC Bus Short Circuit Fault under Steady State Operation - 14V Bus Current Waveform

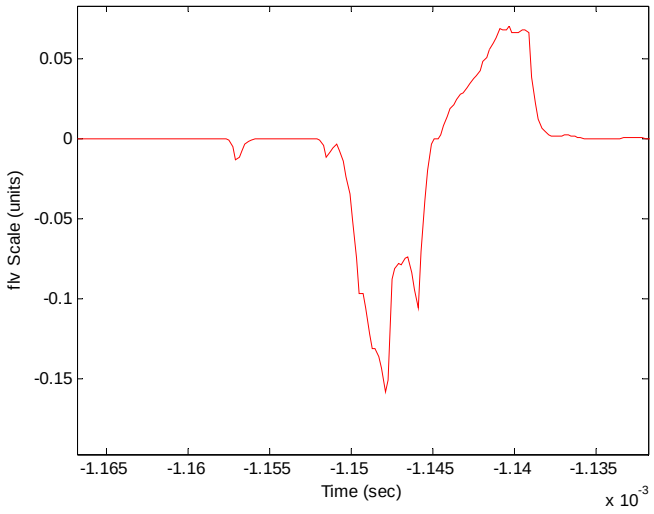

Fig 32. Third Moment of Measured Load O/P Voltage (flv signal) Detects a possible 14V DC Bus Short Circuit Fault in 10 Microseconds

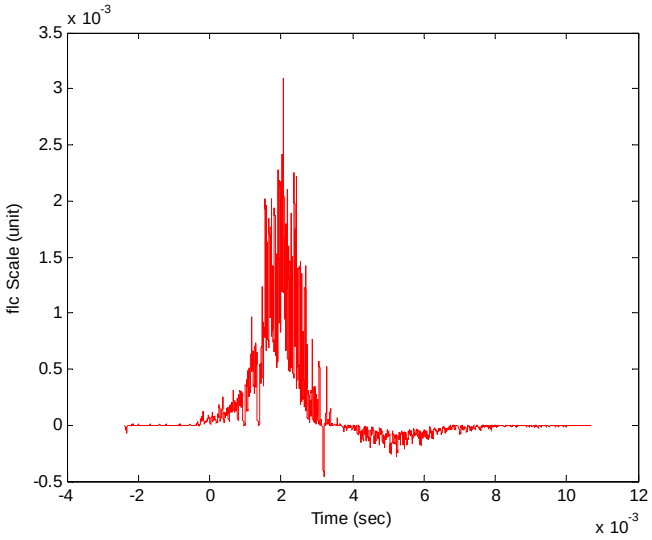

Fig 33. Third Moment of Measured Load O/P Current (flc signal) Detects a 14V DC Bus Short Circuit Fault in 1.5 Milliseconds

CHAPTER 5

NAVAL SHIPBOARD POWER SYSTEMS

Currently, different shipboard power systems for next generation naval vessels are being investigated. The DC zonal distribution system has gained significant interest. In replacing the current AC radial distribution system, substantial gains in terms of survivability, enhanced fight-through capability with fewer component count and reduced cost of ownership can be achieved. However, the system calls for a large interconnected multi-converter environment of tightly regulated power converter with large control bandwidth in a stiff network that may lead to unwanted system resonance. Further, the challenge of contingency management to restore failing systems within acceptable casualty recovery time and prevent cascading of faults under battle damage requires incorporating fault detection, failure assessment and restoration strategies into PMS (Platform Management System) automation systems for survivability and effective Resource Management.

Traditionally, segregate power system architecture was used in ships and submarines that served different electrical loads by independent generator sets. This resulted in locking up nearly 80% of the total power for propulsion alone. The concept of Integrated Power System (IPS) architecture allows all the loads to be supplied by a

common electrical power bus. This enables handling of loads and generation sources more optimally and efficiently, and is able to direct power to vital loads on demand. In distribution, there is an increasing interest in zonal architecture compared to ring or radial type for increased accessibility to sources and loads that it offers. A key design element for distribution should be to provide alternative path to critical service loads such as propulsion drives and to be able to seamlessly transfer power under fault conditions. With loads connected to DC buses, care in design and analysis of power system is required due to increased dynamics and probable instability. However, it proves to be a more compelling technology for enhanced fault management and casualty management for survivability.

5.1 Status of Naval Shipboard Power System

5.1.1 Segregate and Integrated Power System

Traditionally, segregate power system architecture used in ships and submarines served different electrical loads by independent generator sets. This involved use of multiple generators units with none operated at full load. From survivability point, the closer the load to source, the higher the survivability. Such collocated system is efficient from survivability perspective that the vital system would never outlive the service that it provides [75].

In integrated power system all service and propulsion loads are supplied by a common electrical bus. The high power propulsion loads are 20MW (megawatt), low-speed 0–220rpm motor drive systems. From a naval architectural perspective, electric drive offers reduced number of prime movers, no direct mechanical coupling, variable

speed control for enhanced maneuverability and simplified propulsion reversal, reduced ship signature and, operational and maintenance cost. The IPS projects substantial reduction in ship acquisition cost, and in comparison to similar mechanical drives, may reduce fuel cost and manning by approximately 24% and 13% respectively [76].

The IPS may have several architectures. The propulsion motors may be driven directly by multiphase ac cables and drive system from synchronous generator or alternatives from DC distribution bus. Currently, cycloconverters and current-source inverters are used for propulsion drive systems. PWM (Pulse-Width Modulated) voltage-source inverter drives using IGBT (Insulated Gate Bipolar Transistor) and MCT (MOS controlled thyristor) limited in power rating to about 2MW may either need to be stacked or alternative new topologies of multi-level converters are required to achieve 20MW propulsion demands.

5.1.2 Radial and Zonal Power System

Radial power systems employed in naval ships such as surface combat have multiple generation units (3–4 generators) operated in split/parallel configuration and connected to a number of switchboard panels. The 450V, 60Hz three-phase AC is distributed throughout the ship to all loads. The electrical service loads aboard these surface combat ships are in the order of 3.5MW at normal cruising and around 4MW at full combat cruising. However, with new load being added, electrical load requirements may extend to 5MW. With each load classified as vital and non-vital loads, during loss of generation capacity, load shedding can be initiated to disconnect non-vital loads from the network. Intelligent power management can ensure additional generators are not

brought into service to supply momentary increase in demand. A large number of transformers are used to supply 115V and other voltage levels. The primary and secondary of these transformers are both delta resulting in no current path from power line to ship hull. This floating delta increases survivability under single-phase fault to hull, by not allowing large currents to flow into the hull as there is no complete low impedance path. In addition, casualty resulting in open circuit of a single line, balanced power can still be supplied with reduced capacity.

The zonal power system employs starboard and port bus, and sections the ship into number of electrical zones [77]-[78]. These buses are passed through watertight bulkhead and placed to maximize distance between them, and in turn maximize survivability of one of the buses during casualty. Thus, one bus may be located above the water line and one below or both buses maybe placed along the ship centerline displaced by several decks. This architecture maximizes protection from battle damage near the skin of the ship. However, this would only be feasible for large class ships.

In zonal system, the zonal loads are connected to both buses through load centers. With only the main buses passing through each zone, a large number of switchboard feeder cables are eliminated resulting in a substantial reduction in cable cost and weight. The zonal architecture may thus substantially reduce material and labor cost in ships.

5.1.3 AC and DC Zonal Distribution System

The AC zonal distribution involves synchronizing bus and generators, and paralleling controls, two 60Hz primary buses, delta-delta transformers, load centers and

ac switchgear. Alternative architecture employing DC distribution involves rectifying generator voltage to 1200–2000VDC and distributing DC power along the port and starboard buses Fig 4. Each bus is connected to the electrical zone via a power converter (Ship Service Converter Module - SSCM) that serves to buffer main bus and intra-zonal loads. In addition, the converter lowers the main bus voltage to commensurate with the zonal loads, such as DC-AC inverter (Ship Service Inverter Module - SSIM) requirements of 850-950VDC. The zonal inverters provide the necessary single/three phase power requirements to the zone. Parallel converters may be used to gain the required power levels and system redundancy.

Resonant Converter are being increasing considered in service modules to minimize losses and facilitate higher switching frequencies, which in turn would reduce airborne audible noise, maximize control bandwidth and minimize filtering requirements. Converter modules are anticipated to extend across multiple ship platforms reducing ship acquisition costs.

The DC distribution offers several advantages [77]. The solid-state SSCM and SSIM are multifunctional. They can perform power conversion, monitoring and current limiting through semiconductor devices and suitably protecting the system during fault conditions by running fault diagnosis routine in main control loop of the converter. The DC zonal electrical system facilitates isolating faults to a zone. Since inputs to the converters are DC currents, current sensors and techniques required to detect fault is easier and faster. As a result, time lag associated with detecting AC fault and initiating Automatic Bus Transfer (ABT) is nearly eliminated and integrity of power to vital loads

is maintained. Thus, the architecture provides survivability to sources through redundancy and separation, and ensures sustainable power supply to service loads by survivability of pathway because of multiple reconfigurable paths available. The availability of DC distribution enable operation of variable speed motors for many applications such as pumps within a zone and to be operated at highest efficiency. In addition, the substantial inrush currents experienced when starting large motors may be limited aiding in maintaining a stable bus voltage.

The DC distribution reduces number of power conversion stage required for 400Hz loads at different voltages for combat systems. It eliminates need for distribution transformers, ac switchgears, intermediate 60Hz power stage thereby reducing weight, size and cost of the system. Further, the DC zonal distribution decouples generator frequency from distribution requirements. Thus, generator and rectifier requirements can be optimized for size and cost. In addition, prime mover design may be optimized for most efficiency speed making efficient use of fuel and reducing emission.

The disadvantage of DC distribution is the main bus voltage level currently limited to 1500 to 2000V due to the voltage rating of the IGBT and MCT semiconductors in SSCM and SSIM. A higher bus voltage is however preferred that would enable high voltage to be supplied directly for high energy loads that require approximately 15,000V for operation. In addition, it would reduce size and weight of transmission cables. However, higher voltage introduces grounding and isolation issues with the SSCM. Regardless, the substantial gains in survivability, size/weight reduction,

increased efficiency and performance, improved architectural flexibility and reduced cost motivate the DC zonal distribution system.

5.1.4 Current Source Current Intensive Power System

Alternative power system architectures considered are the Current Intensive Current Source (CSCI) Power System that uses Superconducting Magnetic Energy Storage Systems (SMES) to deliver large energy over short period of time [79]. The CSCI is a single series system with multiple converters, either inverters or rectifiers Fig 34. The system may be operated even in the absence of the SMES, wherein the circuit current is controlled by a single converter. With SMES connected in the system, short duration current can be controlled by the SMES without a separate converter. With the SMES connected to the system, it charges during low load conditions and discharges during peaking loads thereby providing load leveling. However small load changes are sufficient to discharge 90% of the SMES. In addition, large current switching and the high refrigeration energy and magnetic field radiation are some of the major issues to its implementation.

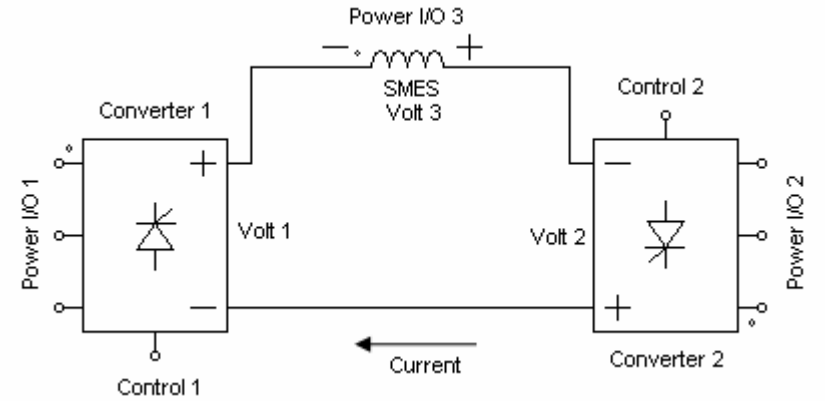

Fig 34. Current Source Current Intensive Power System

5.1.5 AC Articulate Power System

The AC Articulate Power System enables high power transfer with flexible voltage, current and frequency [79]. The use of Unity Displacement Factor Charger (UDFFC) provides constant frequency at the load end regardless of the generator output frequency thereby not requiring accurate speed control of generators and permitting frequency independent transmission. Frequency adjustment helps minimize the generator losses. The UDFFC may be used with a tap changing transformer or alternatively a controlled rectifier for DC conversion followed by an inverter for output frequency control may be employed to connect the load to the AC articulate transmission Fig 35. The system permits full transmission line loading. However the frequency bottleneck limits the power transfer capability due to line capacitance and inductance before insulation and thermal loading capacities are reached. However, this is resolved by continuous adjustment to voltage and current to their optimal values for a given power.

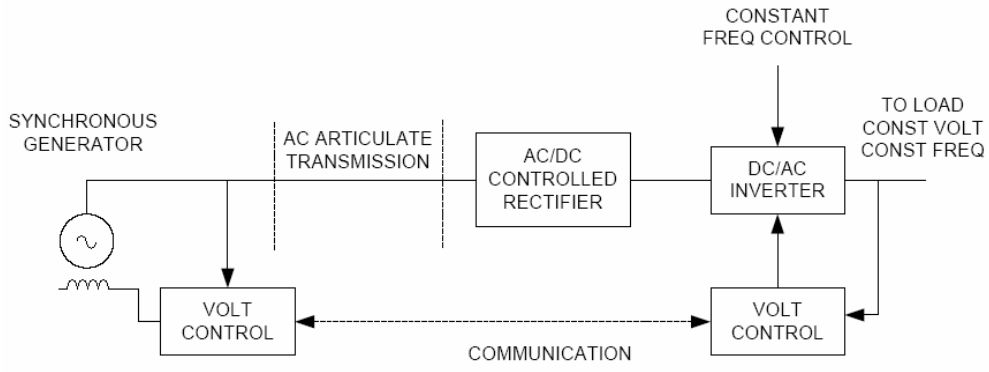

Fig 35. AC Articulate Power System

5.1.6 Challenges in Shipboard Power System

The major challenge with shipboard power system is contingency management - to restore failing systems and prevent cascading of faults under battle damage. This can be achieved by incorporating fault detection, failure assessment and restoration strategies into IPS automation systems for survivability and effective Resource Management. Network reconfiguration for restoring naval power system is a critical task to be performed by automation to restore loads and subsystems from battle damage and system faults, and minimize manning to reduce recovery time and avoid human error [80]. Operation under casualty conditions would be yet another challenge that would depend on the type of casualty.

In the present scenario, casualty (particularly under battle damage) on shipboard power system leads to ship wide electrical outage and loss of combat electronic resulting in complete paralysis for momentary periods. Detection of these faults currently take about 80 microseconds followed by complete recovery from fault and restoring of combat capability in the order of several minutes. However, incorporating comprehensive fault management in IPS automation system - casualty detection, isolation, diagnosis and recovery to combat state would be less than 100 milliseconds Fig 36. Thus, fault diagnosis can prove to be a vital component for contingency management and survivability of naval shipboard power systems.

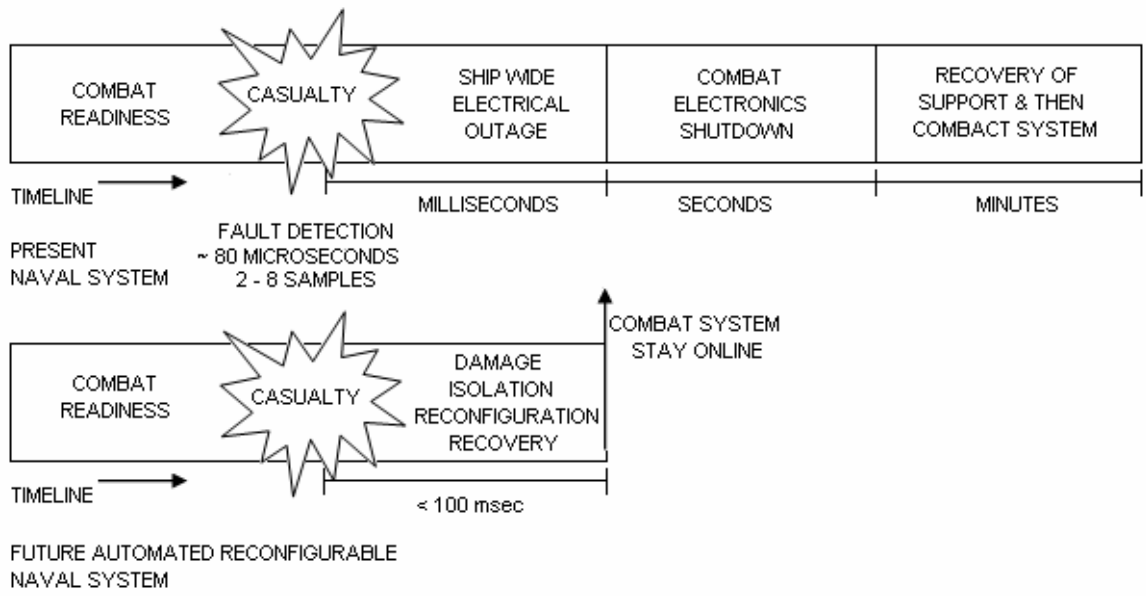

Fig 36. Comparison of the Present and Future Naval Shipboard Power System Casualty Recovery Timeline

5.2 DC Zonal Distribution System Analysis

To analyze the problems and faults associated with DC zonal electrical distribution systems in Naval Vessels the system in Fig. 37 is considered. There are two Power Supplies (PS1, PS2) of 4 kW each. One feeds the port bus, and the other feeds the starboard bus. The power supplies are uncontrolled rectifiers with LC output filters that deliver 200VDC to the buses. There are three zones of DC distribution. Each zone is fed by a converter module on the port bus (CM1, CM2, or CM3) and a converter module on the starboard bus (CM4, CM5, or CM6), operating from one of the two main distribution buses. They are commonly referred to as SSCM and consist of buck converter that steps-down the bus voltage to 160VDC. They have a droop characteristics built in them that allows load sharing between the two SSCM in each zone. Each SSCM is rated for 1kW (1.5kW peak capacity). A load is present in each

zone with SSIM that supplies a 3-phase Load Bank (LB), a Motor Controller (MC) that drives a 3-phase induction motor and a Constant Power Load (CPL). Each of these loads of 1 kW capacities is adjustable over the entire power range.

With each zone connected to both buses through CM and o-ring diodes, prevent fault from one bus being fed by the opposite bus. Fault between SSCM and o-ring diode are mitigated by current limits on the SSCM. Under such scenarios opposite bus can supply the zonal load. In event of PS failure or loss of 200VDC distribution bus, the other PS and opposite distribution bus can take up the entire system load without interruption of service. In addition, the Circuit Breakers (CB) facilitate further control over power flow in the system by disconnecting the part under fault. On a component level, faults are mitigated by their respective control modules.

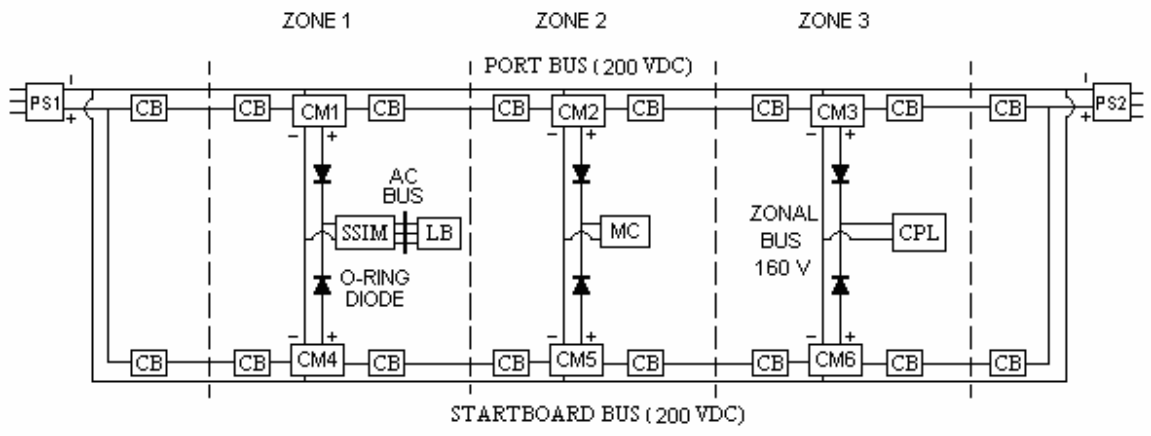

Fig 37. Naval DC Distribution System

For system analysis, a non-linear average model of the system in Fig 37 is used. In system study, initially three-phase source is supplied to both power supplies. The three zonal loads are energized by two main DC buses, the port and starboard supplied by the PS1 and PS2 respectively. Both SSCMs in each zone supply the load. The

system transient on loss of power to PS1 de-energizes the port bus and the full zonal load is transferred to the starboard bus Fig 38. The loss of 3-phase power occurs at 0.5 seconds. Immediately following this, the port bus voltage (VDCPS1) rapidly falls from 200VDC to SSCM output voltage 160VDC as SSCMs on port side increase their duty cycle to 100% to maintain 160V output. Once port side SSCM output falls below 160V, they are cut off due to the o-ring diode as starboard SSCMs maintain the zone voltage and take up the full load supplying power from PS2. Due to the large bus capacitance of port bus and SSCM output, the voltage falls is slow below 160V. The starboard bus voltage (VDCPS2) undergoes oscillation for about 200 milliseconds when full load is transferred to the bus. However, the SSCMs act as buffer and this oscillation does not cascade to the three zonal loads maintaining a steady 160V (CPLVIN, SSIMVDC – zone 1 and 3 voltage respectively).

Fig 39 shows the system transients when power to PS1 is restored and port bus is energized again. The port bus voltage overshoots to 250VDC due to large inrush current to the capacitors and the SSCM controller trying to establish 160V. At the same time, starboard voltage overshoots by about 18V due to a sudden drop in load being supplied as port bus picks up load. The port and starboard bus voltage have an oscillation for 150 and 300 milliseconds respectively. Again, due to the presence of SSCM, it acts as a buffer and the SSCM controller stabilizes the zone voltages well before the oscillations in the port and starboard buses dampen out. Since zone 2 voltage (MCVDC) undergoes similar transient as zone 1 and 3 in Fig 38 and 39, it has been omitted.

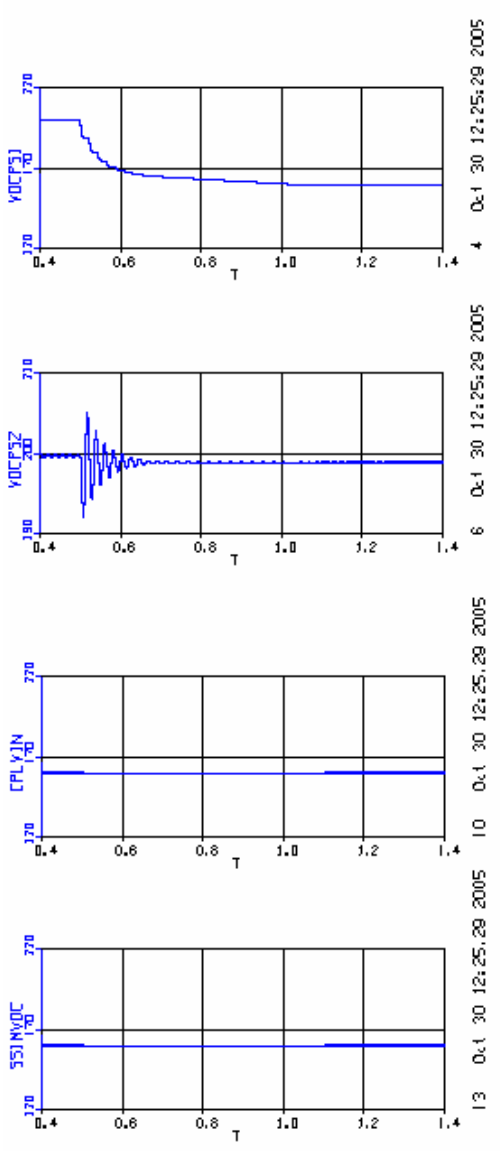

Fig 38. Transients under Loss of Port Bus 3 -Phase Power Supply (Voltage in volts & T in sec)

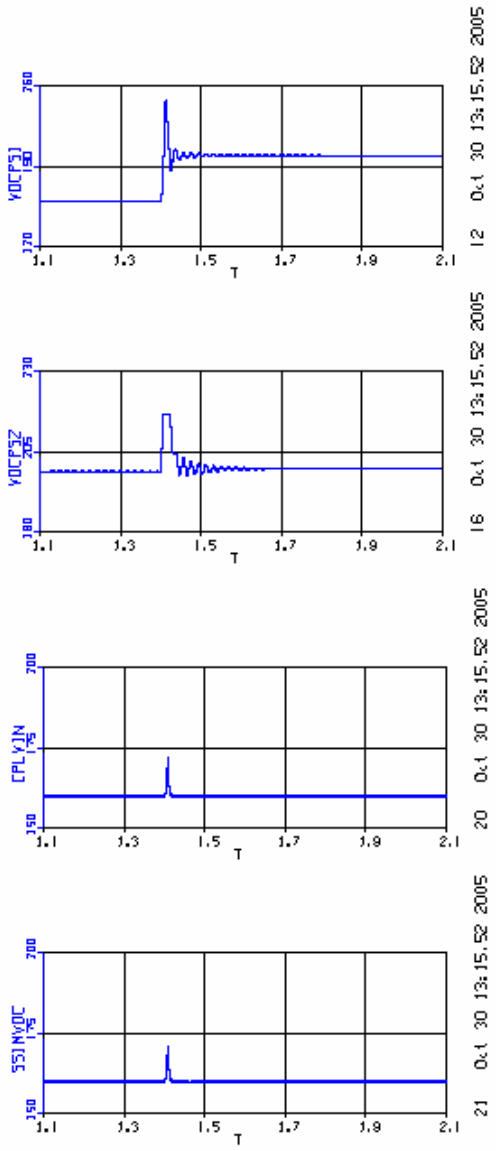

Fig 39. Transient on Recovery of Port Bus 3-Phase Power Supply (Voltage in volts & T in sec)

In the DC zonal electrical distribution system the large number of high bandwidth, nonlinear interconnected power converters lead to stability issues and system dynamics. In addition, the system being time-variant, the overall power system undergoes sequence of topological changes. A possible reconfiguration under fault or casualty to maintain sustained power to the loads, an understanding of stability, system integrity and security is of vital importance [78]. Stability of stiff ac system is known but operation of power converter networks in a stiffly connected system is not well known yet. In a relatively slow dynamics of the source, the networked high bandwidth converters may be assumed and analyzed as equivalent filters and constant power loads and for stable operation requiring source impedance to be smaller than load impedance. An additional constraint is avoiding sustained oscillation in the network which changes with network configuration and load changes. This imposes implication at the design level of the converters to guarantee proper stable operation in the network with all possible system configurations.

5.3 Fault Diagnosis in Naval DC Zonal Shipboard Power System

The technique here suggests the use of statistical moments of higher orders to detect and identify a fault. This utilizes existing system current and voltage sensors (port parameters) without the need for any addition sensors. The technique not only detects system malfunction, but provides information on the nature of the fault.

Analysis indicate third-order statistical moments are effective as they dynamically evaluate and monitor system deviations (voltages, currents) from normal operations and direction of deviations that enable to detect and diagnose fault fast

enough to prevent escalation. The general expression for nth order moment (s^n) is given in (16), wherein, the mean of the moving sampled window measures (M) is compared with the current measure (y) with a defined sample window size of N .

Consider the loss of 3-phase input power to PS1 in Fig 38. The power supply output voltage (VDCPS1) and current (IDCPS1) are again portrayed to indicate the point of 3-phase power loss which shows VDCPS1 fall to 160V in 1 second and a drop in IDCPS1 from 5A to 0A in 10 milliseconds following the malfunction Fig 40 and 41. The third statistical moment of VDCPS1 (fVDCPS1) and IDCPS1 (fVDCPS1) detects this loss of input power at PS1 in 300 microseconds Fig 42 and 43.

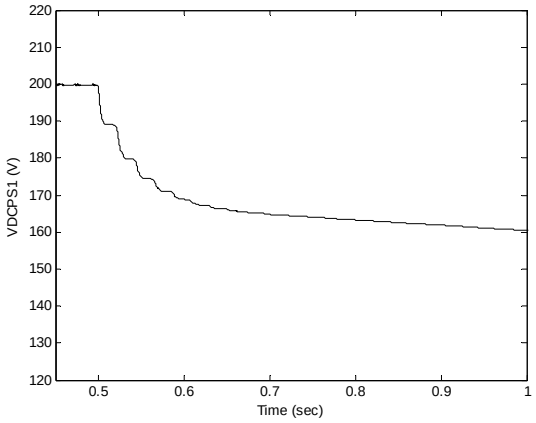

Fig 40. Port Bus Voltage (VDCPS1)

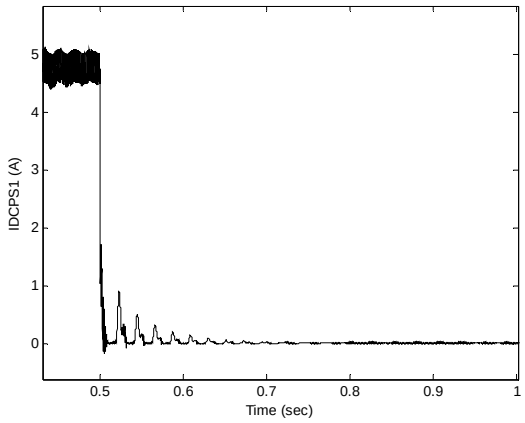

Fig 41. Port Bus Current (IDCPS1)

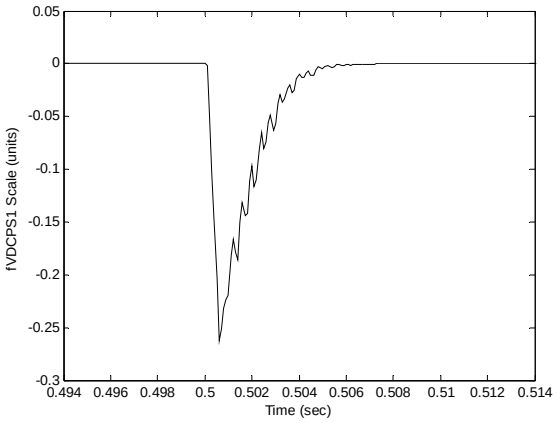

Fig 42. Third moment of VDCPS1

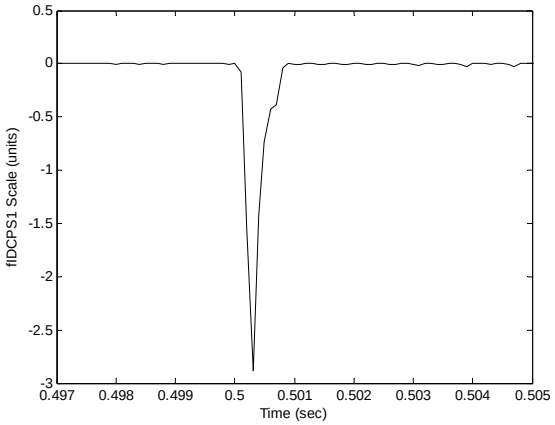

Fig 43. Third moment of IDCPS1

CHAPTER 6

CONCLUSION

In multiconverter systems many power electronic converters such as AC-DC rectifiers, DC-DC choppers and DC-AC inverters are used as sources, loads and distribution networks to provide power in different voltage and form. In recent years power electronics-based systems and components have been increasingly used in land, air, and sea vehicles. This has turned the vehicular products into a primary market for power electronics applications. Moreover, the existing trend in more electrification of the vehicles represents an ever bigger potential for an increase in the existing demand. Although the primary incentive for introduction of multi-converter systems into vehicular technologies was to enhance fuel economy and environmental issues associated with vehicles; today, improvement of fault tolerance, cost, and compactness have boost the motivation for development of the more electric vehicles. However, with increasing electrical and electrically driven loads, there have been increasing concerns on system reliability. Faults occurring in such application specific solid state converters can lead to fatal consequences as compared to their mechanical counterparts. Thus, it is vital to identify faults in such systems so as to develop necessary redundant and safety techniques and methodologies.

Detailed analysis of faults processes has indicated the need to act quickly following a device failure to prevent propagation of faults that may lead to catastrophic failure of the converter affecting the load, source, and connected system. To minimize the effect of fault, it is essential to accurately identify the failed devices and its mode of failure.

The proposed technique for diagnosis of faults involves the use of statistical moments of higher orders to detect and identify a failure. This utilizes the existing current and voltage sensors (port parameters) of the multiconverter system without the need for any additional sensors. The technique not only detects system malfunction, but provides information on the device under fault and the nature of the fault.

Analysis indicate third-order statistical moments are effective as they dynamically evaluate and monitor system deviations (voltages, currents) from normal operations and direction of the deviations enable to detect and diagnose fault fast enough to prevent device failure or escalation of fault. Thus idea behind the techniques is to detect, identify and act quickly on a single device failure to prevent escalation of the fault that would otherwise occur if the controller continued to operate without the knowledge of the fault situation. In addition, failure mode information derived from the system is essential for isolation of fault/reconfiguration of safety critical systems such as in Hybrid Electric Vehicle Power System to ensure sustainable operation and safety.

APPENDIX A

CASCADED CONVERTER CIRCUIT

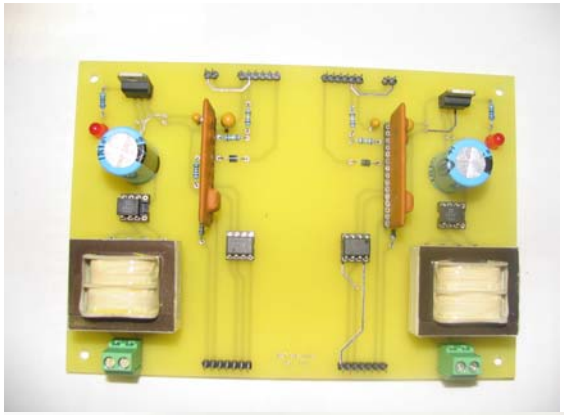

IGBT Gate Driver

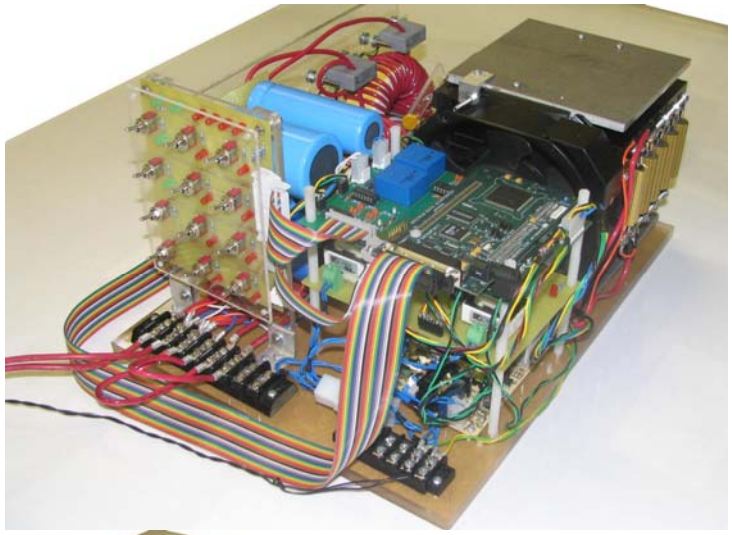

Control Board

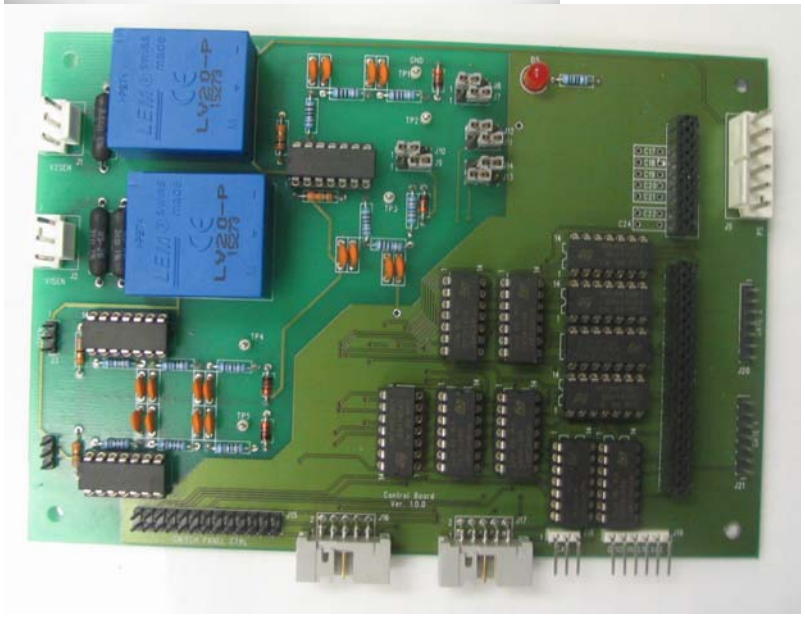

DC/DC Cascaded Converter

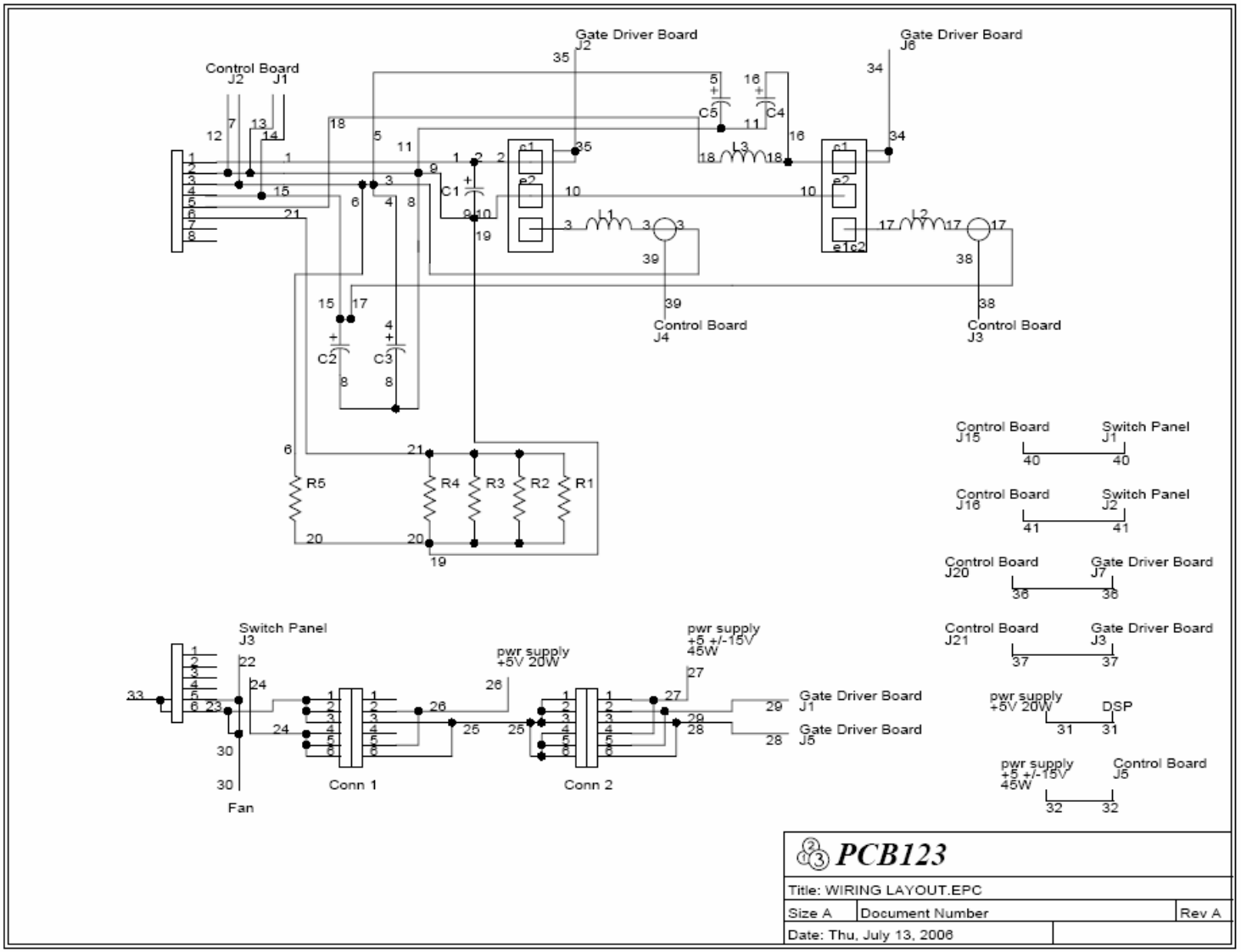
Gate Driver Board
J2
Gate Driver Board
J6
Control Board
J2 J1
C5
C4
L3
C1
L1
L2
C2
C3
R5
R4
R3
R2
R1
Control Board
J4
Control Board
J3
Control Board
J15
Switch Panel
J1
Control Board
J16
Switch Panel
J2
Control Board
J20
Gate Driver Board
J7
Control Board
J21
Gate Driver Board
J3
pwr supply
+5V 20W
DSP
pwr supply
+5 +/-15V
45W
Control Board
J5
Switch Panel
J3
pwr supply
+5V 20W
pwr supply
+5 +/-15V
45W
Conn 1
Conn 2
Gate Driver Board
J1
Gate Driver Board
J5
Fan
PCB123
Title: WIRING LAYOUT.EPC
Size A
Document Number
Rev A
Date: Thu, July 13, 2006

APPENDIX B

PRINTED CIRCUIT BOARDS

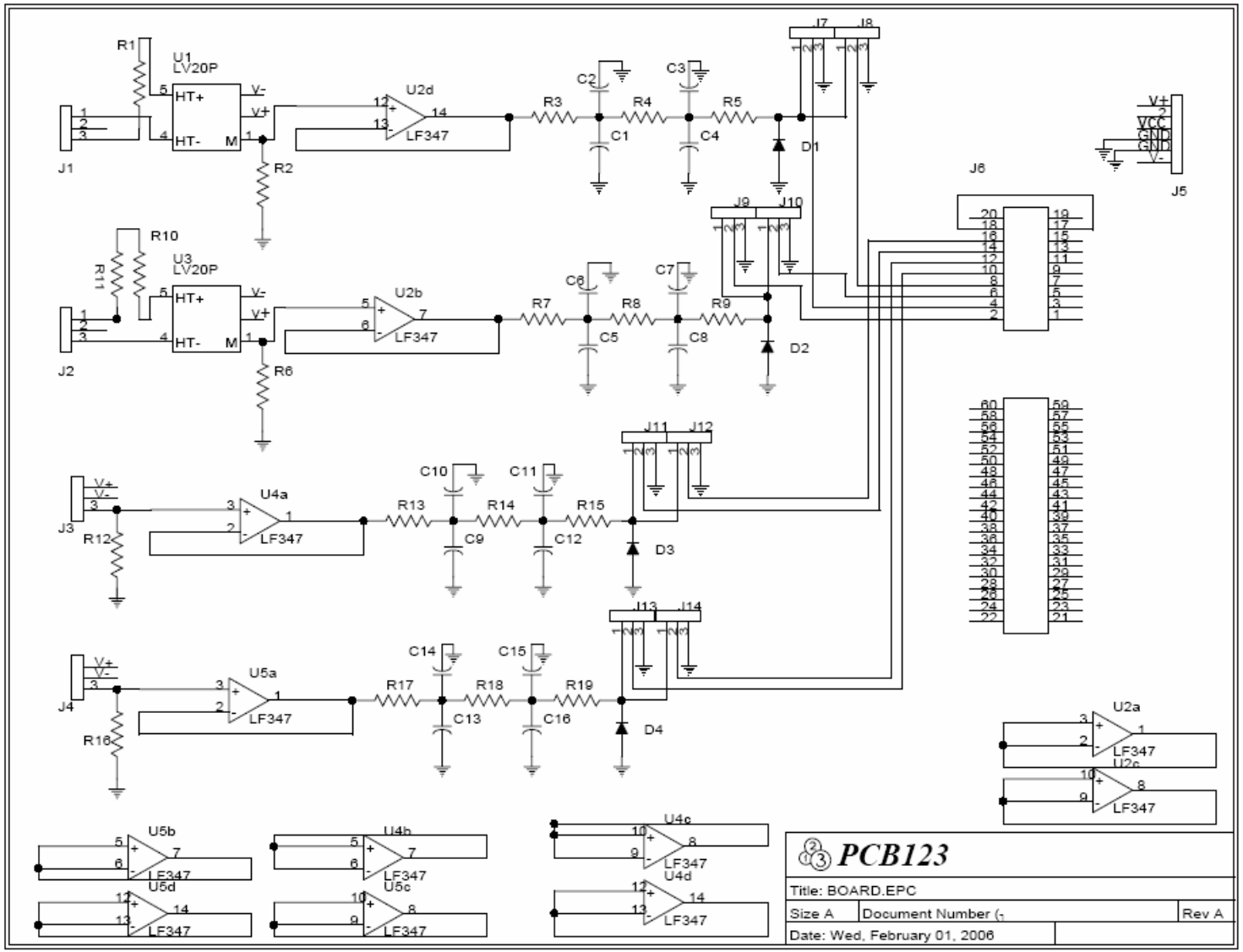
R1
U1
LV20P
HT+
HT-
V-
V+
M
J1
R2
U2d
LF347
R3
C2
C1
R4
C3
C4
R5
J7
J8
D1
J5
V+
VCC
GND
GND
V-
J6
R10
R11
U3
LV20P
J2
R6
U2b
LF347
C6
C5
R7
C7
C8
R8
R9
J9
J10
D2
J11
J12
J3
R12
U4a
LF347
C10
C9
R13
C11
C12
R14
R15
D3
J13
J14
J4
R16
U5a
LF347
C14
C13
R17
C15
C16
R18
R19
D4
U2a
LF347
U2c
LF347
U5b
LF347
U5d
LF347
U4b
LF347
U5c
LF347
U4c
LF347
U4d
LF347
PCB123
Title: BOARD.EPC
Size A
Document Number (-
Rev A
Date: Wed, February 01, 2006

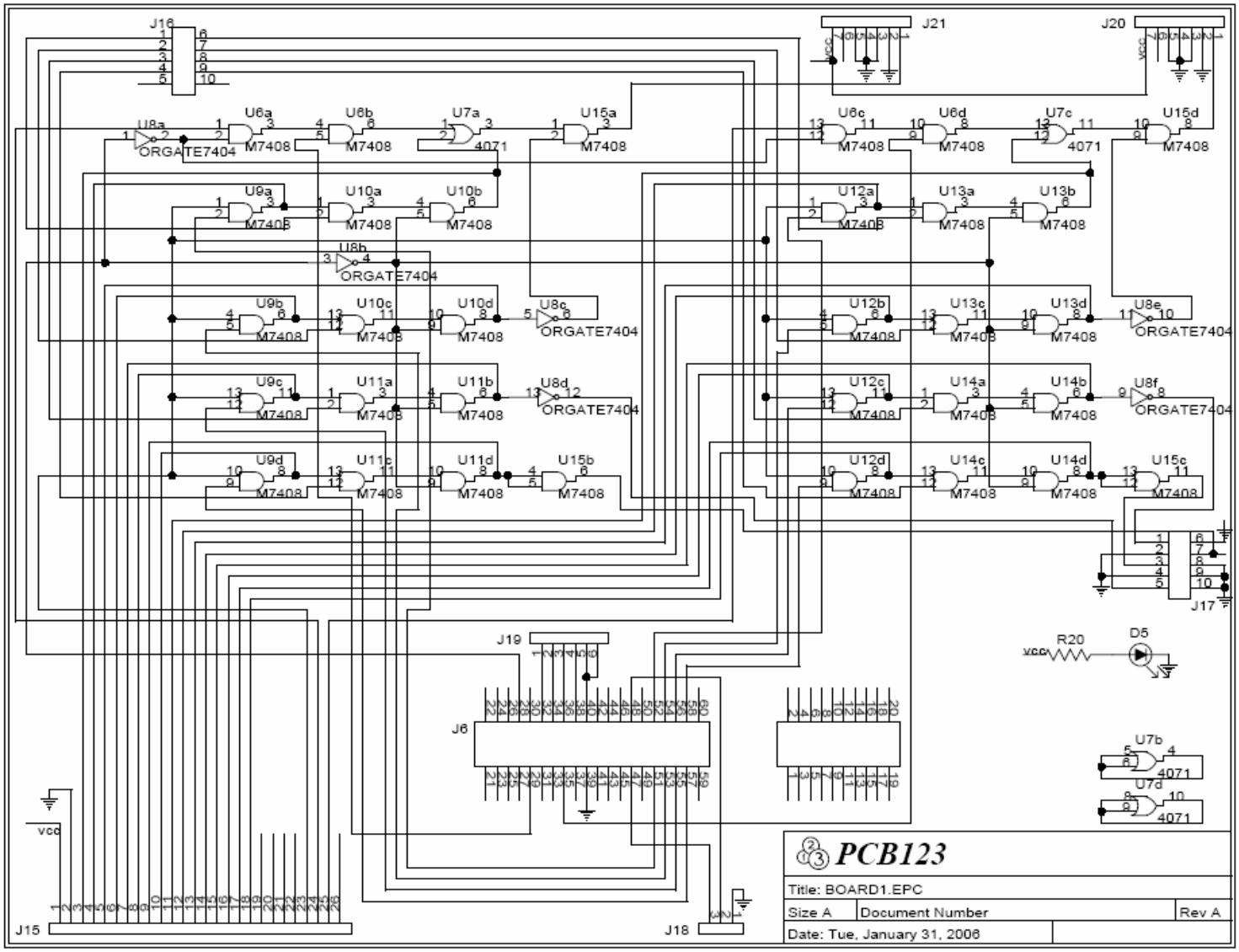
J16
J21
J20
U8a
ORGATE7404
U6a
M7408
U6b
M7408
U7a
4071
U15a
M7408
U6c
M7408
U6d
M7408
U7c
4071
U15d
M7408
U9a
M7408
U10a
M7408
U10b
M7408
U12a
M7408
U13a
M7408
U13b
M7408
U8b
ORGATE7404
U9b
M7408
U10c
M7408
U10d
M7408
U8c
ORGATE7404
U12b
M7408
U13c
M7408
U13d
M7408
U8e
ORGATE7404
U9c
M7408
U11a
M7408
U11b
M7408
U8d
ORGATE7404
U12c
M7408
U14a
M7408
U14b
M7408
U8f
ORGATE7404
U9d
M7408
U11c
M7408
U11d
M7408
U15b
M7408
U12d
M7408
U14c
M7408
U14d
M7408
U15c
M7408
J17
J19
J6
R20
vcc
D5
U7b
4071
U7d
4071
vcc
J15
J18
PCB123
Title: BOARD1.EPC
Size A
Document Number
Rev A
Date: Tue, January 31, 2006

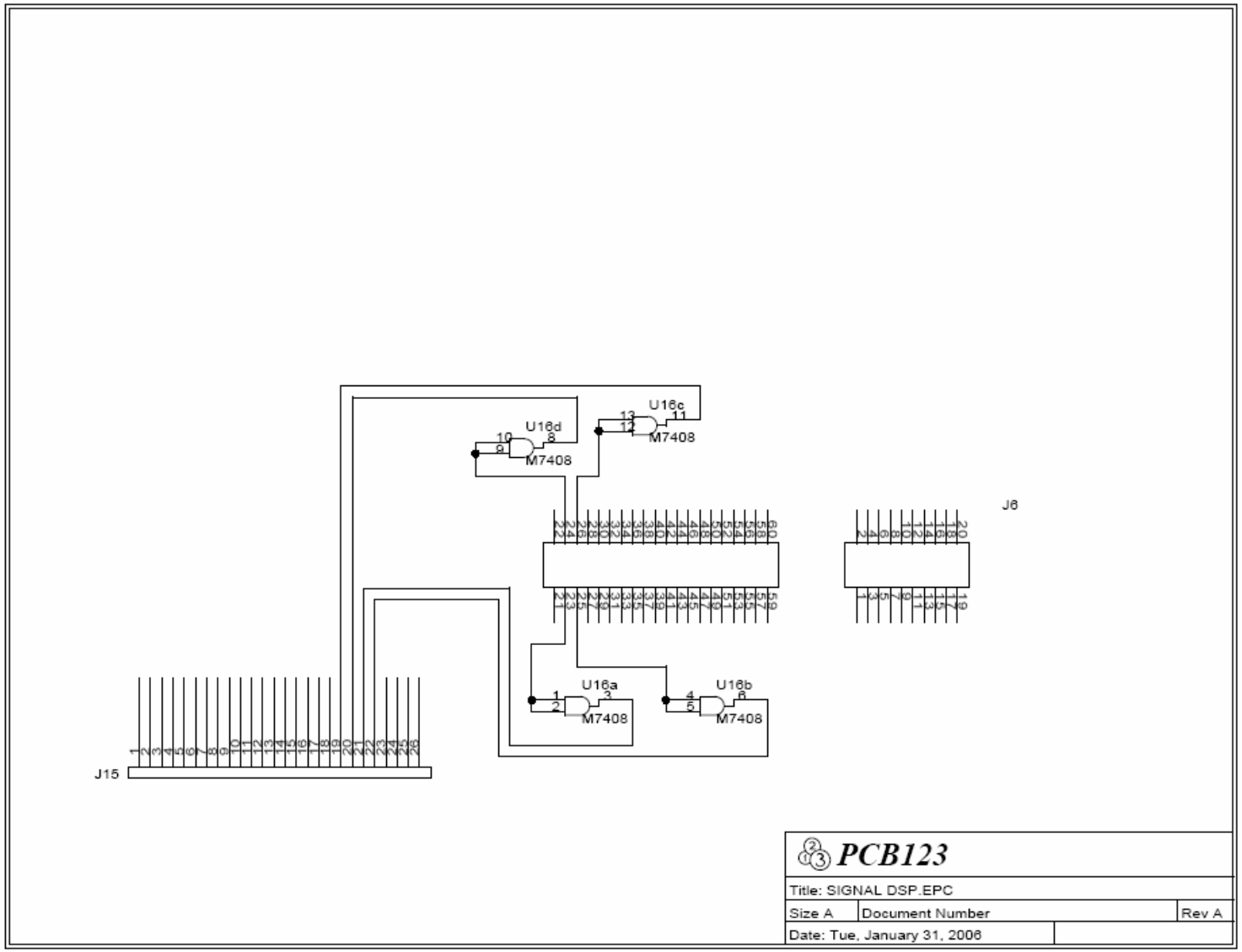
U16c
M7408
U16d
M7408
J6
U16a
M7408
U16b
M7408
J15
PCB123
Title: SIGNAL DSP.EPC
Size A
Document Number
Rev A
Date: Tue, January 31, 2006

Bill of Materials

Control Board

S. No.	Part ID	Description	Distributor/Part No.	Manufacturer	Quantity	Cost (per unit)
1	C1 – C24	Ceramic Capacitor, 2200uF, 50V	140-50Z5-103M Mouser	CDR50Z2-222M Xicon	24	0.08
2	D1 – D3	Zener Diode, 4.3V, 1W	78-1N4731A Mouser	1N4731A-TR Vishay Semiconductor	3	0.07
3	D4	Zener Diode, 4.7V, 1W	78-1N4732A Mouser	IN4732A-TR Vishay Semiconductor	1	0.07
4	D5	LED GREEN, 5 mm, Color Diff, Standard	638-333GD Mouser	EL-333GD Vishay	1	0.09
5	J1, J2	PCB HDR, 3P, Vert, Tin, 0.156”	538-26-60-4030 Mouser	26-60-4030 Molex	2	0.35
6	J3, J4, J7 – J14, J18 - J21	Breakaway Header, Single Row, 36 pole, 0.100” spacing, 0.23” Mating, 0.095” tail, 3A	649-68001-436 Mouser	68001-436 FCI Bergstik	2	1.01
7	J5	PCB HDR, 6P, Vert, Tin, 0.156”	538-26-60-4060 Mouser	26-60-4060 Molex	1	0.61
8	J6	Breakaway Sockets, Double Row, 72 pole, 0.100” spacing, 0.23” Mating, 0.095” tail, 3A	517-975-01-36 Mouser	929975-01-36 3M	1	3.24
9	J15 – J17	Breakaway Headers, Double Row, 72 pole, 0.100” spacing, 0.23” Mating, 0.095” tail, 3A	649-67997-472 Mouser	67997-472 FCI Bergstik	2	1.45
10	R1	Power Resistor, Wire Wound, 3.5kOhm, 3W, 5%	71-CW2B-3.5K Mouser	CW02B3K500JB12 Vishay/Dale	1	0.52
11	R2 – R9, R12 – R19	Metal Film Resistor, 1.8kOhms, 1/4W, 1%	271-1.8K-RC Mouser	271-1.8K-RC Xicon	16	0.09
12	R10, R11	Power Resistor, Wire Wound, 3.0kOhm, 3W, 5%	71-CW2B-3.0K Mouser	CW02B3K000JB12 Vishay/Dale	2	0.44
13	R20	Metal Film Resistor, 1.0kOhms, 1/4W, 1%	271-1K Mouser	271-1K Xicon	1	0.09

14	TP1 – TP5	Test Points, SM, White, 0.04”	151-201-RC Mouser	151-201-RC Kobioconn	5	0.30
15	U1, U3	Voltage Sensor, PCB Mount, 10mA	398-1020-ND Digikey	LV-20P LEM	2	36.60
16	U2, U4, U5	OpAmp, Wideband JFET, Quad	511-LF347N Mouser	LF347N ST Microelectronics	3	0.56
17	U6, U9 – U16	AND Gate, 2-Input, 5V, 14 Pin, Quad	511-M74HC08 Mouser	M74HC08B1R ST Microelectronics	9	0.28
18	U7	OR Gate, 2-Input, 5V, 14 Pin, Quad	511-4071 Mouser	HCF4071BEY ST Microelectronics	1	0.28
19	U8	Inverter/Buffer Gate, 5V, 14 Pin, HexQuad	511-M74HC04 Mouser	M74HC04B1R ST Microelectronics	1	0.28

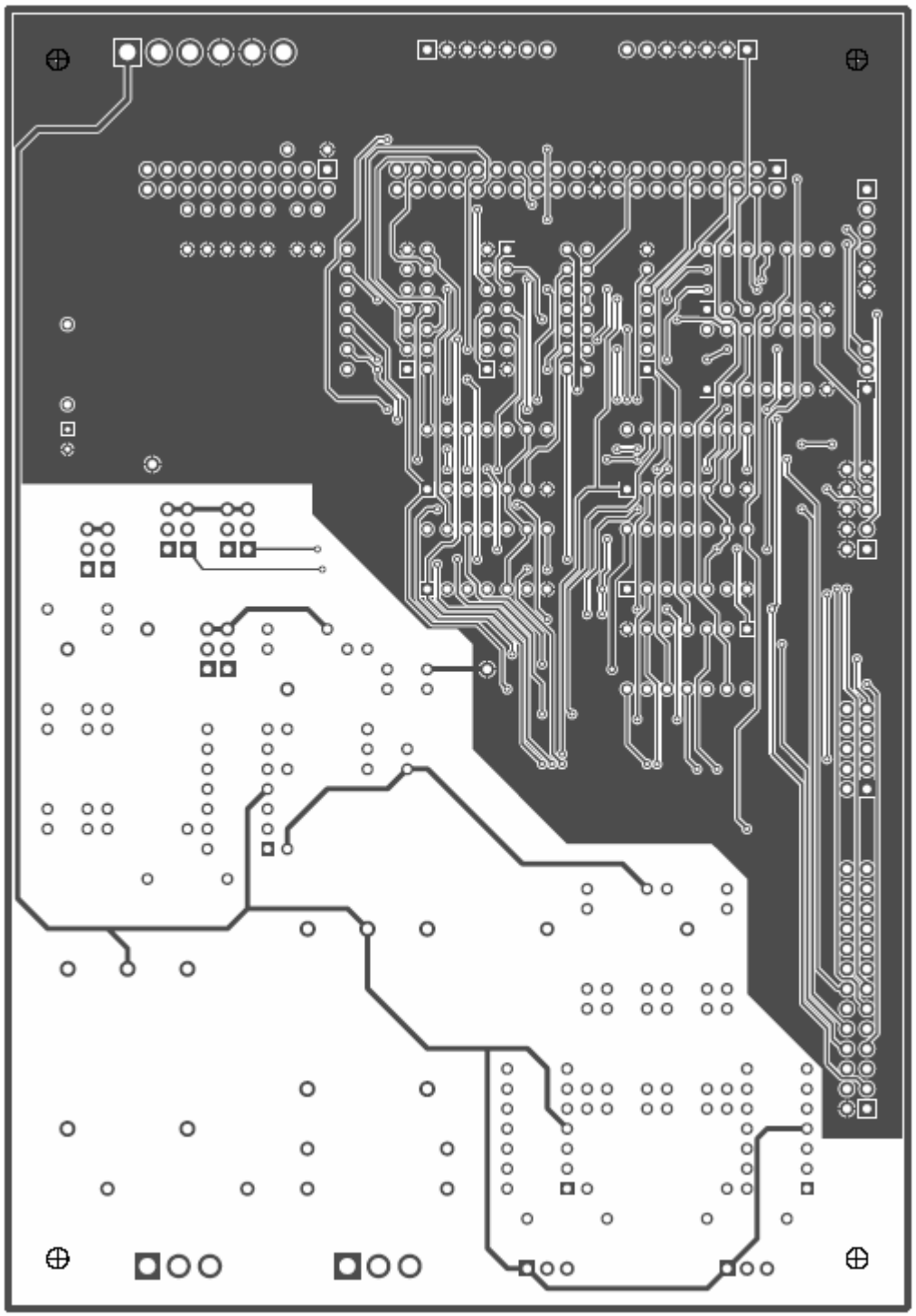

Top Layer

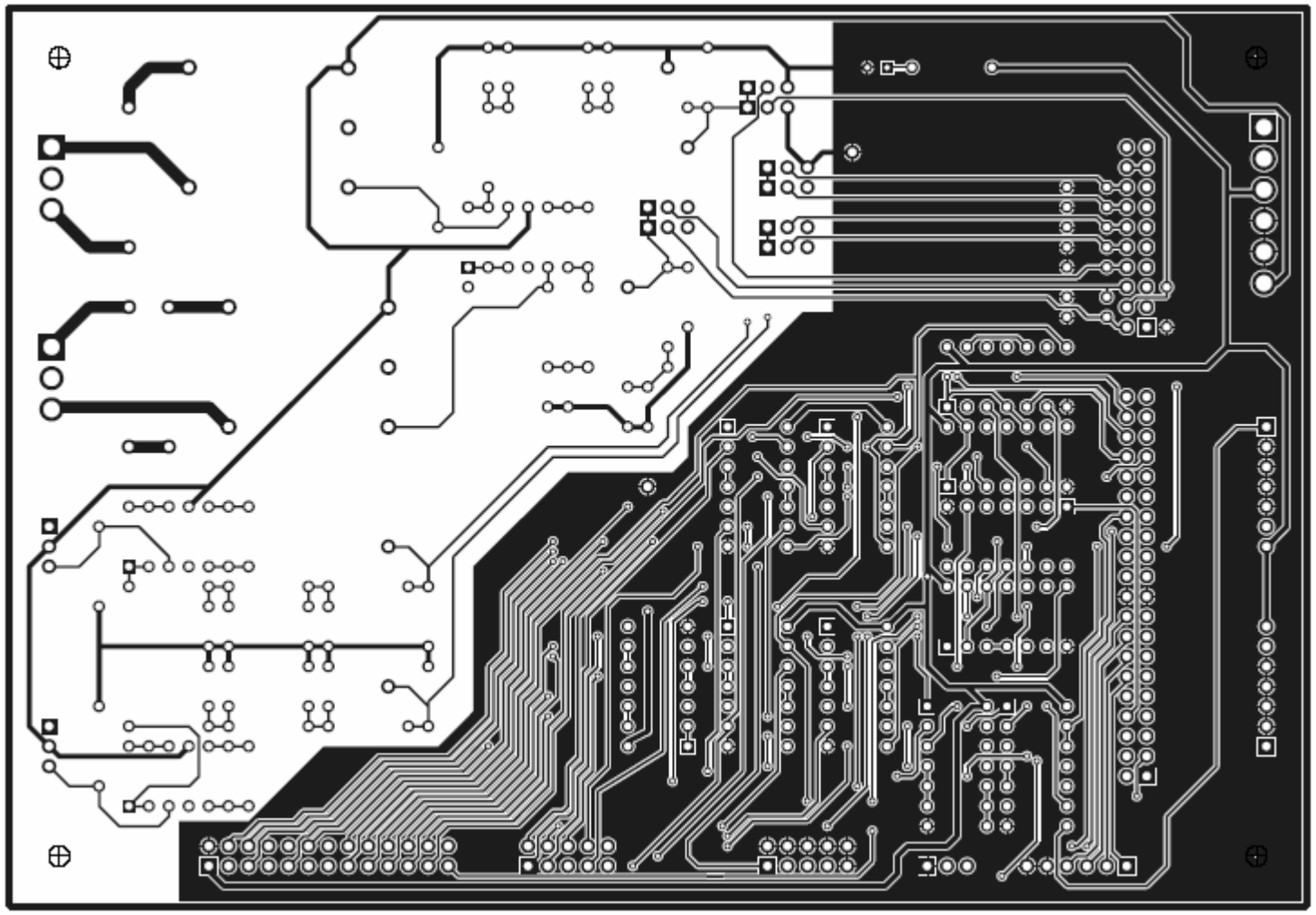

Bottom Layer

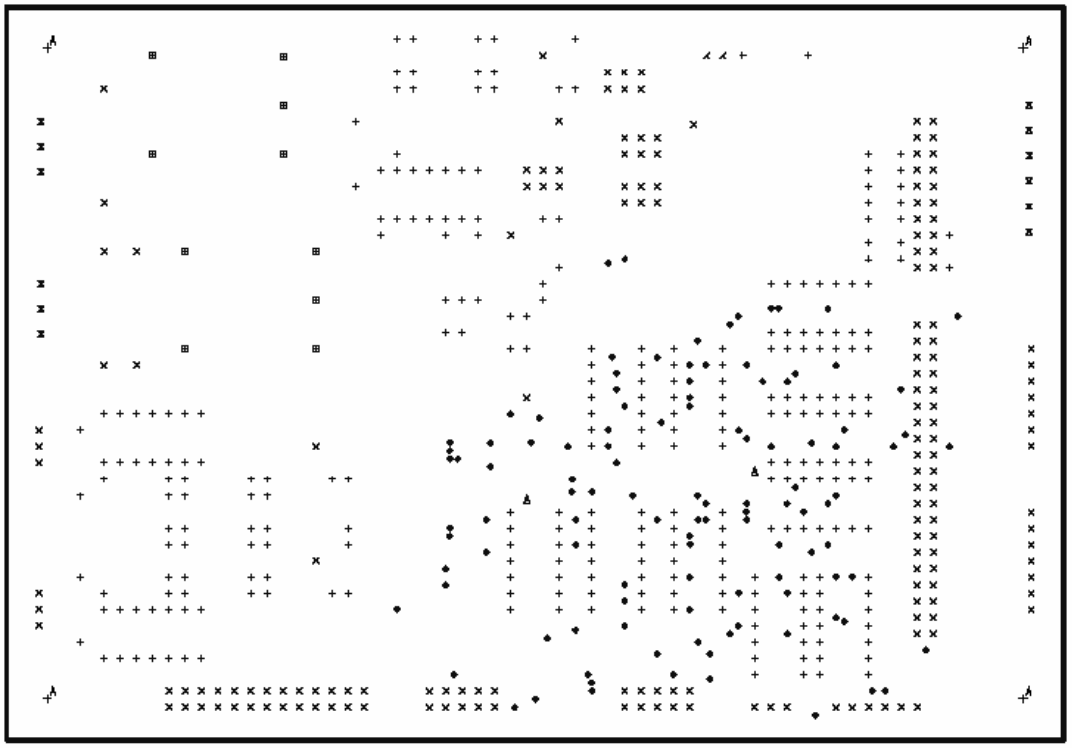

Drill Drawing

Drill Chart				
Sym	Size	Qty	Tol	Type
◈	0.02in	114	+/−0.004"	Plated
◬	0.025in	2	+/−0.004"	Plated
◸	0.029in	2	+/−0.004"	Plated
+	0.035in	286	+/−0.004"	Plated
×	0.04in	173	+/−0.004"	Plated
⊞	0.046in	10	+/−0.004"	Plated
⧗	0.079in	12	+/−0.004"	Plated
⊹	0.1065in	4	+/−0.004"	Non-Plated

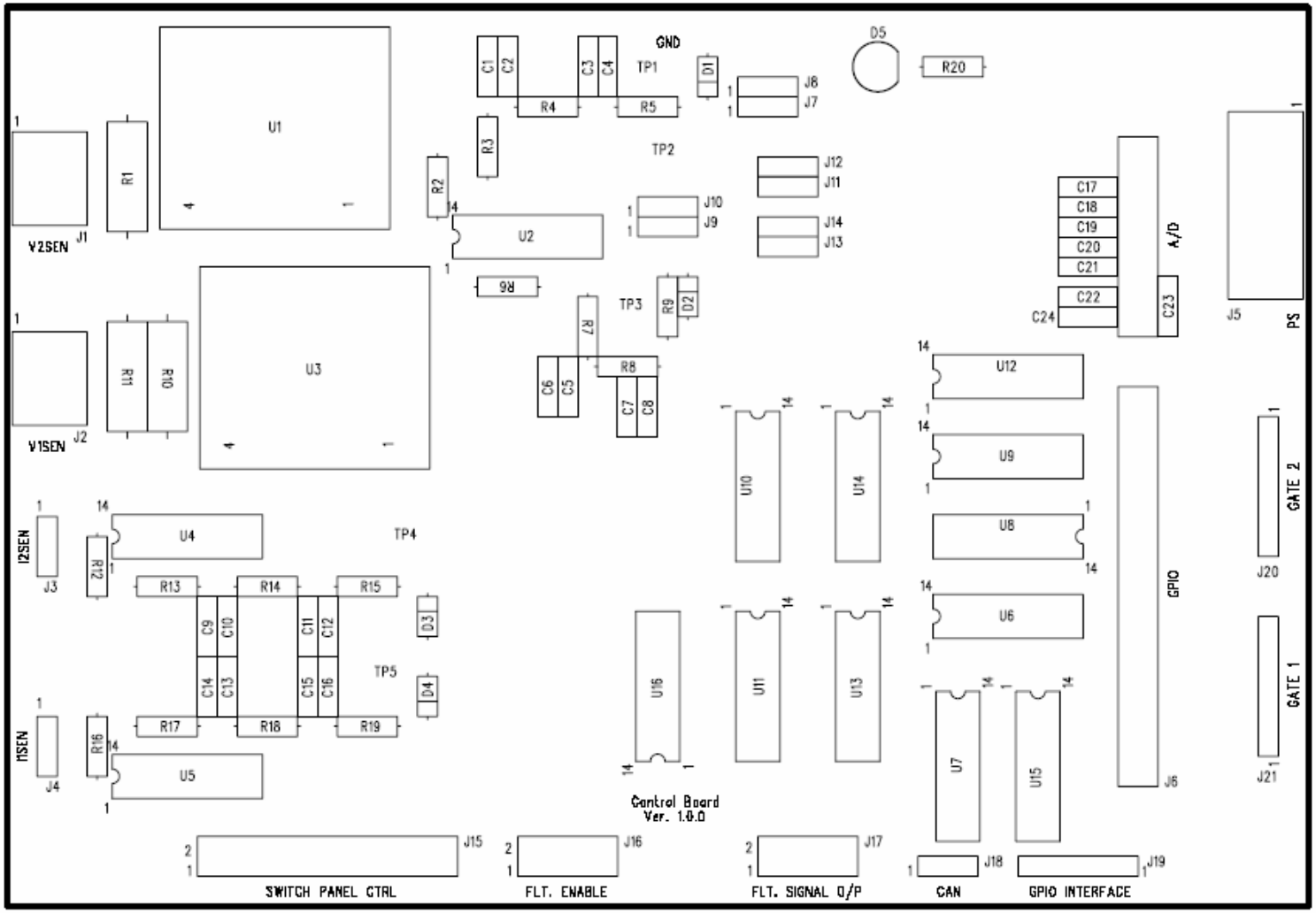

Top Silkscreen

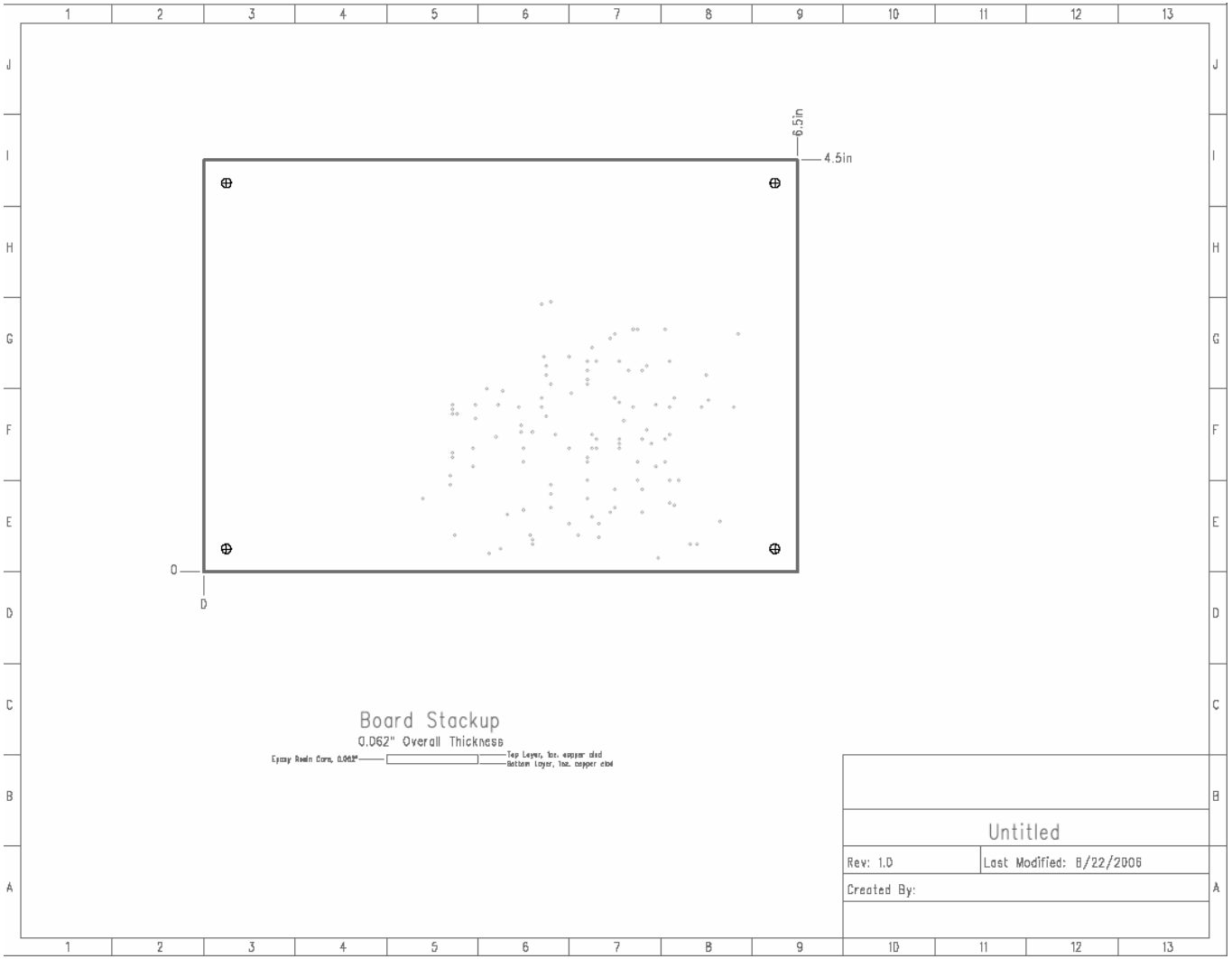

Mechanical Layout

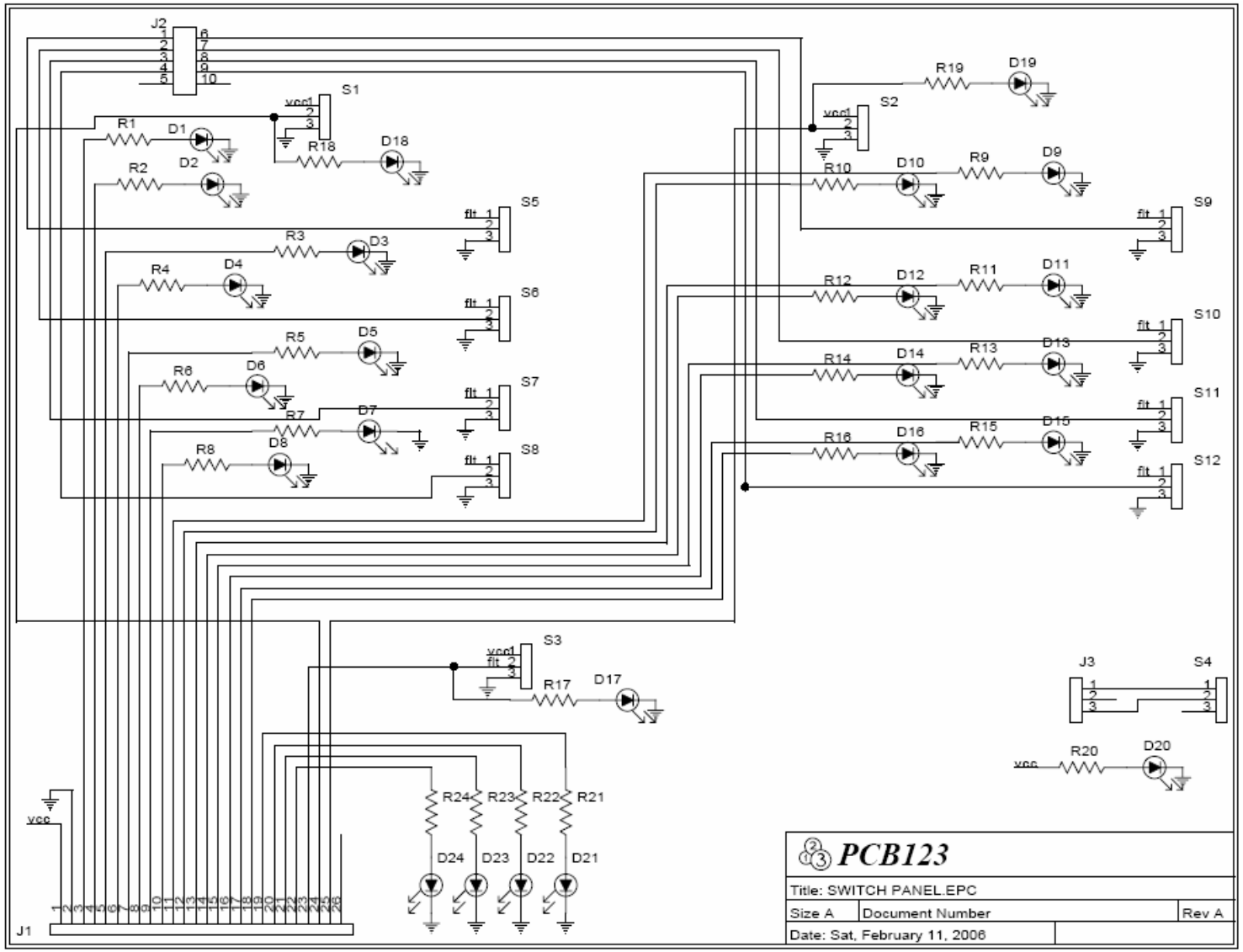
J2
S1
S2
S3
S4
S5
S6
S7
S8
S9
S10
S11
S12
J1
J3
R1
R2
R3
R4
R5
R6
R7
R8
R9
R10
R11
R12
R13
R14
R15
R16
R17
R18
R19
R20
R21
R22
R23
R24
D1
D2
D3
D4
D5
D6
D7
D8
D9
D10
D11
D12
D13
D14
D15
D16
D17
D18
D19
D20
D21
D22
D23
D24
vcc
vcc1
flt
PCB123
Title: SWITCH PANEL.EPC
Size A
Document Number
Rev A
Date: Sat, February 11, 2006

Bill of Materials

Switch Panel

S. No.	Part ID	Description	Distributor/Part No.	Manufacturer	Quantity	Cost (per unit)
1	D1 – D24	LED RED, 5 mm, Hi-Eff Red, color diff, 625 nm, 60 Degrees	638-333ID Mouser	EL-333ID Vishay	24	0.10
2	J1	26 Pole 2x13, IDC Header, Right Angled, 0.1”	649-71922-126 Mouser	71922-126 FCI	1	1.44
3	J2	10 Pole Header, Right Angled, 0.1”	649-71922-110 Mouser	71922-110 FCI	1	0.93
4	J3	3 Pole, 0.156”, Right Angled	538-26-60-5030 Mouser	26-60-5030 Molex	1	1.27
4	R1 – R24	Metal Film Resistor, 2kOhms, 1/4W, 1%	271-2K Mouser	271-2K Xicon	24	0.09
5	S1 – S12	Toggle Switch, ON-ON SPDT, PC Mount, 6A	611-7101-002 Mouser	7101SYCQE IIT/Cannon	12	4.26

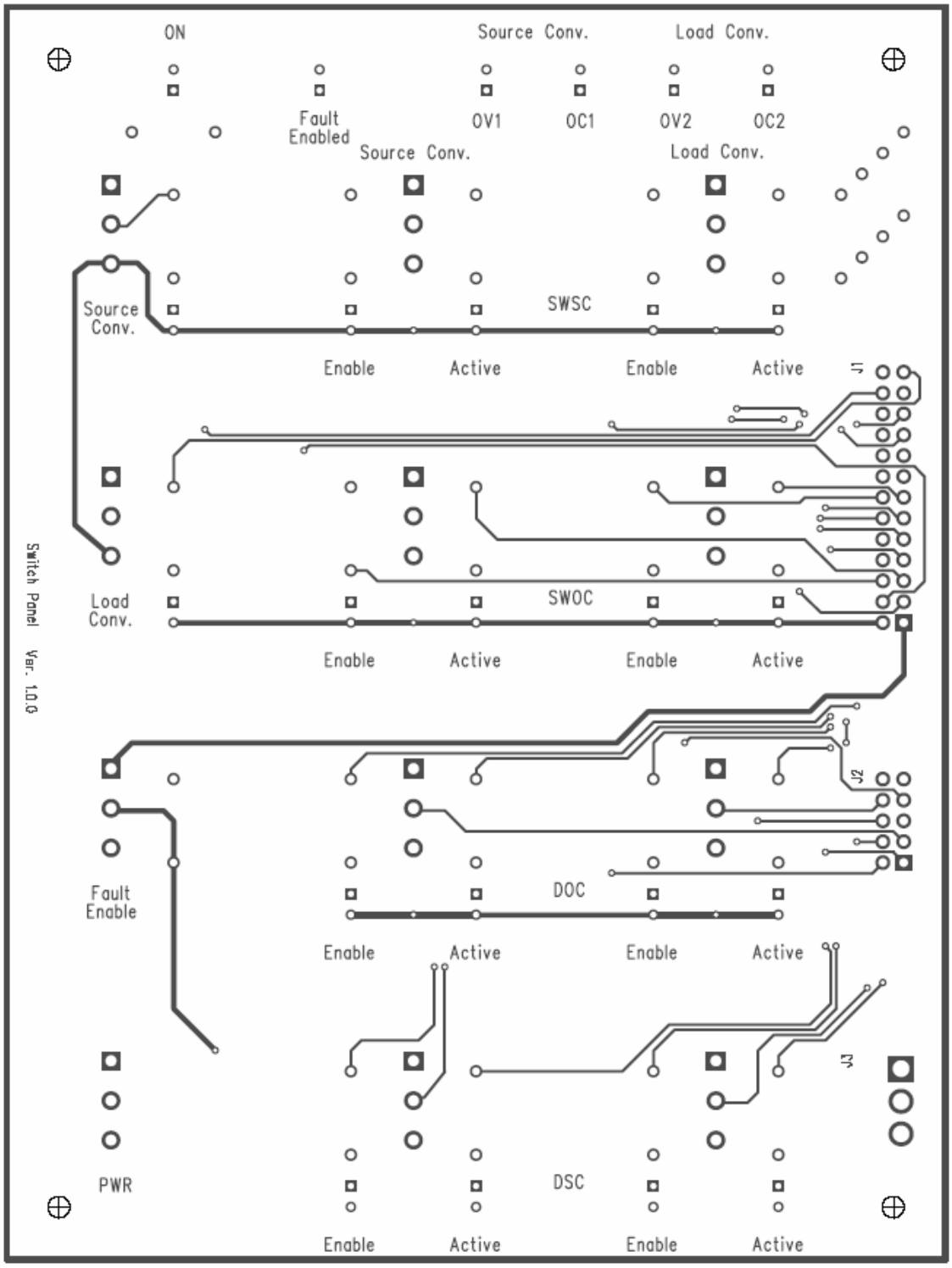
ON
Source Conv.
Load Conv.
Fault Enabled
OV1
OC1
OV2
OC2
Source Conv.
Load Conv.
Source Conv.
SWSC
Enable
Active
Enable
Active
J1
Load Conv.
SWOC
Enable
Active
Enable
Active
Switch Panel Ver. 1.0.0
J2
Fault Enable
DOC
Enable
Active
Enable
Active
J3
PWR
DSC
Enable
Active
Enable
Active

Top Layer

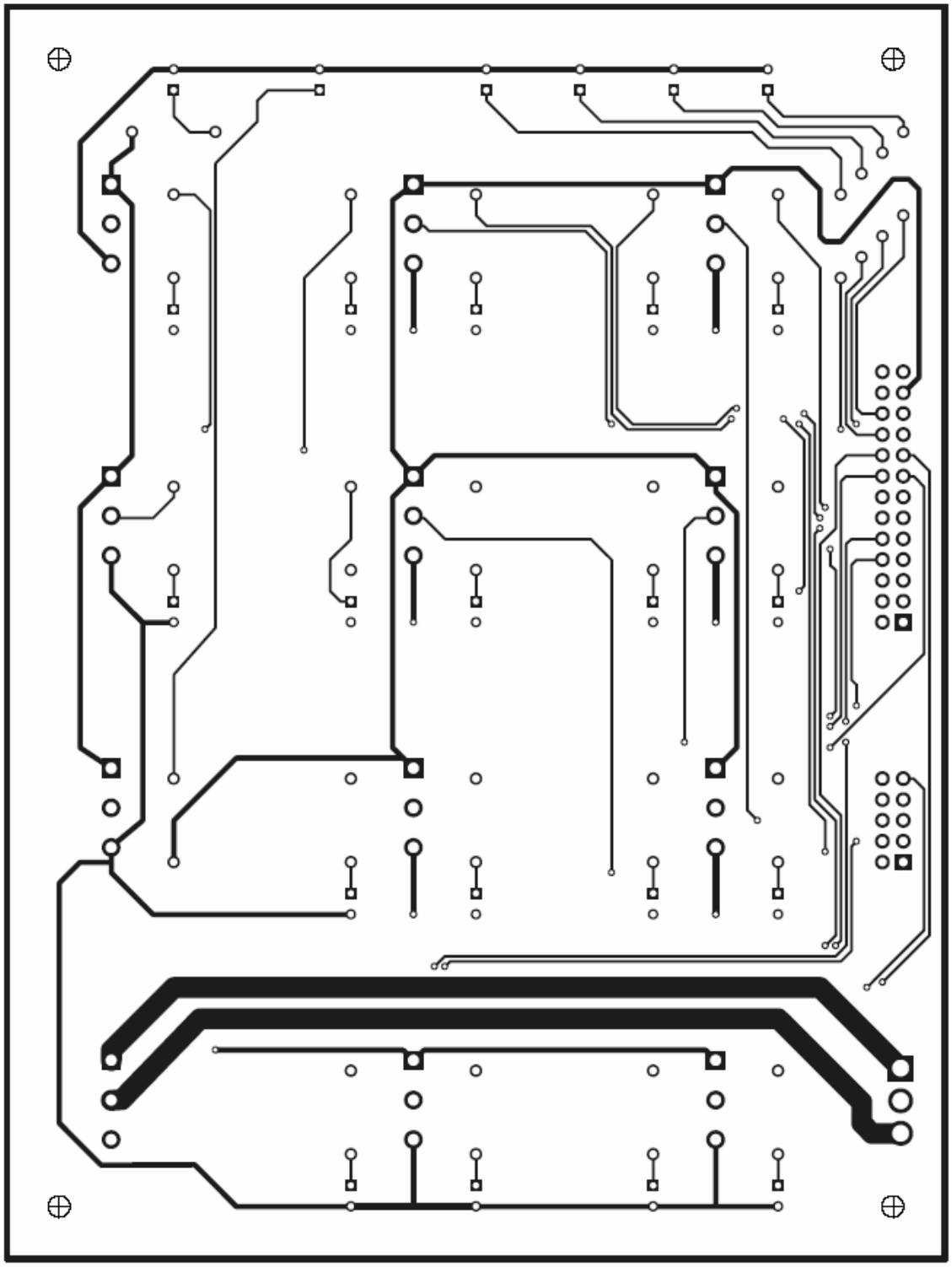

Bottom Layer

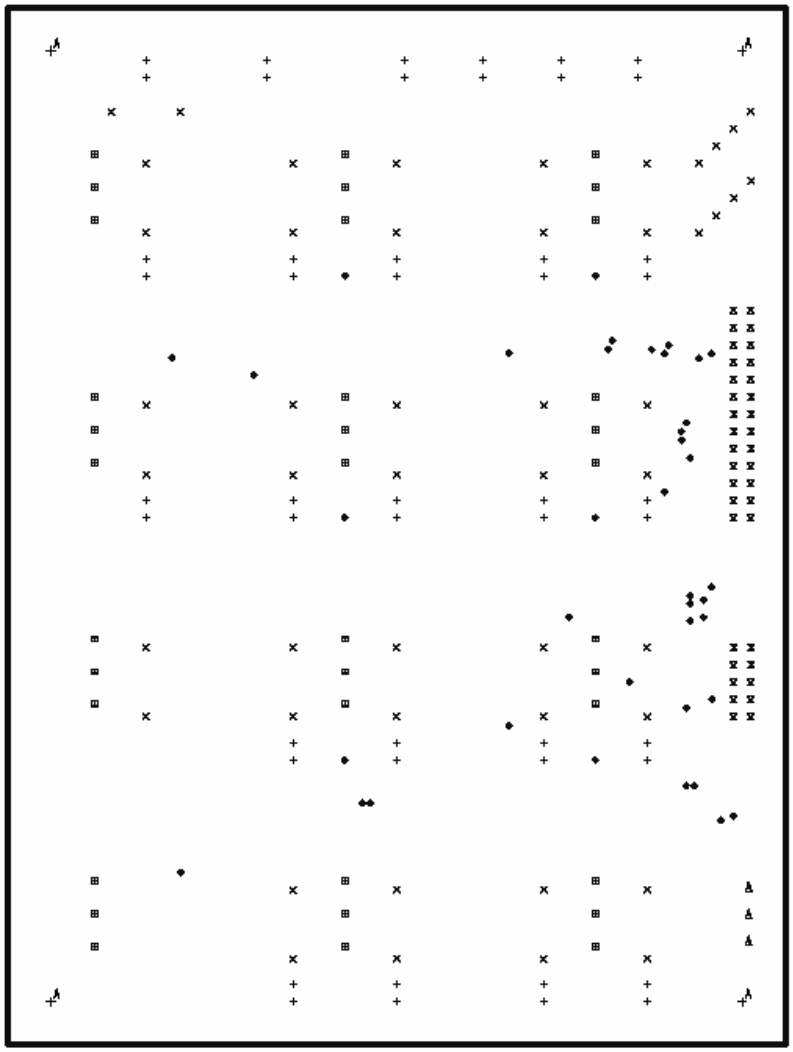

Drill Drawing

Drill Chart				
Sym	Size	Qty	Tol	Type
◈	0.02in	44	+/−0.004"	Plated
+	0.029in	48	+/−0.004"	Plated
×	0.035in	48	+/−0.004"	Plated
⧖	0.04in	36	+/−0.004"	Plated
⊞	0.052in	36	+/−0.004"	Plated
⧋	0.079in	3	+/−0.004"	Plated
⊹	0.1065in	4	+/−0.004"	Non-Plated

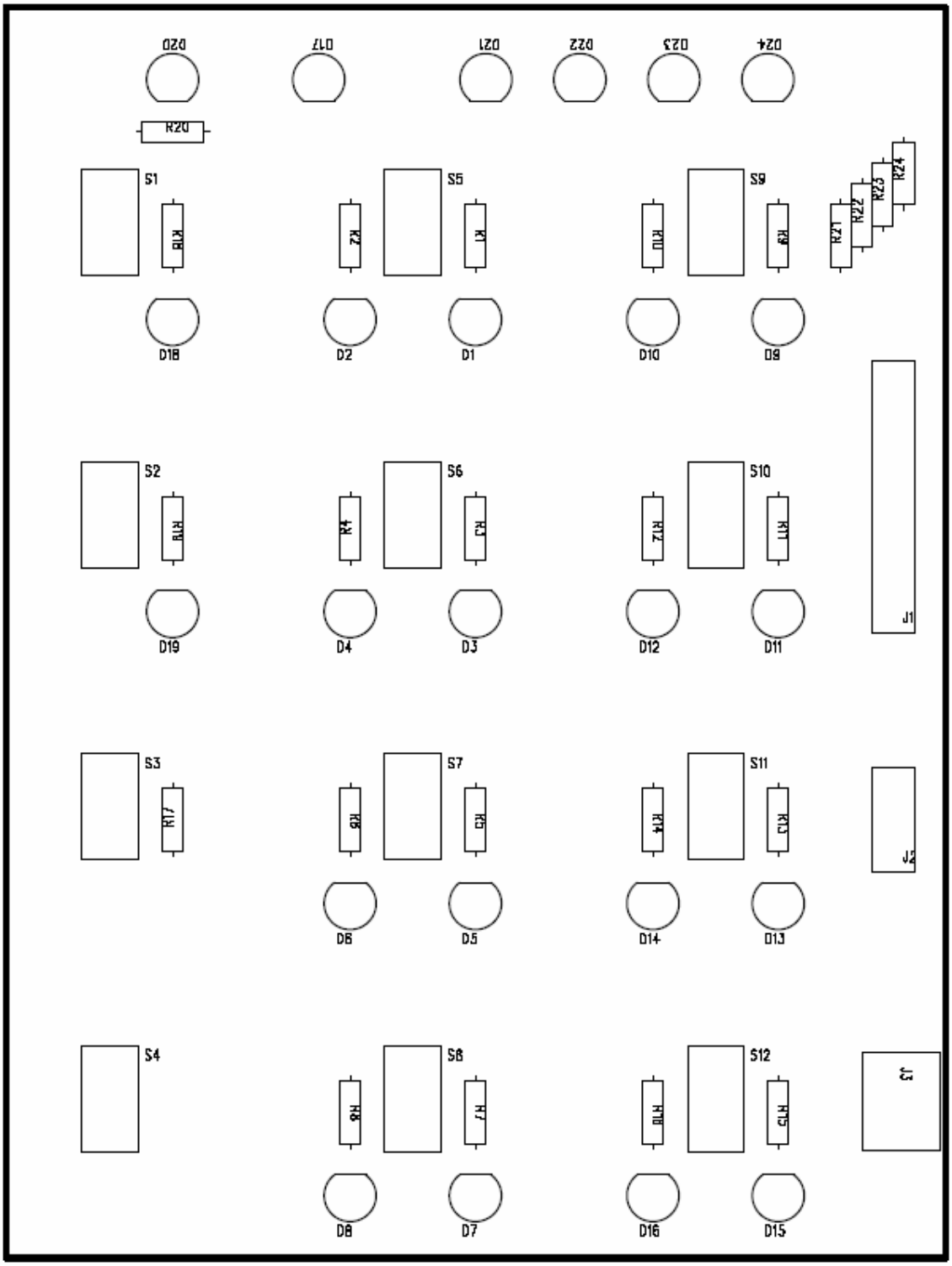

Silkscreen Top

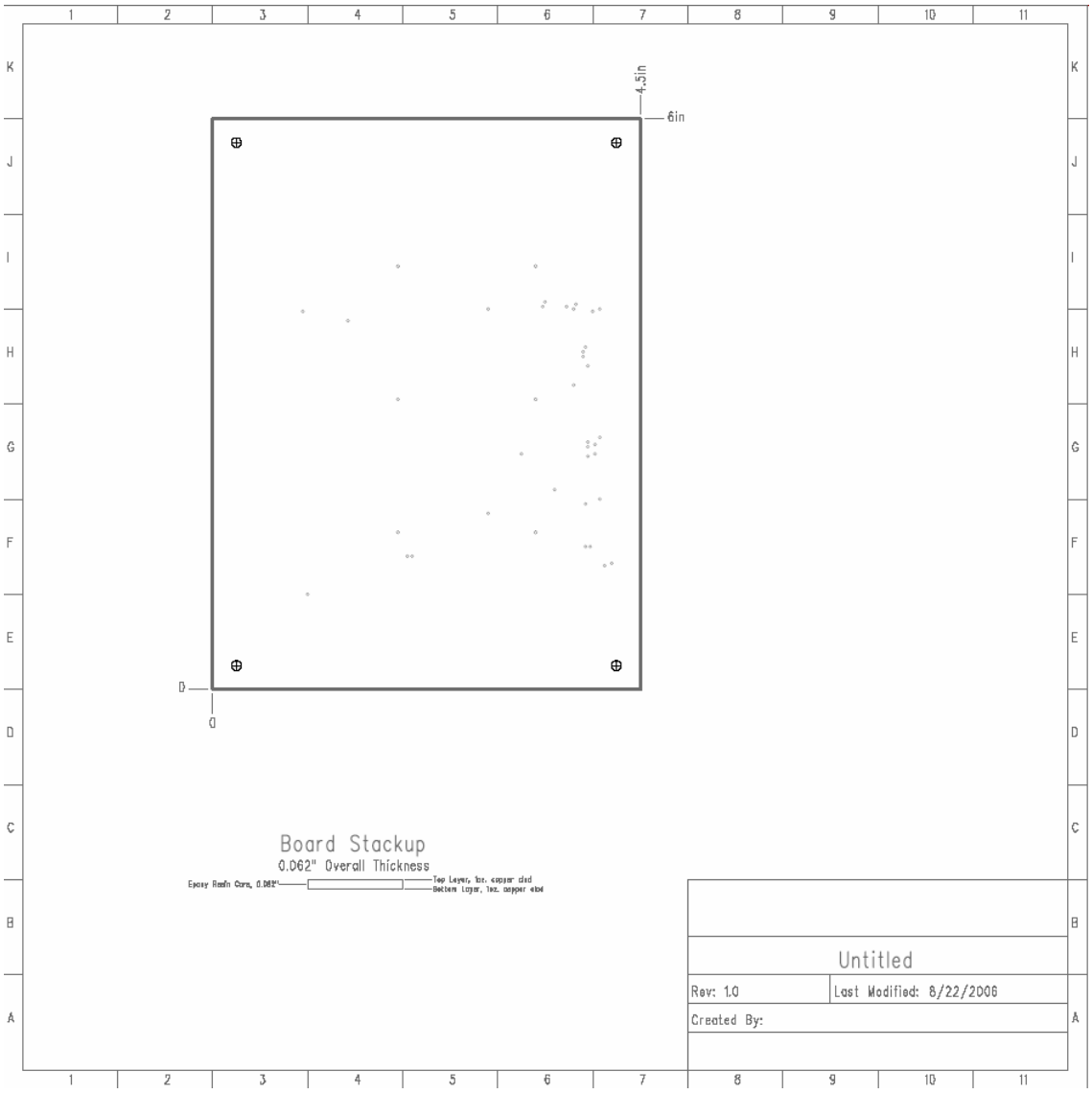

Mechanical Layout

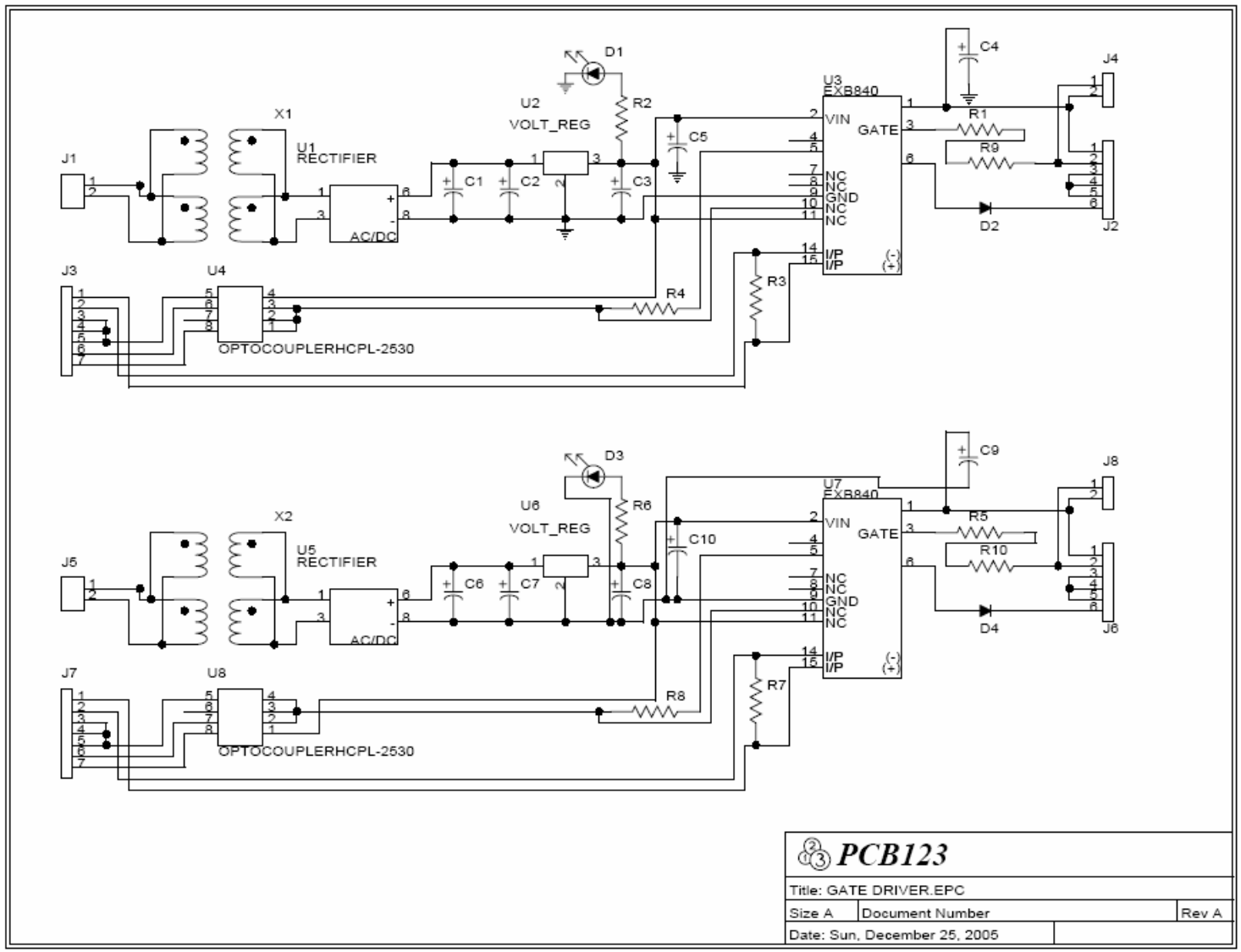
D1
U2
VOLT_REG
R2
C5
X1
U1
RECTIFIER
J1
C1
C2
C3
AC/DC
U3
EXB840
VIN
GATE
NC
NC
GND
NC
NC
I/P
I/P
C4
R1
R9
D2
J4
J2
J3
U4
R4
R3
OPTOCOUPLERHCPL-2530
D3
U6
VOLT_REG
R6
C10
X2
U5
RECTIFIER
J5
C6
C7
C8
AC/DC
U7
EXB840
C9
R5
R10
D4
J8
J6
J7
U8
R8
R7
OPTOCOUPLERHCPL-2530
PCB123
Title: GATE DRIVER.EPC
Size A
Document Number
Rev A
Date: Sun, December 25, 2005

Bill of Materials

Gate Driver Circuit

S. No.	Part ID	Description	Distributor/Part No.	Manufacturer	Quantity	Cost (per unit)
1	C1,C6	Electrolytic Capacitor, 1000uF, 50V	140-HTRL50V1000 Mouser	140-HTRL50V1000 Xicon	2	0.90
2	C5,C10	Tantalum Capacitor, 33uF, 25V	74-199D25V33 Mouser	199D335X9025B1V1 Vishay	2	2.91
3	C4,C9	Tantalum Capacitor 33uF, 6.3V	74-199D6.3V33 Mouser	199D336X96R3C1V1 Vishay	2	0.71
4	C2, C7	Tantalum Capacitor, Radial, 0.33uF, 50V, 10%	74-199D50V0.33 Mouser	199D334X9050A1V1 Vishay	2	0.50
5	C3, C8	Tantalum Capacitor, Radial, 0.1uF, 50V, 10%	74-199D50V0.1 Mouser	199D104X9050A1V1 Vishay	2	0.45
6	D1, D3	LED RED, 5 mm, Hi-Eff Red, color diff, 625 nm, 60 Degrees	638-333ID Mouser	EL-333ID Vishay	2	0.10
7	D2, D4	Fast Reverse Recovery Diode	ERA34-10 Fuji	ERA34-10 Fuji	2	0.55
8	R1, R5, R9, R10	Metal Film Resistor, 24.9Ohms, 1/4W, 1%	271-24.9 Mouser	271-24.9 Xicon	4	0.09
9	R3, R7	Metal Film Resistor, 10kOhms, 1/4W, 1%	271-10K Mouser	271-10K Xicon	2	0.09
10	R4, R8	Metal Film Resistor, 1kOhms, 1/4W, 1%	271-1K Mouser	271-1K Xicon	2	0.09
11	R2, R6	Metal Film Resistor, 2kOhms, 1/4W, 1%	271-2K Mouser	271-2K Xicon	2	0.09
12	U1,U5	Bridge Rectifier IC, 100V, 1A	583-DB102 Mouser	DB102 Rectron	2	0.33
13	U2,U6	Fixed Positive Voltage Regulator, 20V, 1A	511-L7820ACV Mouser	L7820ACV ST Microelectronics	2	0.40
14	U3,U7	IGBT Gate Driver, Hybrid IC, High Speed	EXB840 Fuji	EXB840 Fuji	2	17.38
15	U4,U8	High Speed Transistor Optocouplers,	512-HCPL-2531	HCPL-2530	2	2.07

		Dual Channel	Mouser	Fairchild		
16	J1,J5	PCB Terminal Block, 5 mm, 2 Pole, Screw Clamp	651-1711026 Mouser	1711026 Phoenix Contact	2	1.38
17	J2, J3, J4, J6, J7, J8	Breakaway Header, Single Row, 36 pole, 0.100” spacing, 0.23” Mating, 0.095” tail, 3A	649-68001-436 Mouser	68001-436 FCI Bergstik	2	1.01
18	X1,X2	Transformer, 6 VA, 36V, 0.065A Split Pack, 8 Pin	553-FS36-65 Mouser	FS36-65 Triad Magnetics	2	9.00

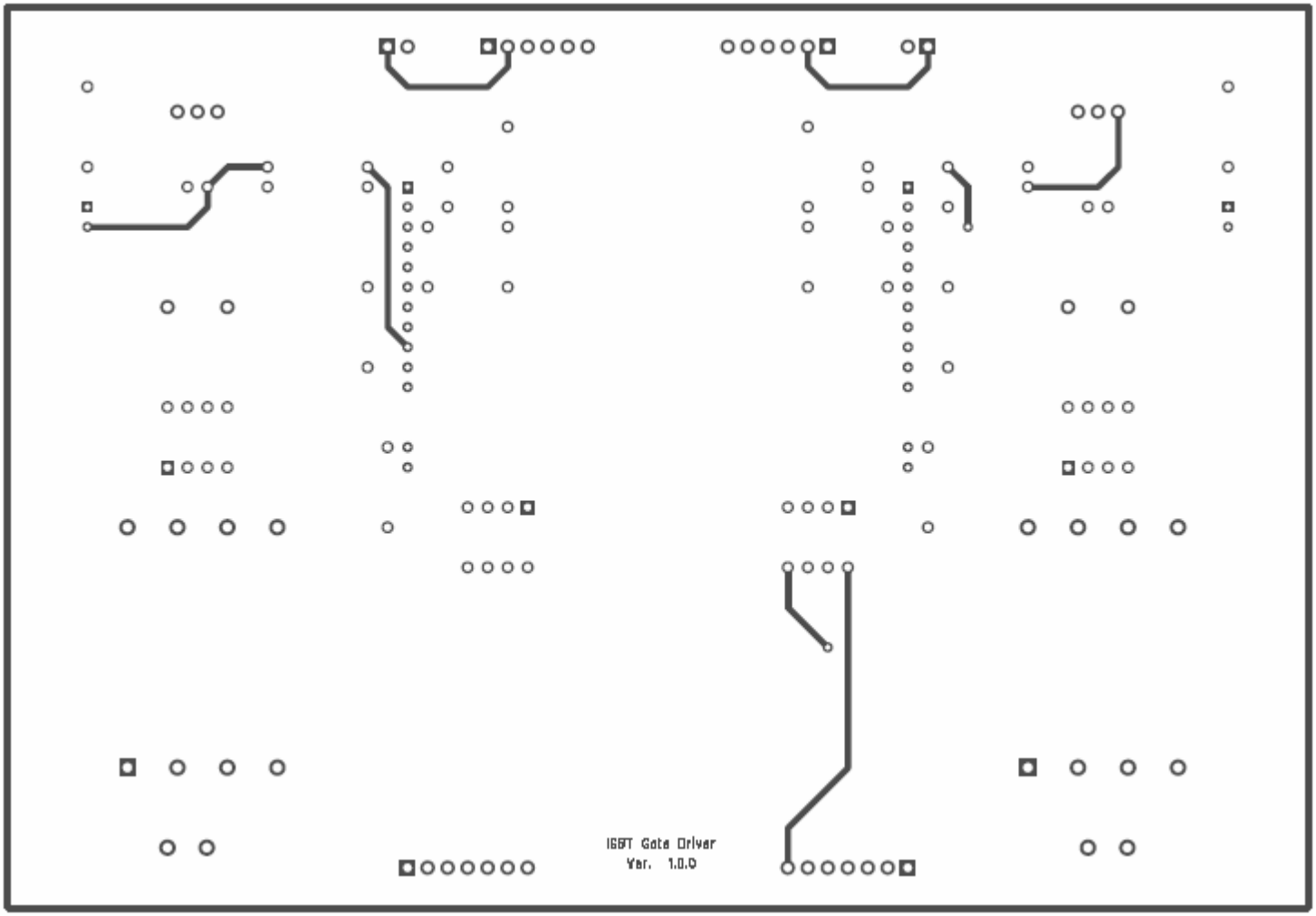

Top Layer

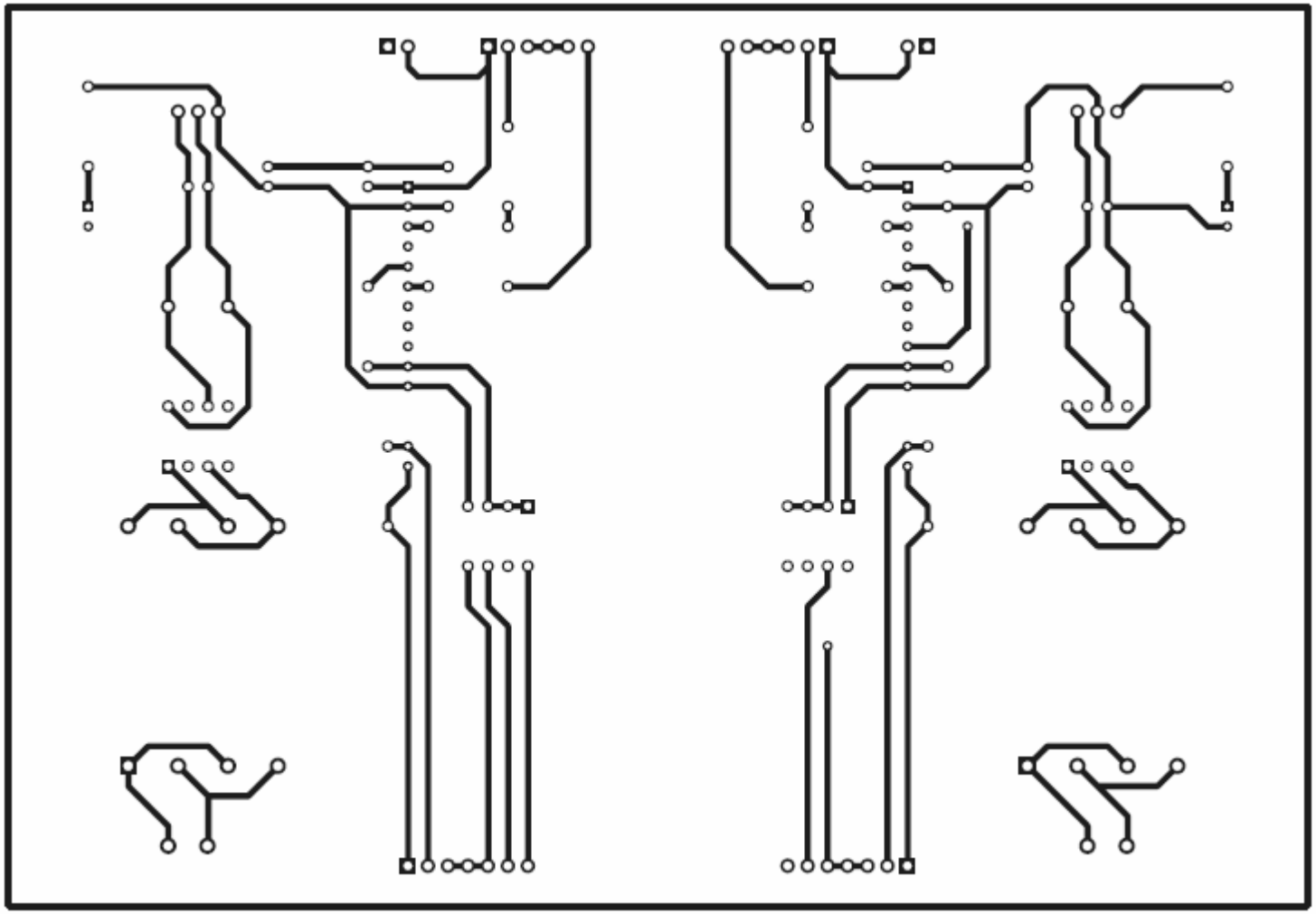

Bottom Layer

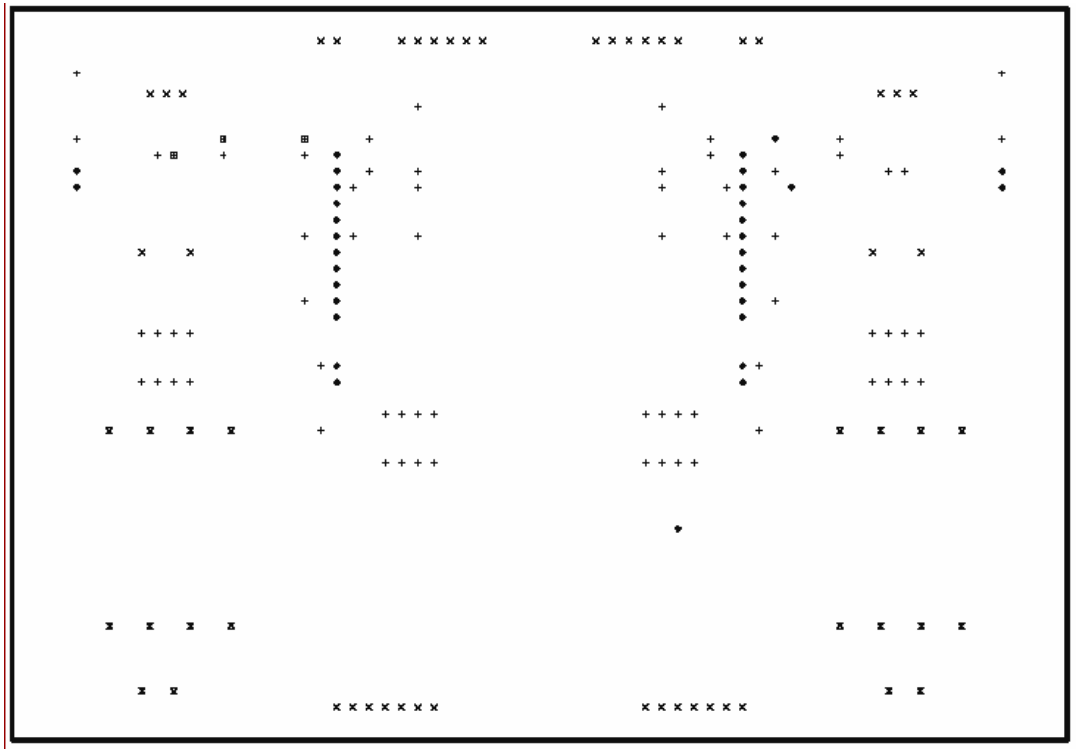

Drill Drawing

Drill Chart				
Sym	Size	Qty	Tol	Type
⊡	0.02in	3	+/−0.004"	Plated
◈	0.029in	33	+/−0.004"	Plated
+	0.035in	72	+/−0.004"	Plated
×	0.04in	40	+/−0.004"	Plated
⧖	0.046in	20	+/−0.004"	Plated

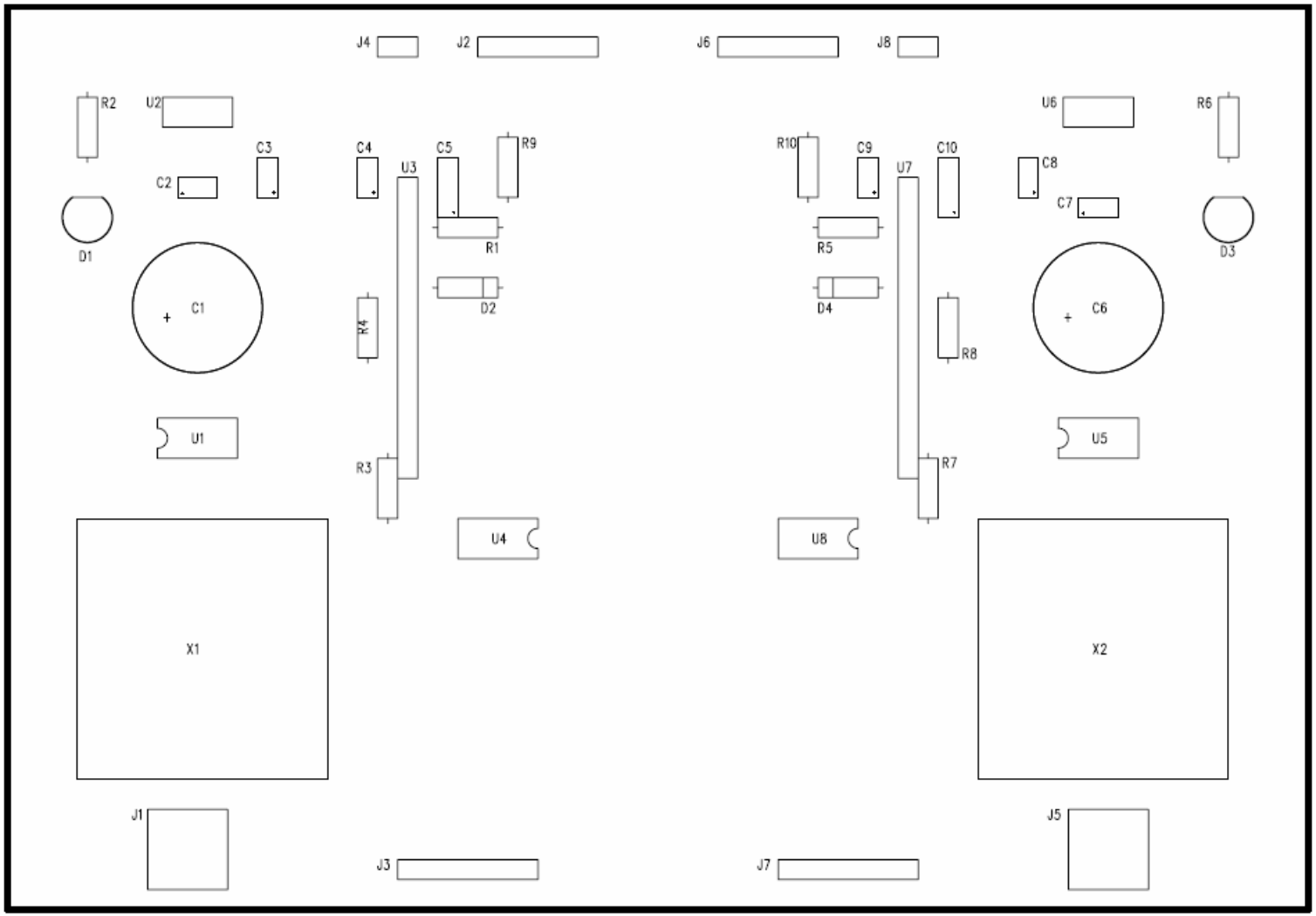

Silkscreen Top

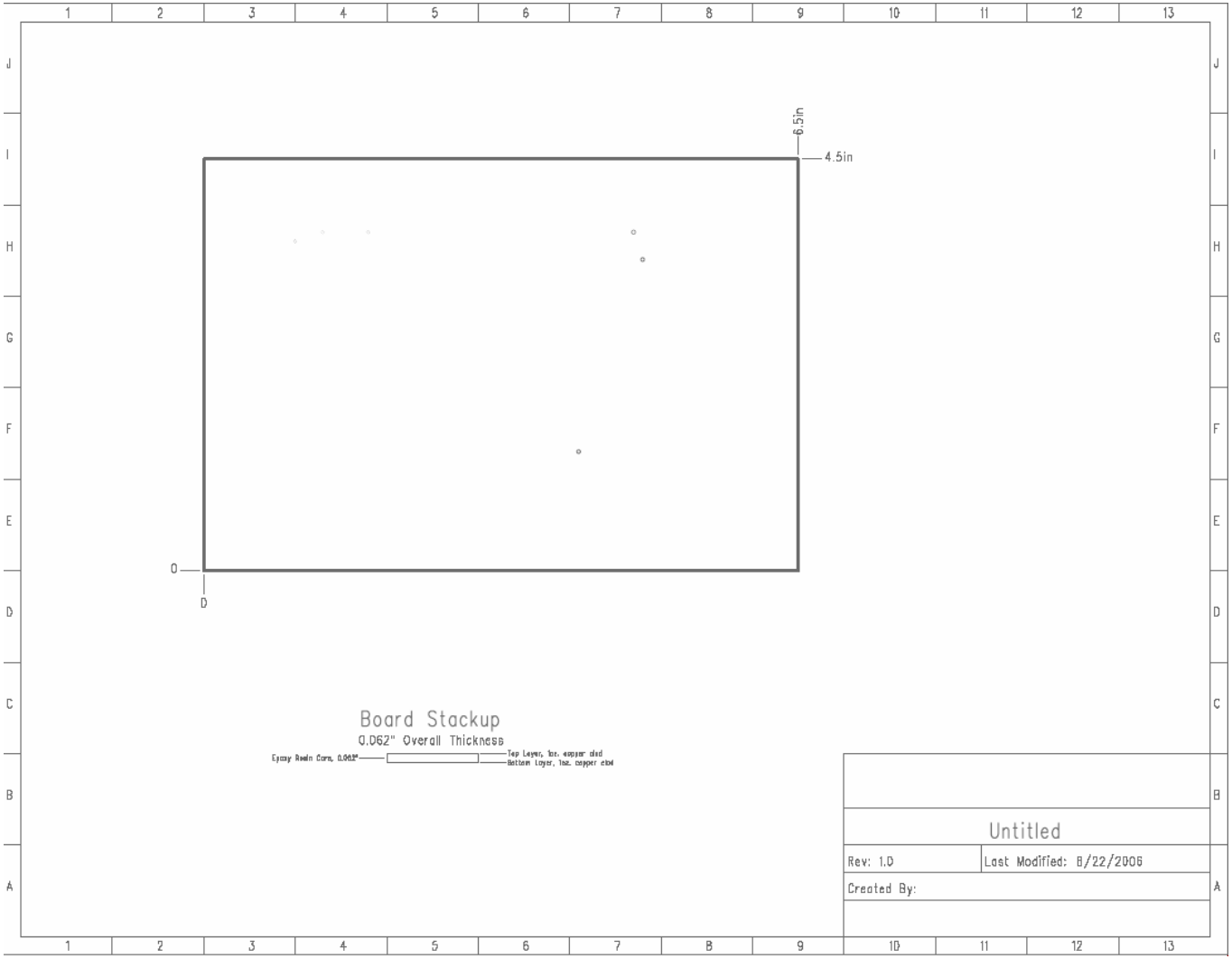

Mechanical Layout

REFERENCES

[1] S. P. Robb, J. L. Sutor, L. E. Terry, "Smartdiscretes, new products for automotive applications," *Automotive Power Electronics*, pp 109-113, Aug 1989.

[2] J. M. Miller, "Multiple voltage electrical power distribution system for automotive application," *Proc. of 31st Energy Conversion Engineering Conference*, vol. 3, pp 1930-1937, Aug. 1996.

[3] S. M. Lukic, A. Emadi, "Performance analysis of automotive power systems: effect of power electronic intensive loads and electrically-assisted propulsion systems," *Proc. of 56th Vehicular Technology Conference*, vol. 3, pp. 1835-1839, Sep. 2002.

[4] J. M. Miller, P.R. Nicastri, "The next generation automotive electrical power system architecture: issues and challenges," Proc. of *17th Digital Avionics Systems Conference*, vol. 2, pp. I15/1-I15/8, Oct/Nov. 1998.

[5] A. Emadi, M. Ehsani, J. M. Miller, " Advanced silicon rich automotive electrical power system," *Proc. of 18th Digital Avionics Systems Conference*, vol. 2, pp. 8.B.1-1 - 8.B.1-8, Oct. 1999.

[6] J. M. Miller, A. Emadi, A. V. Rajarathnam, M. Ehsani, " Current status and future trends in more electric car power systems," *49th Vehicular Technology Conference*, vol. 2, pp. 1380 – 1384, May 1999.

[7] X. Xingyi, "Automotive power electronics – opportunities and challenges," *International Conference on Electric Machines and Drives*, pp. 260 – 262, May 1999.

[8] M. Frister, G. Henneberger, "New concepts for vehicle electrical systems," *IEE Colloquium on Vehicle Electrical Power Management and Smart Alternators*, pp. 6/1 – 6/4, 15th April 1988.

[9] I. A. Khan, "Automotive electrical systems: Architecture and components," *Proc. of 18th Digital Avionics Systems Conference*, vol. 2, pp. 8.C.5-1 - 8.C.5-10, Oct. 1999.

[10] J. G. Kassakian, D. J. Perreault, "The future of electronics in automobiles," *Proc. of 13th Int. Symposium on Power Semiconductor Devices and ICs*, pp. 15-19, June 2001.

[11] J. H. Evans, "42Volts – impact on electrical distribution systems and components." *IEE Seminar, Passenger Car Electrical Architecture* (Ref. No. 2000/088), pp. 5/1 – 5/7, 21st June 2000.

[12] T. Heurung, "42Volt electrical systems design," *IEE Seminar, Passenger Car Electrical Architecture* (Ref. No. 2000/088), pp. 2/1 – 2/3, 21st June 2000.

[13] I. Moir, "The all-electric aircraft – major challenges," *IEE Colloquium on All Electric Aircraft*, digest no. 1998/260, pp. 2/1 – 2/6, June 1998.

[14] W. G. Homeyer, E.E. Bowles, S. P. Lupan, C. Rodriguez, P. S. Walia, N. M. Shah, M. A. Maldonado, "Advanced power converters for more electric aircraft applications," *Proc. of 31st Intersociety Energy Conversion Engineering Conference*, vol. 1, pp. 137– 142, Aug. 1996.

[15] L. J. Feiner, "Power-by-wire aircraft secondary power systems," *AIAA/IEEE 12th Digital Avionics Systems Conference*, pp. 439 – 444, Oct. 1993.

[16] M. A. Maldonado, N. M. Shah, K. J. Cleek, P. S. Walia, G. J. Korba, "Power management and distribution system for a more-electric aircraft (MADMEL) – program status," *Proc. of 32nd Intersociety Energy Conversion Engineering Conference*, vol. 1, pp. 274– 279, July/Aug. 1997.

[17] R. I. Jones, "The more electric aircraft: the past and the future," *IEE Colloquium on Electrical Machines and Systems for the More Electric Aircraft*, ref no. 1999/180, pp. 1/1 – 1/4, Nov. 1999.

[18] E. J. Woods, C. S. Rubertus, I. S. Mehdi, "Advanced aircraft secondary power system design," *Proc. of 25th Intersociety Energy Conversion Engineering Conference*, vol. 1, pp. 500– 510, Aug. 1990.

[19] R. E. Quigley, "More electric aircraft," *Proc. of 8th Applied Power Electronics Conference and Exposition*, pp. 906 – 911, March 1993.

[20] A. Emadi, M. Ehsani, "Aircraft power systems: technology, state of the art, and future trends," *IEEE Aerospace and Electronic Systems Magazine*, vol. 15, issue 1, pp. 28 – 32, Jan. 2000.

[21] C. G. Hodge, "Modern application of power electronics to marine propulsion systems," *Proc. of 14th International Symposium on Power Semiconductor Devices and ICs*, pp. 9 – 16, June 2002.

[22] D. Webstar, "Naval experience of power electronics maintenance," *IEE Colloquium on Power Electronics Reliability – Promise and Practice*. Does it deliver ?," Digest no. 1998/202, pp. 7/1 – 7/4, Feb. 1998.

[23] M. Baran, N. R. Mahajan, A. W. Kelley, J. J. Grainger, "A distribution system simulator for protection and control," *IEEE/PES Transmission and Distribution Conference and Exposition*, vol. 1, pp. 307 – 310, Oct/Nov. 2001.

[24] S. D. Sudhoff, S. Pekarek, B. Kuhn, S. Glover, J. Sauer, D. Delisle, "Naval combat survivability testbeds for investigation of issues in shipboard power electronics based power and propulsion systems," *IEEE Power Engineering Society*, vol. 1, pp. 347 – 350, July 2002.

[25] R. G. Blakey, "Power electronics in warships," *Power Engineering Journal*, vol. 7, issue 2, pp. 65 – 70, April 1993.

[26] T. Ericsen, "Power electronics building blocks – a systematic approach to power electronics," *IEEE Power Engineering Society*, vol. 2, pp. 1216 – 1218, July 2000.

[27] K. T. Kornegay, "Design issues in power electronic building block (PEBB) System Integration," *IEEE Proc. Computer Society Workshop on VLSI System Level Design*, pp. 48 – 52, April 1998.

[28] F. C. Lee, D. Peng, "Power electronics building block and system integration," *Proc. of 3rd International Power Electronics and Motion Control Conference*, vol. 1, pp. 1 – 8, Aug. 2000.

[29] T. Ericsen, "Power electronics building blocks and potential power modulator application," *Conf. Record of 23rd International Power Modulator Symposium*, pp. 12 – 15, June 1998.

[30] J. L. Hudgins, J. Mookken, B. Beker, R. A. Dougal, "The new paradigm in power electronics design," *IEEE Proc. of International Conference on Power Electronics and Drives Systems*, vol. 1, pp. 1 – 6.

[31] L. D. Massie, "Space power systems requirements and issues: The next decade," *IEEE Aerospace and Electronic Systems Magazine*, vol. 5, issue 12, pp. 4 – 9, Dec. 1990.

[32] D. J. Weeks, S. A. Starks, "Advanced automation approaches for space power systems," *IEEE Trans. Computer Applications in Power*, vol. 2, issue 4, pp. 13 – 16, Oct. 1989.

[33] G. L. Kusic, W. H. Allen, E. W. Gholdston, R. F. Beach, "Security for space power systems," *IEEE Trans. Power Systems*, vol. 2, issue 1, pp. 140 – 147, Feb. 1990.

[34] P. M. Anderson, R. Thibodeaux, "Power distribution study for 10 – 100 kW baseload space power systems," *Proc. of 25th Energy Conversion Engineering Conference*, vol. 1, pp. 428 – 433, 1990.

[35] I. Lazbin, B. R. Needham, "Analysis of the stability margins of the space station freedom electrical power system," *24th Power Electronic Specialist Conference*, pp. 839 – 845, June 1993

[36] M. Ehsani, M. O. Bilgic, A. D. Patton, J. Mitra, "New architectures for space power systems," *IEEE Aerospace and Electronic Systems Magazine*, vol. 10, issue 8, pp. 3 – 8, Aug. 1995.

[37] A. Emadi, M. Ehsani, "Multi-converter power electronic systems: definition and applications," *IEEE 32nd Power Electronics Specialist Conference*, vol. 2, pp. 1230 – 1236, June 2001.

[38] A. Emadi, "Modeling, analysis, and stability assessment of multi-converter power electronic systems," *Ph.D. Dissertation*, Texas A&M University, College Station, TX, Aug. 2000.

[39] A. Emadi, "Modeling and analysis of multi-converter DC power electronic systems using the generalized state space averaging method," *IEEE 27th Industrial Electronics Society*, vol. 2, pp. 1001 – 1007, Nov./Dec. 2001.

[40] X. Sun, Y. Lee, D. Xu, "Modeling, analysis, and implementation of parallel multi-inverter systems with instantaneous average-current-sharing scheme,"

IEEE Transactions on Power Electronics, vol. no. 18, issues 3, pp. 844 – 856, May 2003.

[41] K. J. Karimi, A. Booker, A. Mong, "Modeling, simulation, and verification of large DC power electronics systems," *IEEE 27th Power Electronics Specialist Conference*, vol. 2, pp. 1731 – 1737, June 1996.

[42] P. C. Krause, et. al., "Analysis of electric machinery and drive systems," *IEEE Press*.

[43] R. D. Middlebrook, S. Cuk, "A general unified approach to modeling switching converter power stages," IEEE Power Electronics Specialist Conference Records, 1976, pp. 18–34.

[44] S. D. Suhoff, S. F. Glover, "Three-dimensional stability analysis of DC power electronics based systems," *IEEE 31st Power Electronics Specialist Conference*, vol. 1, pp. 101 – 106, June 2000.

[45] C. M. Wildrick, "Stability of distributed power supply systems," *Masters Thesis*, Virginia Polytechnic Institute and State University, Blackburg, VA, Jan 1993.

[46] A. Emadi, J. P. Johnson and M. Ehsani, "Stability analysis of large DC solid – state power systems for space," *IEEE Aerospace and Electronic Systems Magazine*, vol. 15, issue 2, pp. 24 – 30, Feb. 2000.

[47] E. W. Gholdston, K. Karimi, F. C. Lee, J. Rajagopalan, Y. Panov, B. Manners, "Stability of large DC power systems using switching converters, with application to the international space station," *Proc. of 31st Intersociety Energy Conversion Engineering Conference*, vol. 1, pp. 166 – 171, Aug. 1996.

[48] T. L. Skvarenina, S. Pekarek, O. Wasynczuk, P. C. Krause, R. J. Thibodeaux, J. Weimer, "Simulation of a more – electric aircraft power system using an automated state model approach," *Proc. of 31st Intersociety Energy Conversion Engineering Conference*, vol. 1, pp. 133 – 136, Aug. 1996.

[49] J. Jatskevich, O. Wasynczuk, S. Pekarek, E. A. Walters, C. E. Lucas, P.T. Lamm, "Automated identification of the operation modes of switched electric circuits," *SAE Power Systems Conference*, document no. 2000 – 01 – 3650, Oct. 2000.

[50] A. Emadi, B. Fahimi, M. Ehsani, "On the concept of negative impedance instability in the more electric aircraft power systems with constant power loads," *SAE 34th Intersociety Energy Conversion Engineering Conference*, document no. 1999 – 01 – 2545, Aug. 1999.

[51] A. Emadi, M. Ehsani, "Dynamics and control of multi-converter DC power electronics systems," *IEEE 32nd Power Electronics Specialist Conference*, vol. 1, pp. 248 – 253, June 2001.

[52] A. Emadi, M. Ehsani, "Negative Impedance stabilizing controls for PWM DC/DC converters using feedback linearization techniques," *35th Intersociety Energy Conversion Engineering Conference*, vol. 1, pp. 613 – 620, July 2000.

[53] J. Mahadev, A. Emadi, H. A. Toliyat, " Application of state space averaging method to sliding mode control of PWM DC-DC converter," 32nd IEEE Industrial Application Society, vol. 2, pp. 820-827, Oct. 1997.

[54] Y. K. Chen, T. F. Wu, Y. E. Wu, C. P. Ku, "A current-sharing control scheme for paralleled multi-inverter systems using microprocessor-based robust control," *IEEE International Conference on Electrical and Electronic Technology*, vol. 2, pp. 647 – 653, Aug. 2001.

[55] R. Zhang, F. C. Lee, D. Boroyevich, C. Liu, L. Chen, "AC load conditioner and DC bus conditioner for a DC distribution power system," *IEEE 31st Power Electronics Specialist Conference*, vol. 1, pp. 107 – 112, June 2000.

[56] A. Emadi, A. Abur, "Real time state estimation of multi-converter DC power electronic systems using generalized state space averaging method," *IEEE 33rd Power Electronics Specialist Conference*, vol. 2, pp. 881 – 886, June 2002.

[57] J. A. Momoh, S. S. Kaddah, W. Salawu, "Security assessment of DC zonal naval – ship power system," *Large Engineering Systems Conference on Power Engineering*, pp. 206 – 212, July 2001.

[58] J. Riedesel, "A survey of fault diagnosis technology," *Proc. of 24th Energy Conversion Engineering Conference*, vol. 1, pp. 183 – 188, Aug. 1989.

[59] T. F. Glennon, "Fault tolerant generating and distribution system architecture," *IEE Colloquium on All Electric Aircraft*, Digest no. 1998/260, pp. 4/1 – 4/4, June 1998.

[60] A. C. Renfrew, J. X. Tian, "The use of a knowledge-based system in power electronic circuit fault diagnosis," *5th European Conference on Power Electronics and Applications*, vol. 7, pp. 57 – 62, Sep. 1993.

[61] R. E. Johnson, "Practical considerations in the design of power system architecture for fault tolerant systems," *20th Digital Avionics Systems Conference*, vol. 1, pp. 1A2/1 – 1A2/12, Oct. 2001.

[62] J. G. Kassakian, M. F. Schlecht, G. C. Verghese, Principles of Power Electronics, Addison-Wesley, 1991.

[63] Y. V. V. S. Murthy, G. K. Dubey, R. M. K. Sinha, " Fault diagnosis in three-phase thyristor converters using microprocessors," *IEEE Trans. Industry Application*, vol. 1A-20, 1984, pp. 1490-1496.

[64] C. S. Moo, S. Y. Chan, Y. C. Chuang, Y. N. Chang, "Investigation on fault operations of full-converter fed DC drives," *Proc. of IEEE Industry Application Society Annual Meeting*, vol. 1, pp. 3 – 8, Oct. 1995.

[65] A. J. M. Cardoso, E. S. Saraiva, "Fault diagnosis in electric drives and systems," *Proc. of Electric Drives Symposium*, pp 71 – 77, 1990.

[66] K. Waaryn, W. Zinka, "A prototype expert system for fault diagnosis in electronic devices," *European Conference on Circuit Theory and Design*, pp. 667 – 680, Sep. 1989.

[67] K. Debebe, V. Rajagopalan, T. S. Sankar, "Expert systems for fault diagnosis of VSI fed AC drives," *Proc. of IEEE Industry Application*, vol. 1, pp. 368 – 373, 1991.

[68] H. Jia-Zhou, Z. Zhi-Hua, Y. Xu-Ri, C. Shi-Fu, "Using neural networks for fault diagnosis," *Proc. of IEEE – INNS – ENNS International Joint Conference on Neural Networks*, vol. 5, pp. 217 – 220, July 2000.

[69] I. Dalmi, I. Kovacs, I. Lorent, G. Terstyanszky, "Adaptive learning and neural networks in fault diagnosis," *Proc. of IEE International Conference on Control*, vol. 1, pp. 284 – 289, Sep. 1998.

[70] C. Rodriguez, S. Rementeria, C. Ruiz, A. Lafuente, J. I. Martin, J. Muguerza, "A modular approach to the design of neural networks for fault diagnosis in power systems," *Proc. of IEEE International Joint Conference on Neural Networks*, vol. 3, pp. 16 – 23, June 1992

[71] D. Gayme, S. Menon, C. Ball, D. Mukavetz, E. Nwadiogbu, "Fault detection and diagnosis in turbine engines using fuzzy logic," *Proc. of IEEE 22nd International North American Fuzzy Information Processing Society Conference*, pp. 341 – 346, July 2003.

[72] T. Oyama, "Fault section estimation in power system using Boltzmann machine," *Proc. of the 2nd International Form on Application of Neural Networks to Power Systems*, pp. 3 – 8, April 1993.

[73] T. S. Sidhu, O. Cruder, G. J. Huff, "An abduction inference technique for fault diagnosis in electrical power transmission networks," *IEEE Trans. On Power Delivery*, vol. 12, No. 1, Jan. 1997.

[74] A. Bhoomaiah, P. Krishna Reddy, K. S. Linga Murthy, P. Appla Naidu, B. P. Singh, "Measurement of neutral currents in a power transformer and fault detection using wavelet techniques," *Proc. of IEEE Conference on Electrical Insulation and Dielectric Phenomena*, pp. 170 – 173, 2004.

[75] J. Hill, "Survivable architecture for vital systems," *Proc of the Symposium of ASNE Reconfiguration and Survivability*, (Feb. 2005) [Online]. Available: http:// www.navalengineers.org.

[76] N. Doerry, J. Davis, "Integrated Power System for Marine Application," *Naval Engineering Journal*, vol. 106. pp. 77 – 90, (May 1994).

[77] N. Doerry, "Zonal Ship Design," *Proc of the Symposium of ASNE Reconfiguration and Survivability*, (Feb. 2005) [Online]. Available: http:// www.navalengineers.org.

[78] J. A. Momoh, S. S. Kaddah, W. Salawu, "Security assessment of DC zonal naval – ship power system," Proc of the Conf of Large Engineering Systems on Power Engineering, pp. 206-212 (July 2001).

[79] K. L. Butler, M. Ehsani, "Flexiable Ship Electric Power System Design," Proc of the Symposium of Engineering the Total Ship, (1998).

[80] E. L. Zivi, 'Integrated shipboard power and automation control challenge problem', *Proc of IEEE Power Engineering Society Summer Meeting*. vol. 1, pp 325 – 330 (2002).

BIOGRAPHICAL INFORMATION

Ranjit Jayabalan graduated from BE from A K. College of Engineering, India and MS in Electrical Engineering from Illinois Institute of Technology, Chicago. He completed Ph. D. in Electrical Engineering at University of Texas at Arlington. His interests are in Power Electronics, Motor Drives and Vehicular Power Systems.